Aerodynamic Performance Measurements of a Fully Scaled, Film-Cooled, Turbine Stage

by

Christopher M. Spadaccini

S.B. Aeronautics and Astronautics, Massachusetts Institute of Technology, 1997

Submitted to the Department of Aeronautics and Astronautics
in partial fulfillment of the requirements for the degree of

Master of Science

at the

Massachusetts Institute of Technology

September 1999

Author_____
Department of Aeronautics and Astronautics
August 30, 1999

Certified by_____
Dr. Gerald R. Guenette
Principal Research Engineer
Department of Aeronautics and Astronautics, Gas Turbine Laboratory
Thesis Supervisor

Accepted by_____
Professor Nesbitt W. Hagood
Associate Professor of Aeronautics and Astronautics
Chair, Department Graduate Programs

Aerodynamic Performance Measurements of a Fully Scaled, Film-Cooled, Turbine Stage

by

Christopher M. Spadaccini

Abstract

The MIT Blowdown Turbine short duration test facility was used to experimentally measure the aerodynamic performance of a film-cooled turbine stage. Turbine torque, speed, mass flow, temperature, and pressure were measured and used to calculate efficiency. Pressure ratio, corrected speed, and coolant mass flow were varied parametrically over a range of conditions and compared to a baseline. No distinct trend was seen in the pressure ratio tests. Efficiency increased approximately 2.2% with a corrected speed increase of 20%. This trend is a result of a corresponding decrease in blade loading. An efficiency decrease of 2% was shown for a two-fold increase in coolant mass flow. A preliminary comparison to a previous uncooled test series showed a 2% decrease in efficiency with a 12% coolant-to-mainstream mass flow ratio.

To complete these tests, an uncooled turbine configuration was modified to a film-cooled configuration. A solid blade and nozzle guide vane set was machined via electro-discharge machining, laser drilling, and laser welding to provide film-cooling holes and manifold channels. The effective area (C_dA) of the film-cooling holes was measured and part-to-part variations quantified.

A coolant feed system was constructed to provide coolant flow to the turbine. Flow to the rotor blades, nozzle guide vanes, and tip casing was metered and controlled independently. Thick walled, squared edged, choked orifices were used. A set of experiments were performed to show that supersaturated coolant flow could be adequately controlled by this method.

Thesis Supervisor: Dr. Gerald R. Guenette
Title: Principle Research Engineer
Department of Aeronautics and Astronautics
Gas Turbine Laboratory

ACKNOWLEDGMENTS

I would like to thank Dr. Gerald Guenette for his guidance advising this research and for contributing to nearly every aspect. Also, Professor Alan Epstein for his suggestions and academic counseling.

I am greatly indebted to Lori Martinez, Holly Anderson, Viktor Dubrowski, James Letendre, Bill Ames, Mariano Hellwig, and Tom Ryan for their administrative and technical support.

A special thanks to the students who worked with me on the Blowdown Turbine: Jason Jacobs, Leo Grépin, Yi Cai, and especially, Rory Keogh who was more of a mentor than a fellow student.

I would also like to thank the other students at the Gas Turbine Laboratory who have made my experience here a more enjoyable one, especially Dan Kirk and Dave Underwood. Also, my office-mates, Adam, Mez, Waleed, and Bruno, as well as my other friends at the GTL: Amit, Luc, Zolti, Kevin, Brian, Tony, Jon, and Margarita.

Over the past two years many friends outside of the lab have helped to make this experience a memorable one. Especially my roommates Erin, Marco, and Jon, as well as Ming, Andrew, Amy, Ivy, Eva, and Bergen. Also my friends from CT: Pat, Joe, Amy, Chris, Pete, Rico, and Matt.

Finally, I would like to thank my family for all of the support and encouragement they have given me over the past two years of this work.

This program was sponsored by the US Department of Energy and ABB Power Generation Systems. Their support is gratefully acknowledged.

Contents

List of Figures

List of Tables

NOMENCLATURE

Roman

a	speed of sound [m/s]
A	area [m^2]
$A_{geometric}$	geometric area [m^2]
$A_{effective}$	effective area [m^2]
C_d	discharge coefficient
C_R	critical flow coefficient
h	enthalpy [J/kg]
I	moment of inertia [kg·m^2]
L_{ref}	reference length [m]
$\dot{m}$	mass flow rate [kg/s]
M	Mach Number
N	angular velocity [rps]
N_{mech}	mechanical speed [rps]
N_{cor}	corrected speed
P	pressure [Pa]
Q	heat per unit mass [J/kg]
R	gas constant [J/kg·K]
Re	Reynolds Number
s	entropy [J/kg·K]
t	time [s]
T	temperature [K]

u	velocity [m/s]
V	volume [m^3]
W_c	corrected flow

Greek

γ	specific heat ratio, C_p/C_v
ϵ	error
η	efficiency
μ	dynamic viscosity [kg/m·s]
π	pressure ratio
ρ	density [kg/m^3]
τ	temperature ratio
ω	angular velocity [rad/s]

Script

$\mathcal{P}$	power [Watts]
$\mathcal{T}$	torque [N·m]

Superscripts

*	sonic conditions, M=1

Subscripts

0	stagnation quantity
1	turbine inlet
2	turbine exit
c	coolant conditions

CHAPTER 1
INTRODUCTION

1.1 Background

The aerodynamic performance of axial flow turbines has increased dramatically over the past fifty years. Currently, polytropic efficiencies exceed 90% and turbine inlet temperatures are on the order of 1800°K. Improvements in efficiency have been driven by a better understanding of turbine fluid mechanics and more powerful computational tools. The relatively high turbine inlet temperatures have been achieved via advances in blade materials and internal and external cooling schemes. Thus, modern turbine designs have culminated in a much higher power per unit mass flow and a substantial increase in efficiency compared to their predecessors. Empirical observations acquired through years of turbine testing on engines, rotating rigs, cascades, and other sub-scale experiments are largely responsible for these advances.

Currently, steady state turbine testing has become expensive and impractical at the academic level. A rig test with inlet temperatures of only 450°K will typically cost around $5 million. As a result, experimental turbine research at this level is no longer common. A typical engine development program will usually include one or even zero turbine rig tests. In the case of the power generation industry, where large gas turbines are used, test rigs are simply not considered due to the immense size and power requirements. These components are tested in service and lead to conservative turbine designs and little or no performance improvement. Aerodynamic efficiency measurement accuracy in a full scale engine is only on the order of 1-2% and is considerably less than that required for today's sophisticated turbine design systems.

A similar situation existed for turbine heat transfer and cooling. However, during the 1980s, a new technology based on transient testing techniques has been developed at MIT's Gas Turbine Laboratory (GTL)[1]. Researchers at the GTL have been able to obtain highly accurate and detailed measurements of turbine heat transfer characteristics using this method. Time scales characteristic of heat transfer phenomena within a turbine are on the order of hundreds of microseconds. The technique is based on this realization. With instrumentation of adequate time response, tests less than a second long may be sufficient to establish steady state behavior. Although the instantaneous power generated during such a short duration test may be quite high (several megawatts), the energy required to conduct the test is relatively low. Also, by scaling all relevant non-dimensional properties, such as Reynolds Number, total pressure ratio, gas-to-wall temperature ratio, and corrected speed, turbine inlet temperature and rotor tip velocity can be reduced significantly[2]. These factors reduce the construction, maintenance, and power costs of turbine testing in addition to increasing safety margins.

Researchers also believe that transient testing may be useful for aerodynamic performance measurements (e.g., blade loading, efficiency). With the development of aerodynamic instrumentation with fast time response and the ability to measure shaft torque and turbine mass flow, Guenette[3] has proposed measuring turbine efficiency to an accuracy of 0.5%. Based on this realization, a test program to measure the adiabatic efficiency of both an uncooled and a corresponding cooled turbine, has been undertaken. This thesis is a result of these efforts.

1.2 Previous Work

The MIT Blowdown Turbine transient test facility was one of the first successful short duration turbine experiments. Since its development in the early 1980s, the Blowdown Turbine has been used to study many aspects of turbomachinery fluid physics and heat transfer. This work is briefly reviewed.

1. The Blowdown Turbine facility was designed and constructed by Guenette[4]. This initial work focused on the individual component design and fabrication, instrumen-

tation, and the importance of time and physical scaling. Heat transfer testing of the tip casing and nozzle guide vanes (NGVs) was also conducted.

2. The effect of film cooling on blade heat transfer was studied by Abhari[5]. Heat transfer coefficients, measured on both a cooled and uncooled turbine, were compared. The time unsteady nature of blade heat transfer was examined using these data, as well as cascade data and a physics-based model.

3. Shang[6] examined the influence of turbine inlet temperature non-uniformities on blade heat transfer. Radial temperature distortions were found to have a large effect on turbine heat transfer, while circumferential distortions did not. The experimental study was conducted in conjunction with a computational investigation.

4. Particle-image velocimetry (PIV) was used to study the unsteady nature of turbine fluid mechanics by generating an image of the instantaneous velocity field in the Blowdown Turbine. These data were then compared to CFD calculations by Grépin[7].

5. The latest research focuses on measuring the aerodynamic performance of both an uncooled and a corresponding film-cooled turbine. Ultimately, the efficiency loss due to coolant flow injection will be quantified. Initial research conducted by Keogh[8] and Cai[9] resulted in the development of the instrumentation and facility modifications required for these measurements. Preliminary analyses of these data were carried out by Jacobs[10].

1.3 Motivation

In an effort to improve the performance of the gas turbine cycle, turbine researchers and designers have devoted most of their resources to increasing turbine inlet temperature. In addition to the development and implementation of high temperature alloys and other advances in materials technology, this increase is the result of improved cooling techniques. Full coverage of the turbine blading by film-cooling is one of the most effective means of sustaining higher temperatures and is commonly employed in all high performance engine designs.

It can be expected that further rises in inlet temperature will require not only more effective application of the cooling flow, but also increases in the fraction of flow used for this cooling. Some advanced design concepts are now projecting overall coolant-to-main flow ratios approaching 33%. At these levels, the injected flow is a major component of the overall turbine through-flow. If the advanced life and performance goals of future systems are to be met, these coolant/main flow interactions must be identified and understood.

However, little research in rotating facilities has focused on the effect of these coolant/main flow interactions on turbine aerodynamic performance. This is due to the high level of experimental and analytical capability required to study such phenomena. With recent advances at the MIT Blowdown Turbine facility, this area will begin to receive more attention. Analysis by Guenette[3] and facility modifications and instrumentation developed by Keogh[8] now allow for accurate measurement of turbine adiabatic efficiency. Therefore, this facility can be utilized to study coolant/main flow interactions in axial flow turbines.

1.4 Objectives

The primary objectives of this work are:

1. To construct a geometrically scaled, fully rotating, single stage, film cooled turbine for testing in the MIT Blowdown Turbine facility.

2. To modify the facility to allow for independent control of coolant flow to the rotor blades, NGVs, and tip casing. This includes all associated coolant system instrumentation.

3. To test a film-cooled turbine stage under fully scaled conditions in the Blowdown Turbine facility and obtain aerodynamic performance measurements.

4. To conduct a preliminary comparison of the cooled turbine performance with that of the corresponding uncooled turbine. Uncooled data were obtained in a previous test series and were analyzed by Jacobs[10].

5. To provide a detailed data set for use in physics-based modeling efforts and CFD code validation.

1.5 Thesis Outline

This chapter introduces the content of the thesis, reviews previous Blowdown Turbine research, and outlines the motivation and objectives of this work.

Chapter 2 introduces the MIT Blowdown Turbine facility and reviews all primary components. Facility scaling issues and typical run conditions are discussed. Modifications to the facility to allow for coolant flow are also presented.

In chapter 3, the manufacturing of a scaled, film-cooled turbine is presented. The use of advanced machining techniques, including electro-discharge machining (EDM), laser drilling, and laser welding are discussed.

Knowledge of the discharge coefficients of each row of film cooling holes is required for later calculations and modeling. In chapter 4, an apparatus for measuring these discharge coefficients is presented along with data for the rotor blade cooling holes.

Chapter 5 discusses the problems associated with the flow of supersaturated CO_2 in the coolant feed system. Metastable flow metering with thick walled, square edged, choked orifices was validated by comparison with flow through a toroidal throat, critical flow venturi nozzle.

Chapter 6 reviews the uncooled turbine performance data first analyzed by Jacobs[10]. The method of calculating efficiency propounded by Keogh[8] is also re-examined.

Chapter 7 includes a description of the cooled turbine tests, as well as a detailed discussion of the data. Some analysis and a preliminary comparison of the cooled and uncooled turbine aerodynamic performance is also presented.

Chapter 8 concludes the thesis with some final observations and recommendations for future work.

Chapter 2

Blowdown Turbine Test Facility

2.1 Introduction

The MIT Blowdown Turbine test facility is a short-duration, blowdown wind tunnel for testing a fully rotating turbine stage. The facility is capable of rigorously simulating the fluid physics and heat transfer phenomena which occur in a turbine. This is accomplished by matching all critical non-dimensional parameters including Reynolds Number, total pressure ratio, gas-to-wall temperature ratio, coolant-to-mainstream mass flow ratio and coolant-to-mainstream momentum flux ratio. The transient environment of the blowdown facility provides up to 800 ms of quasi-steady state turbine operation. The important fluid and heat transfer phenomena occur on extremely small time scales, on the order of the inverse of the blade passing frequency, and can be observed in the 800 ms test window. Therefore, quasi-steady state measurements can be made in a fraction of a second, capturing several hundred flow time scales provided that instrumentation with adequate time response is available. Although the facility was originally designed around a 0.75 scale turbine from the Rolls Royce Advanced Core Engine (ACE), it now houses a 0.25 scale ABB GT24 first low pressure turbine stage.

This chapter reviews the MIT Blowdown Turbine facility. Overall configuration and operational procedures are described. Scaling of the turbine operating point for achieving full scale similarity is discussed. Individual components are examined as well as instrumentation and the recently modified coolant feed system. The data acquisition system is also briefly presented.

2.2 Facility Configuration

2.2.1 Introduction

The MIT Blowdown Turbine test facility is shown in Figure 2-1. The facility consists of seven primary components: the supply tank, fast acting valve, test section, eddy current brake torque meter, critical flow venturi nozzle, coolant feed system (not shown), and dump tank. Each of these components will be discussed and a detailed review of the overall design of the facility can be found in reference [4].

2.2.2 Supply Tank and Main Valve

The supply tank is a large cylindrical tank which is capable of holding gas up to pressures of 150 psia. The supply tank can also be heated to obtain the appropriate test gas temperature. The tank is wrapped in a metal jacket through which heat transfer oil is circulated. By regulating the temperature of this oil, the tank temperature can be controlled. A gas mixing fan is mounted inside the tank to ensure gas temperature uniformity.

The supply tank is separated from the rest of the tunnel by the main valve. This valve is a fast acting, axially traversing, plug valve. When closed, the valve seals the supply tank from the test section and when open, forms a smooth annular flow path. Figure 2-2 shows the valve. The valve is initially actuated by 1200-1400 psi argon supply bottle. The force from the argon begins to open the valve and the test gas, usually at pressures of 50-105 psia, flows out of the supply tank and forces the valve completely open. Valve dynamics are controlled by the expansion of the test gas into internal damping chambers. The valve is opened in approximately 50 ms and the flow transient due to this opening is 300 ms. A detailed review of the main valve design and dynamics can be found in reference [4].

2.2.3 Test Section

A cut-away of the test section is shown in Figure 2-3. The test section houses the forward frame, rotor assembly, and downstream translator. The forward frame mates to the main valve upstream and contains the nozzle guide vanes (NGVs) downstream. The forward

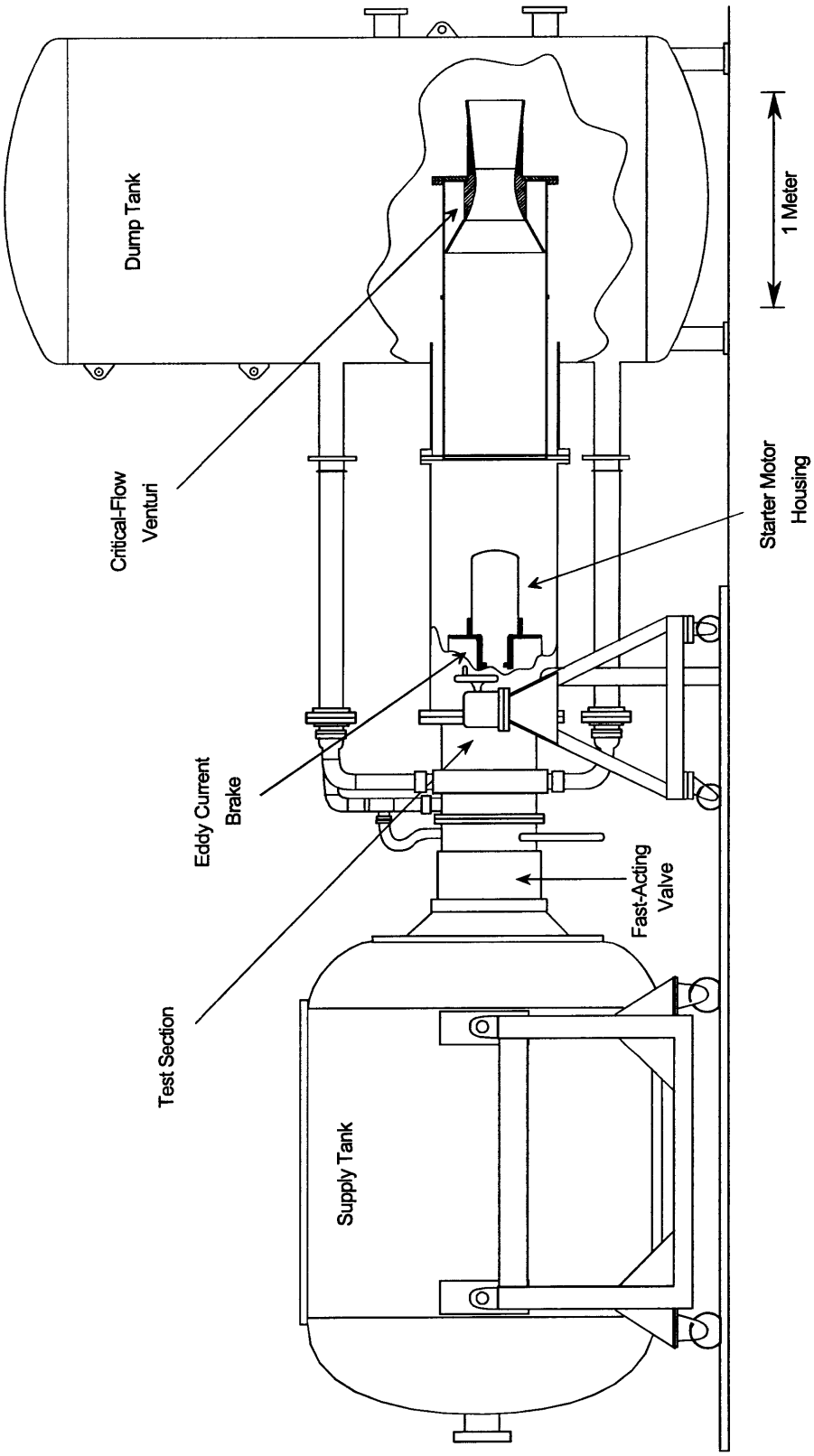

Figure 2-1: MIT Blowdown Turbine test facility.

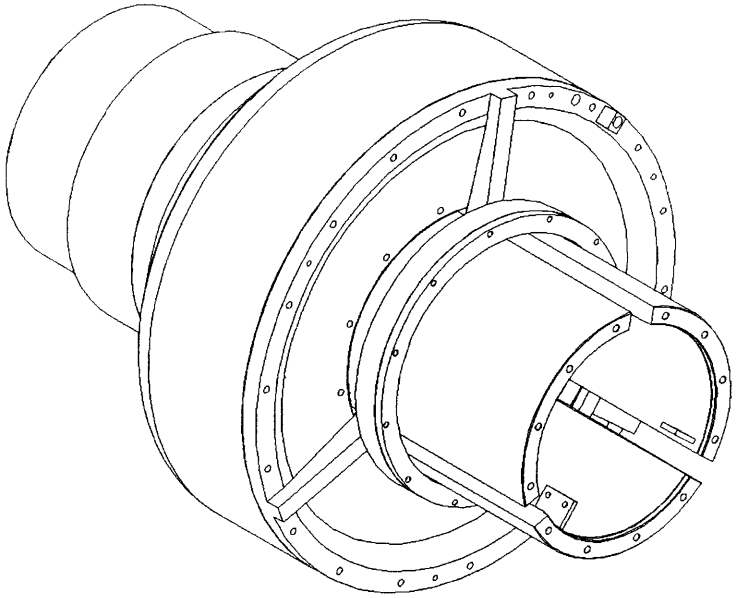

Figure 2-2: Blowdown Turbine facility main valve.

frame is followed by the rotor assembly which consists of the rotor discs, blades, and a large cylindrical drum (not shown). The drum is inserted into the eddy current brake torque meter which will be discussed in subsection 2.2.5.

Figure 2-4 shows a cross-sectional view of the test section flow path. Upstream of the turbine stage a boundary layer bleed provides clean inlet flow. Downstream of the rotor the flow is exhausted through an adjustable throttling area. During the usable portion of the test, this area is choked. By varying this area via a throttle plate, the desired pressure ratio across the turbine can be achieved. Also shown in Figure 2-4 are upstream and downstream measurement locations. Downstream total temperature and pressure probes are mounted on a circumferential translator. This device will be discussed in subsection 2.2.4.

2.2.4 Downstream Translator

Upstream of the turbine stage it can be assumed that the flow is circumferentially symmetric. This allows for stationary upstream measurements to be representative of the entire

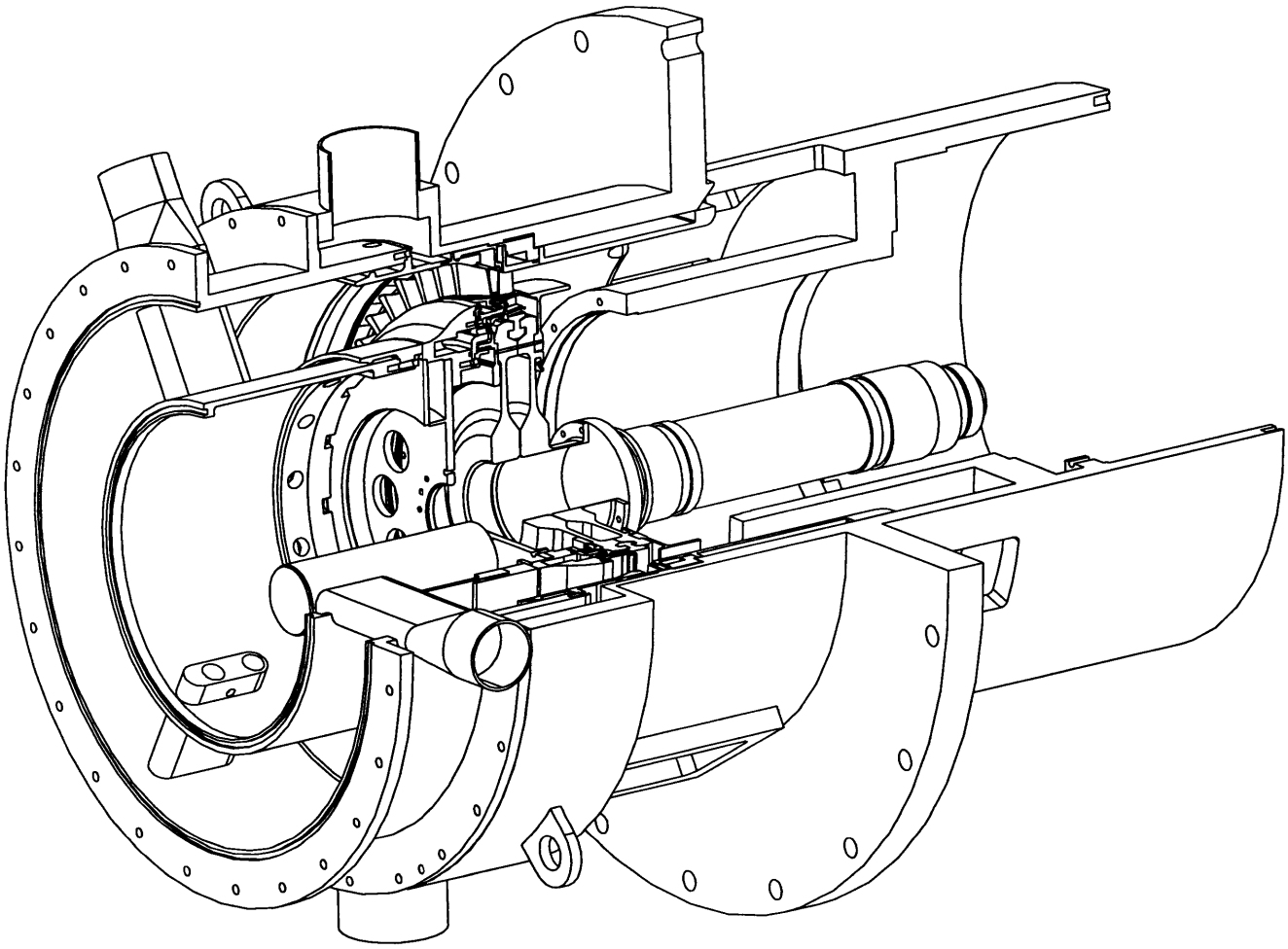

Figure 2-3: Test section cut-away.

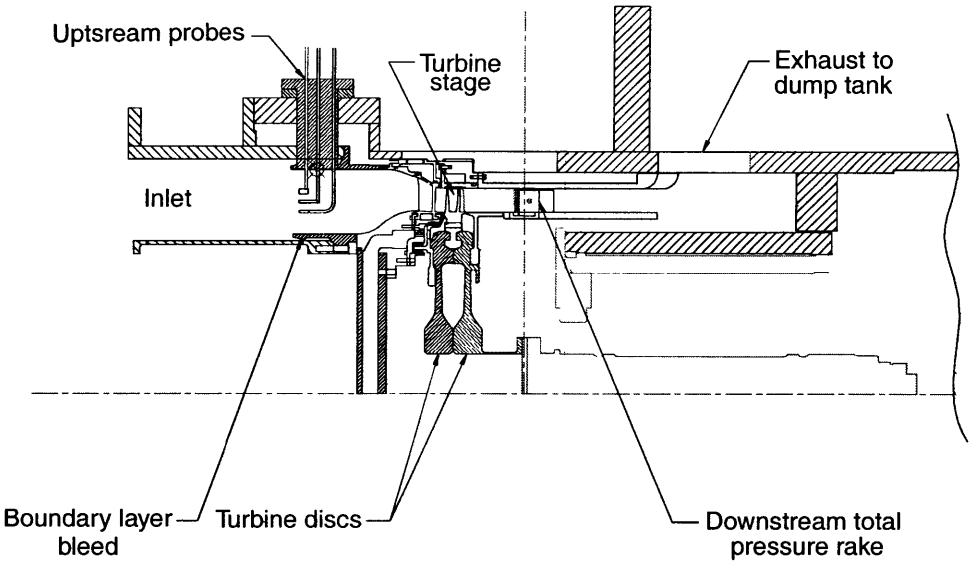

Figure 2-4: Test section flow path.

flow field. Downstream of the turbine this is not the case. The presence of the NGVs causes a circumferential non-uniformity in the form of a wake. Thus, stationary flow field measurements will be biased by their circumferential location; the temperature and pressure inside and outside of a wake are not the same. In order to avoid this complication the downstream probes must be circumferentially traversed during the usable test window. This is the purpose of the downstream translator.

The translator is a large cylindrical drum located downstream of the rotor. It contains three "canisters" in which probes can be mounted. They are spaced 20^o apart and contain the appropriate electrical connections for either a total temperature or pressure rake. Located 40^o ahead of the first canister is a static pressure tap, labeled P45HUB.

The translator is free to rotate 350^o and is restricted by a spring loaded hard stop. This stop is designed to prevent the translator from freely spinning and destroying the canisters' electrical wiring. The translator is driven by a servo-motor which provides approximately 3 in-lbs of torque through an equivalent 13.5:1 gear ratio and is computer controlled.

Figure 2-5 shows typical translator motion during an experiment. The translator rotates at a constant angular velocity of approximately 0.25 rps during the usable test window. All instruments are between 0^o and 120^o during this time. These locations correspond to wind tunnel strut locations behind which measurements are contaminated.

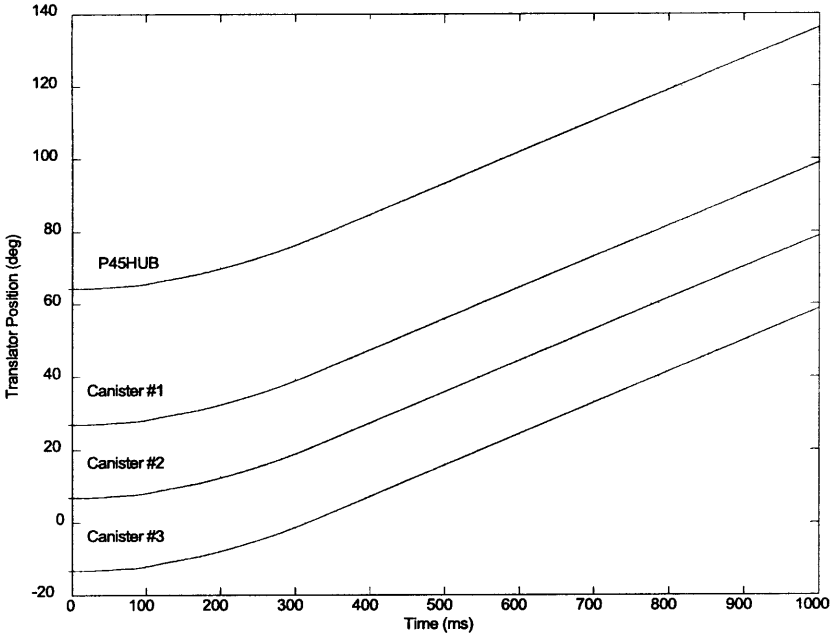

Figure 2-5: Downstream translator motion.

2.2.5 Eddy Current Brake Torque Meter

The eddy current brake torque meter serves the purpose of braking the turbine and holding a relatively constant corrected speed during the test window. It also provides a measure of shaft torque. A large, cylindrical, inconel drum which is connected to the rotor assembly inserts into the eddy current brake torque meter. The braking mechanism consists of a series of electromagnets arranged circumferentially inside the facility. Spinning the drum in the magnetic field induces a current. This current, through resistive heating of the drum, dissipates the power produced by the turbine. In the presence of the magnetic field, the current opposes the rotation of the drum and provides a braking torque. By adjusting the brake excitation voltage, the torque provided by the brake can be varied. This is how turbine corrected speed is controlled.

The braking system was modified by Keogh[8] so that it can be used to measure shaft torque. By mounting the brake assembly on bearings and reacting the braking torque through load cells, torque can be measured. Ultimately, this measurement is used to compute turbine power.

2.2.6 Critical Flow Venturi Nozzle

A large critical flow venturi nozzle is located downstream of the test section and is used to measure the total facility mass flow. After passing through the test section, the test gas flows through the venturi nozzle and its total temperature and pressure are measured. From these data and knowledge of the venturi discharge coefficient, the mass flow can be calculated. After passing through the venturi the flow exhausts into the dump tank. The venturi itself is a smooth-walled, geometrically well defined nozzle. It was built by Flow Systems Inc. and it's discharge coefficient was calibrated by Colorado EESI. This calibration is traceable to the National Institute for Standards and Technology (NIST). A cross section of the critical flow venturi nozzle is shown in Figure 2-6 and a more detailed review of its design and usage can be found in reference [8].

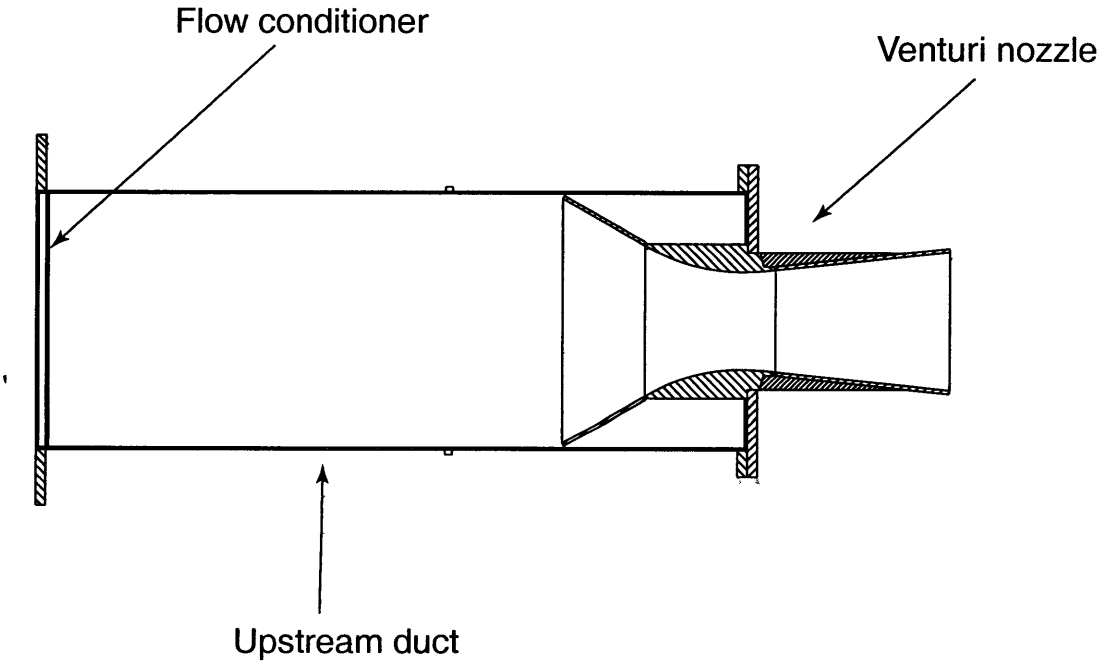

Figure 2-6: Critical flow venturi nozzle.

2.2.7 Coolant Feed System

Previous testing of the ABB turbine was done with an uncooled configuration. There were no film-cooling holes and as a result, no need for a coolant feed system. However, recent testing on the film-cooled version of the turbine stage required such a system. There was

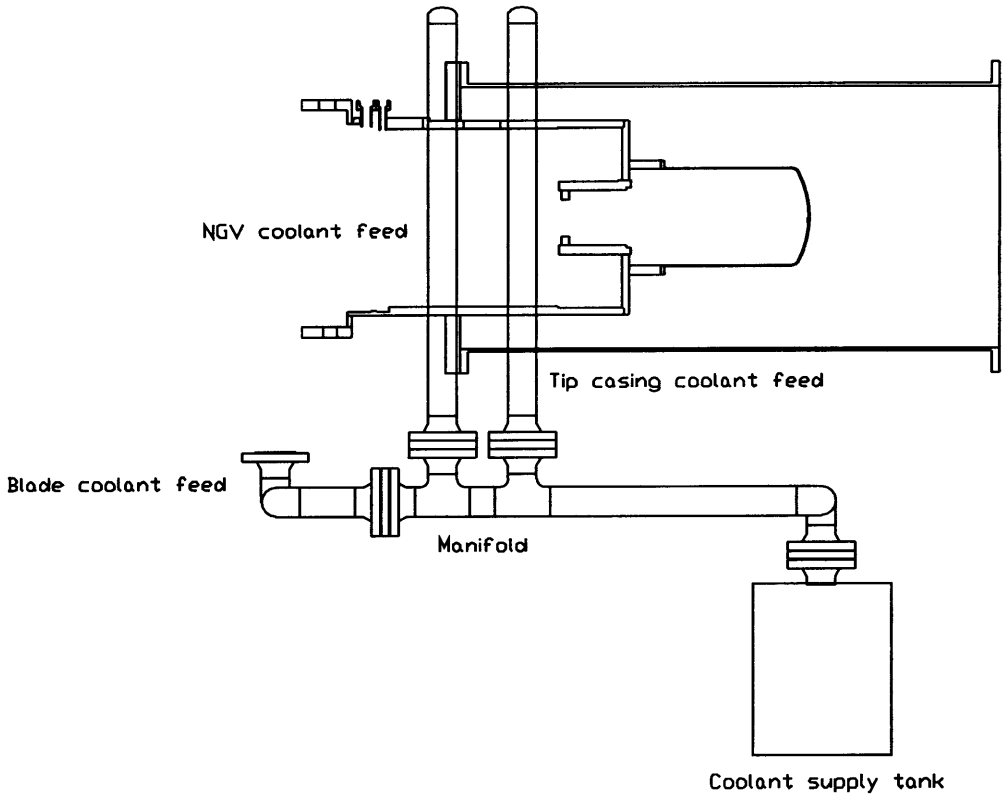

Figure 2-7: Coolant feed system.

an existing coolant system which would need modifications to be used. It was necessary to install additional plumbing to feed the coolant into the turbine and to control the coolant mass flow splits to the rotor blades, NGVs, and tip casing independently. The system consists of a coolant supply tank, a fast-acting pneumatic ball valve, a pipe network, and several orifice plates for metering the flow. Like the facility itself, the cooling system operates in a blowdown mode.

The coolant supply tank is 3.97 ft^3 and has a pressure rating of 450 psia. Like the main supply tank, it is surrounded by a metal jacket and insulation for controlling tank temperature. A flow of liquid nitrogen mixed with compressed air is used to cool the tank lining and the test gas to the desired temperature.

The fast-acting ball valve at the tank exit is actuated by a 1000 psi argon bottle. It is triggered simultaneously with the main valve and closes approximately 1.2 seconds later.

The piping network feeds the coolant from the supply tank into the test section and to the turbine. An overhead view of this network can be seen in Figure 2-7. Three independent feeds are required. One each to the rotor blades, NGVs, and tip casing. The flow is split in a manifold downstream of the ball-valve. Each split is metered by a thick, square edged, choked orifice with known discharge coefficient. This sets the mass flow ratios to each turbine component in an accurate, reliable, and inexpensive manner.

2.3 Test Procedures

Preparations for a blowdown experiment begin by determining the desired conditions for achieving full-scale turbine operating similarity. This analysis is presented in section 2.4. For the purposes of this discussion, it is assumed that these conditions consist of the upstream total temperature and pressure, coolant total temperature and pressure, test gas composition, mechanical speed, throttle area, and brake excitation. The experiment then proceeds as follows:

1. The entire facility is evacuated to approximately 0.5 torr and the throttle plate is positioned for the predetermined area.

2. The main supply tank is heated to the desired upstream total temperature and is brought to thermal equilibrium.

3. The main valve is sealed and the supply tank is filled with the test gas to the desired upstream total pressure.

4. Simultaneously, the coolant supply tank is filled with it's test gas to the desired pressure and cooled to the predetermined temperature.

5. At this post-fill state, all differential pressure transducers are calibrated by cycling their back-pressure between vacuum and atmosphere. This provides a scale factor for each transducer. Instrumentation and calibration are discussed in further detail in section 2.5.

6. The brake excitation is set.

7. The data acquisition system and translator servo-motor controller are set to stand-by mode and are waiting to be triggered.

8. The turbine rotor is then accelerated to the desired mechanical speed by a starter motor.

9. Once this speed is exceeded, the motor is powered down and the rotor spins freely in the vacuum. It is decelerated by bearing friction.

10. When the decelerating rotor reaches the preset speed, triggering occurs causing the main valve and coolant ball valve to open. Simultaneously, the data acquisition system begins collecting data, the downstream translator begins it traverse, and the eddy current brake torque meter is energized.

11. The test gases then flow through the test section and quasi-steady state operation is reached after a 300 ms transient. The useful test window is approximately 300-1000 ms.

12. After approximately 1.2 seconds the coolant ball-valve closes and the brake is turned off.

13. The rotor decelerates and comes to a stop.

14. Once the gas inside the tunnel stabilizes, all differential pressure transducers are re-calibrated to check for drift.

15. The tunnel is re-evacuated and cooled to room temperature.

2.4 Scaling of Test Conditions

Validity of scaled wind tunnel experiments depends on similarity between the test flow and the actual flow being simulated. In dimensionless form, the equations for momentum and energy transfer produce non-dimensional parameters which characterize the flow field. Similarity between experiment and reality only requires that these non-dimensional parameters are matched. For a turbine stage, corrected mass flow and total temperature ratio depend

on four dimensionless parameters: total pressure ratio, corrected speed, Reynolds number, and specific heat ratio γ[4]. Equation 2.1 shows the functional form of this relationship.

$$\left[\frac{\dot{m}\sqrt{RT_{0,1}}}{P_{0,1}L_{ref}^2}, \tau\right] = f\left(\pi, \frac{NL_{ref}}{\sqrt{RT_{0,1}}}, \frac{\dot{m}}{\mu L_{ref}}, \gamma\right) \tag{2.1}$$

These are the parameters that govern similarity in the Blowdown Turbine and can be matched with the proper operating conditions. Operating conditions consist of a test gas composition, upstream total temperature and pressure, coolant total temperature and pressure, mechanical speed, throttle area, and brake excitation.

For an uncooled turbine test, supply tank total temperature and pressure are set to simultaneously match Reynolds Number and specific heat ratio. Reynolds number can be written in terms of mass flow as

$$Re = \frac{\dot{m}}{\mu L_{ref}} \tag{2.2}$$

Corrected flow is equal to the stage design corrected flow and is known. It can also be expressed in terms of mass flow as

$$W_c = \frac{\dot{m}\sqrt{RT_{0,1}}}{P_{T0,1}L_{ref}^2} \tag{2.3}$$

A relationship for total temperature, total pressure, and Reynolds number for a given corrected flow can be obtained by combining equations 2.2 and 2.3.

$$P_{0,1} = \frac{\mu\sqrt{RT_{0,1}}}{L_{ref}} \cdot \frac{Re}{W_c} \tag{2.4}$$

With this relationship, a total temperature can be selected and the pressure required for Reynolds Number similarity can be calculated. From this temperature and pressure, γ can be obtained from a table of gas properties and compared to the desired value. Total temperature is adjusted until specific heat ratio similarity is obtained. This process is demonstrated graphically in Figure 2-8 where lines of constant Reynolds number and γ are plotted on a total temperature and pressure plane.

Once the supply tank temperature and pressure are known, the mechanical speed can be

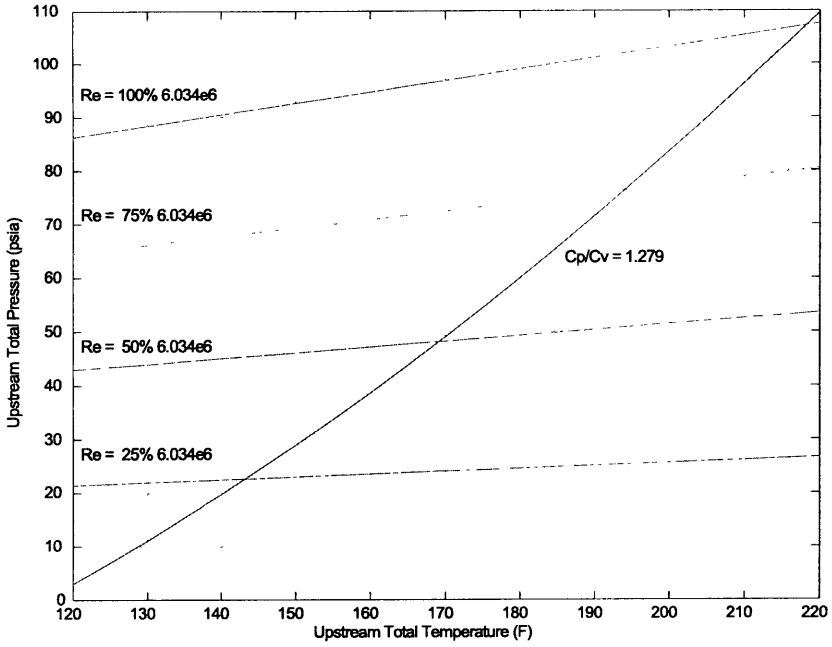

Figure 2-8: Total temperature and pressure for matching Reynolds Number and γ. A test gas of pure CO_2 is assumed.

set to match full scale corrected speed by applying the definition of corrected speed:

$$N_{mech} = \frac{\sqrt{\gamma R T_{0,1}}}{L_{ref}} N_{cor} \tag{2.5}$$

For a film-cooled turbine test two additional parameters must be satisfied. Momentum flux ratio and coolant-to-mainstream mass flow ratio are matched. To match the full scale momentum flux ratio, the coolant-to-mainstream temperature ratio must be simulated. This requires a main supply tank temperature which is very high and a low coolant temperature. As a result, the afore mentioned method of matching Reynolds Number and specific heat ratio no longer holds. In some cases, Reynolds Number can not be matched because the initial pressure of the supply tank would be greater than safety limits would allow. To match γ, the test gas composition must be varied. Mixtures of argon and CO_2 are typical. The coolant total pressure is selected to match the coolant-to-main flow mass fraction of the full scale engine. This is based on the areas of the choked orifices in the coolant feed system and is discussed further in Chapter 5.

The target total pressure ratio is equal to the stage design pressure ratio and is known. To

Table 2.1: Typical Blowdown Turbine operating conditions.

Parameter	Full Scale Engine	MIT BDT
Working Fluid	Air	CO_2
Specific Heat Ratio γ	1.28	1.28
Mean Metal Temperature	1100 K	300 K
Metal/Gas Temp. Ratio	0.647	0.647
Midspan NGV Chord	0.15 m	0.0365 m
Reynolds Number	5.6 x 10^6	5.6 x 10^6
Inlet Total Pressure	15 atm	7 atm
Exit Total Pressure	7.43 atm	3.47 atm
Inlet Total Temperature	1700 K	464 K
Exit Total Temperature	1470 K	401 K
Prandtl Number	0.928	0.742
Design Rotor Speed	3600 rpm	5954 rpm
Design Mass Flow	312 kg/s	23.3 kg/s
Coolant/Main Flow	9.8%	9.8%
Turbine Power Output	91 MW	1.2 MW
Test Time	continuous	$\approx$500 ms

set the test pressure ratio the downstream throttle plate must be adjusted. The throttle area can be approximated using average values for γ, and assumed values for discharge coefficient, C_d, and adiabatic stage efficiency, η. However, several blowdown experiments are required to fine tune the pressure ratio and simple scaling from previous tests is more effective.

The eddy current brake torque meter excitation voltage must be set at a certain level to absorb the turbine power and maintain a constant corrected speed. The calculation of this voltage is based on a model of the device which was developed by Guenette[4] during its design.

Table 2.1 summarizes the conditions of a typical blowdown experiment and compares them to that of a full scale engine.

2.5 Instrumentation

2.5.1 Introduction

In a transient testing environment there are stringent requirements on the accuracy and time response of instrumentation. Several highly accurate, fast time response temperature and pressure probes were developed by Cai[9] for use in these conditions. Some of these probes as well as other instrumentation which was used in the Blowdown Turbine will be reviewed here. In addition, the calibration of differential pressure probes will be discussed.

2.5.2 Total Temperature Instrumentation

Upstream of the turbine stage are three fast time response total temperature probes. The type K thermocouple junctions are 0.0005" diameter and are accurate to 0.13^o K. The three probes are spaced 120^o apart on the inlet annulus.

There are two total temperature probes located in the critical flow venturi nozzle and one just upstream. These probes are also type K thermocouples with 0.0005" diameter junction and have similar time response and accuracy to the upstream probes.

The cooling system is instrumented with seven type K thermocouples. These probes have 0.003" junctions and do not have the time response of the afore mentioned sensors due to their larger size. These probes are located at points upstream of the choked orifices and as close as possible to where the coolant enters the test section.

All of the thermocouples are referenced to an Omega TRCIII Ice Point reference cell. Their signals are also amplified prior to be recorded by the data acquisition system.

2.5.3 Total Pressure Instrumentation

The primary concerns in the design of a pressure sensor are fast time response and flow angle insensitivity. The second criteria is particularly important for downstream measurements where a probe is exposed to NGV wakes and is circumferentially translated.

To achieve the desired time response, piezoresistive strain gauge type pressure transducers

manufactured by Kulite, were used. The primary disadvantage of these transducers are that they tend to drift with changes in temperature. This is the reason for the extensive calibration routines used during every experiment.

Downstream of the turbine stage a rake type pressure probe with eight heads is employed to survey the pressure in the radial direction. The probe is mounted on the downstream translator to resolve flow characteristics in the circumferential direction. To allow a large range of inlet flow angles to the probe, a 15^o beveled impact head was employed. Acceptable flow angles are estimated to be $\pm 27.5^o$. The transducers on this rake are 100 psig differential Kulites. More information on the design of this probe is available in reference [9].

In addition to this rake, there are differential sensors located upstream of the turbine and in the supply, coolant, and dump tanks. There are also several highly accurate pressure sensors mounted throughout the facility for use as a calibration reference. These transducers are manufactured by Sensotec. The coolant system is instrumented with several lower accuracy Sensotec 100 psig transducers and one 300 psig transducer.

2.5.4 Other Instrumentation

Several other pieces of instrumentation are used in the Blowdown Turbine facility. Turbine speed and translator motion are monitored by their respective digital encoders. Several vibrometers are mounted on the shaft and bearings to record vibrations during an experiment. The eddy current brake torque meter is instrumented with two load cells which provide a measure of shaft torque. The brake voltage and current are also recorded by the data acquisition system. A list of all instrumentation is provided in Table 2.2.

2.5.5 Transducer Calibration

All differential pressure transducers are calibrated immediately after the supply tank is filled and at the conclusion of each test. Calibration data just before and after each experiment allows transducer drift to be quantified. Figure 2-9 shows a typical calibration trace of a differential pressure transducer. This figure and the calibration sequence are described below.

Table 2.2: Blowdown Turbine instrumentation.

Sensor Name	Type	Location
PREF150	Absolute Pressure	Supply Tank
PREF050	Absolute Pressure	Test Section - Upstream
PREF300	Absolute Pressure	Coolant Supply Tank
FTACH	Digital Speed	Shaft
ATACH	Analog Speed	Shaft
VTOT	Excitation	Eddy Current Brake
ITOT	Current	Eddy Current Brake
IBRK	Current	Eddy Current Brake
DSTPOS	Digital Encoder	Downstream Translator
ECBF,1-2	Load Cells	Eddy Current Brake
FBRING	Vibrometer	Forward Bearing
RBRING	Vibrometer	Rear Bearing
PT0,A-B	Differential Pressure	Supply Tank
PTC0	Differential Pressure	Coolant Tank
PDMP	Differential Pressure	Dump Tank
PT2,A-C	Differential Pressure	Test Section - Upstream
PNOZ	Differential Pressure	Venturi Nozzle
TT2,A-C	Temperature	Test Section - Upstream
PTC1	Gauge Pressure	Cooling System - Manifold
PTC2V	Gauge Pressure	Cooling System - NGVs
PTC2B	Gauge Pressure	Cooling System - Blades
PCCV	Gauge Pressure	Cooling System - NGVs
PCCC	Gauge Pressure	Cooling System - Tip Casing
PT45R,1-8	Differential Pressure	Downstream Translator
P45HUB	Differential Pressure	Downstream Translator
P45A	Differential Pressure	Test Section - Downstream
TTMFM1	Temperature	Venturi Nozzle - Upstream
TTNOZ,1-2	Temperature	Venturi Nozzle
TTC0	Temperature	Coolant Tank Exit
TTC1	Temperature	Coolant System Manifold
TTC2B	Temperature	Coolant System - Blades
TTCBV	Temperature	Coolant System - NGVs
TTCBC	Temperature	Coolant System - Tip Casing
TTCCV	Temperature	Coolant System - NGVs
TTCCC	Temperature	Coolant System - Tip Casing

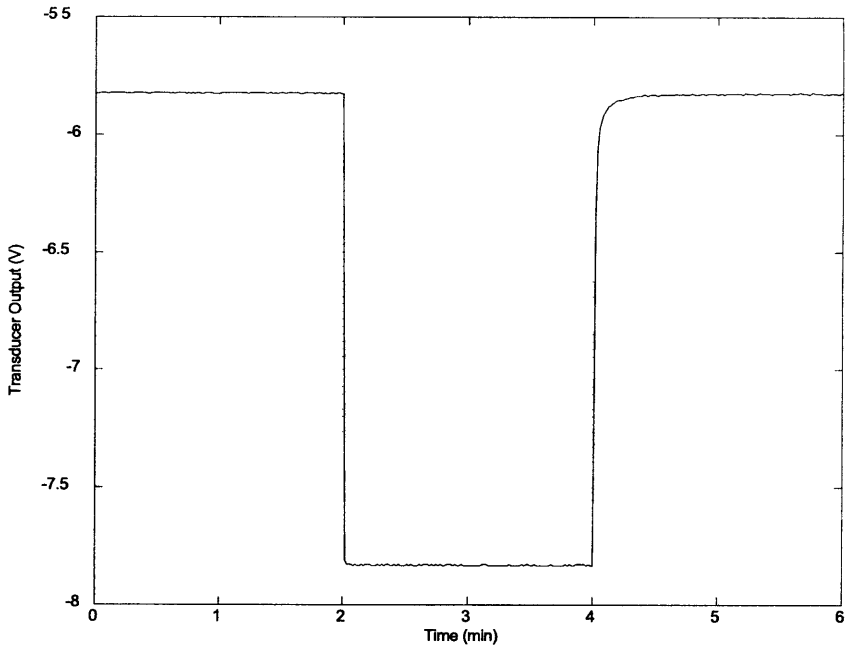

Figure 2-9: Typical differential pressure transducer calibration trace.

1. All transducers are provided a vacuum back-pressure reference by an external vacuum pump. For a post-fill calibration this produces a zero pressure differential across the transducers which are located inside the tunnel. For those in the supply or coolant tanks, a pressure differential equal to the initial tank pressure is recorded.

2. Data is taken at this condition for approximately two minutes as shown by the first segment of the trace in Figure 2-9.

3. After two minutes, the back-pressure reference is exposed to atmospheric pressure. Data is acquired for two minutes as shown in Figure 2-9.

4. After four minutes, the back-pressure reference is returned to vacuum where it remains for the experiment.

5. This procedure is repeated after the blowdown experiment has been completed.

These data provide a voltage change for each differential transducer which corresponds to the local atmospheric pressure. A transducer scale factor can then be computed. Transducer zeros are taken to be the average output prior to the opening of the main valve. The scale

and zero can then be used in the data reduction process via the linear calibration relation:

$$P = (Volts - Zero)\, Scale \tag{2.6}$$

2.6 Data Acquisition

The data acquisition system monitors all instrumented channels at a sampling rate sufficient for capturing time scales of interest during the experiment. For aerodynamic performance measurements, 5 kHz is adequate. The system typically acquires data for 2-4 seconds depending on the experimental conditions being monitored. The current hardware includes a Pentium II 450 MHz computer which is programmed with LabVIEW lab automation software.

2.7 Summary

This chapter reviewed the MIT Blowdown Turbine test facility. Facility configuration and individual components were described as well as typical test procedures. Analysis for scaling of all relevant non-dimensional parameters was presented. Instrumentation and data acquisition were then discussed.

Chapter 3

Film-Cooled Turbine Fabrication

3.1 Introduction

In a previous test series, an uncooled version of the ABB turbine was performance tested[8][10]. In order to quantify the losses due to coolant flow injection, a film cooled turbine was fabricated and tested. This turbine should have a similar overall geometry (blade and NGV shape) to the uncooled turbine, but with film-cooling injection holes and all other associated passages. In this chapter, the fabrication of this film-cooled turbine is described.

Due to monetary considerations and time restrictions, the existing uncooled turbine was converted to the film-cooled turbine. This was accomplished by the use of sophisticated machining techniques, such as electro-discharge machining (EDM) and laser machining. The uncooled turbine blade and NGV geometry can be seen in Figures 3-1 and 3-2.

Fabrication of the film-cooled turbine proved to be difficult, costly, and time consuming. The complex geometry of the holes and passages pushed existing manufacturing technologies to their limits. The cooling hole geometries and machining techniques will be reviewed here.

3.2 Film-Cooled Turbine Geometry

3.2.1 Film-Cooled Turbine Blade

The scaled ABB film-cooled turbine blade can be seen in Figure 3-3. The blade cooling configuration consists of five rows of coolant injection holes: two on the leading edge, one on the suction surface, one on the pressure surface, and one directly out of the trailing edge.

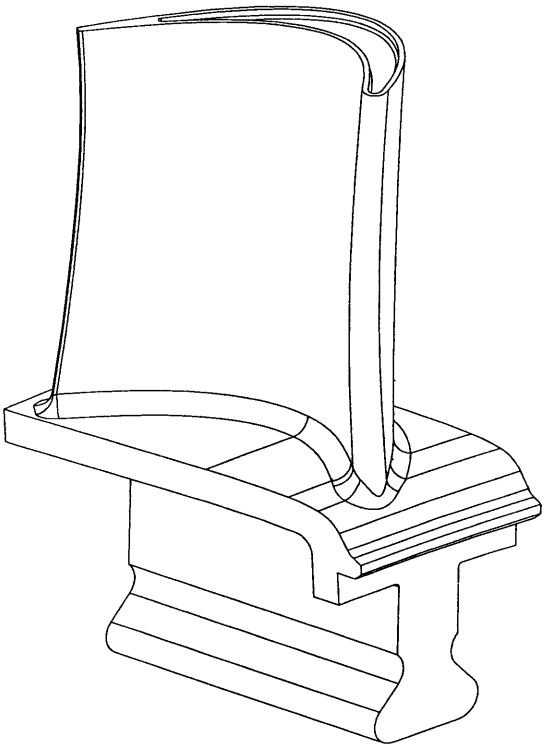

Figure 3-1: ABB uncooled turbine blade.

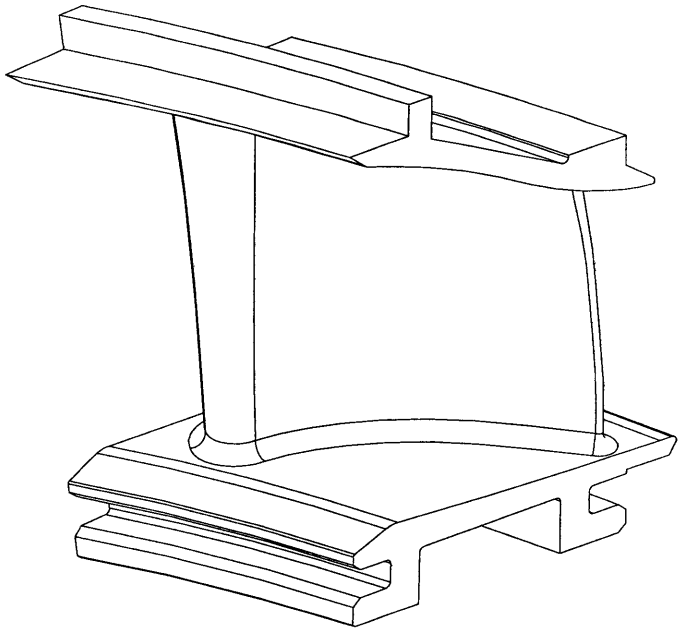

Figure 3-2: ABB uncooled turbine NGV.

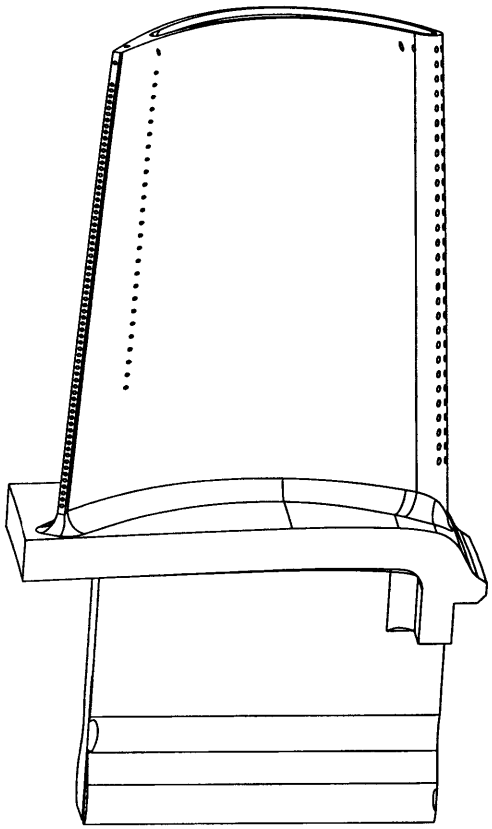

Figure 3-3: ABB cooled turbine blade.

There are also "dust-holes" which are not part of any of the distinguishable rows. Each hole is also oriented at a compound angle. The numbers and sizes of the holes are summarized in Table 3.1. Some details are omitted due to their proprietary nature.

The internal passages of the actual ABB turbine have not been replicated. The purpose of this work is to study the effects of film-coolant injection; therefore, only simple manifold channels through the blade are needed. Two channels will be used to feed the blade cooling holes; one for the leading edge and suction surface rows, and one for the pressure surface

Table 3.1: Blade cooling holes.

Row	Number of Holes	Diameter	Location
1	17	0.008"	suction surface
2	29	0.008"	leading edge
3	29	0.008"	leading edge
4	26	0.008"	suction surface
5	69	0.008"	trailing edge

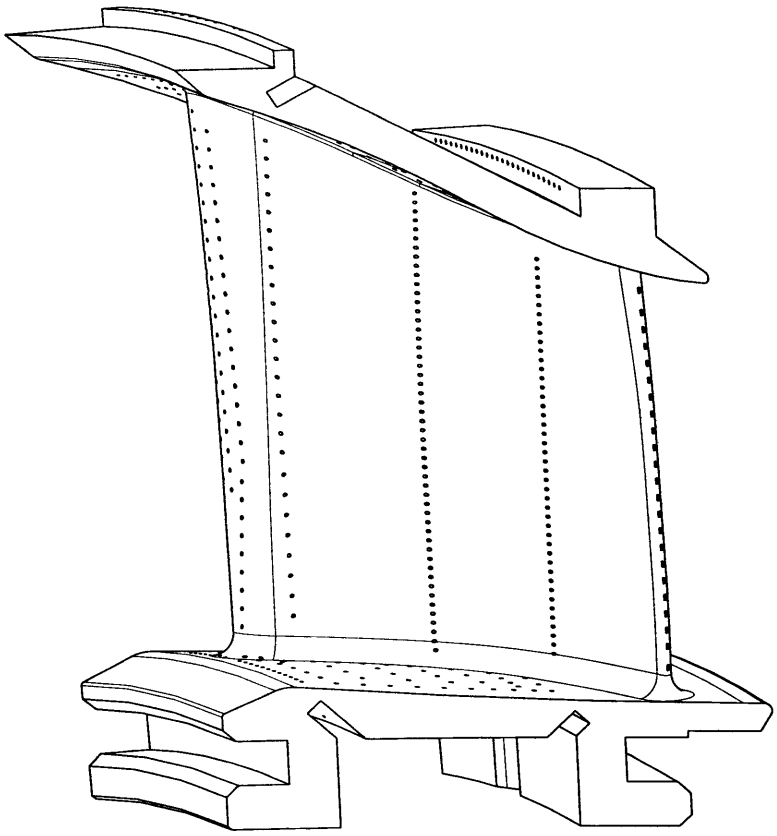

Figure 3-4: ABB cooled turbine NGV.

and trailing edge rows. These passages should provide a relatively constant wall thickness.

3.2.2 Film-Cooled Turbine Nozzle Guide Vane

The scaled ABB film-cooled nozzle guide vane can be seen in Figure 3-4. The NGV cooling configuration consists of 12 rows of coolant injection holes on the airfoil surface, as well as several holes on the upper and lower platforms. Like the blade, each hole is oriented at a compound angle. Table 3.2 summarizes the important features of this layout. Again, some details are omitted for proprietary reasons.

Like the cooled turbine blade, the internal passages of the actual ABB NGV have not been replicated. Two vertical channels were required to feed all of the airfoil surface cooling holes. Coolant will be supplied to the platform holes via manifolds above and below the locations where the NGVs mate to the facility.

Table 3.2: NGV cooling holes.

Row/Group	Number of Holes	Diameter	Location
1	25	0.021"	trailing edge
2	44	0.008"	pressure surface
3	51	0.008"	pressure surface
4	26	0.008"	pressure surface
5	28	0.008"	leading edge
6	21	0.008"	leading edge
7	29	0.008"	leading edge
8	19	0.008"	leading edge
9	45	0.008"	leading edge
10	42	0.008"	leading edge
11	40	0.008"	leading edge
12	22	0.008"	leading edge
A	107	0.008"	upper platform
B	91	0.008"	lower platform

3.2.3 Film-Cooled Turbine Tip Casing

The rotor tip casing (the outer annulus wall surrounding the blade tips) also requires film cooling holes. The actual ABB geometry could not be directly scaled and accommodated in the MIT Blowdown Turbine facility. As a result, a geometry which provided the same coolant flow, but could be fabricated for use in the Blowdown Turbine, was devised. This configuration consists of two rows of film cooling holes located at the leading and trailing edges of the tip casing ring. There are 1544 leading edge holes with a 0.012" diameter and 1200 trailing edge holes with a 0.015" diameter.

3.3 Electro-Discharge Machining

3.3.1 Introduction

Electro-discharge machining (EDM) is a process by which an electrode, usually made of a copper-tungsten alloy, is used to "burn" a detail into a metal piece. The piece which is to be machined is submerged in a water and oil solution while the energized electrode cuts the metal. This is required to keep the part cool and to flush away debris as it is burned away. Different types of metals respond differently to the EDM process and various burn rates can

be achieved. The power used for burning a piece is set based on the type of material being cut, the desired rate of burn, and the desired finish. The quality of the finish is determined by the amount of "over-burn" provided by the electrode. The electrode does not actually come into contact with the part and does not apply any load. It is the field created by the electrode that actually burns the metal. The power of this field, or over-burn, can be adjusted to improve the finish of the cut. Over-burns of 0.002-0.020" are common.

There are two types of EDM processes; wire EDM and plunge, or vertical, EDM. Wire EDM is the simplest and fastest process. The electrode consists of a wire which passes through the material in the same fashion as conventional band saw. The disadvantage of this method is the physical constraint of the wire itself. This limits the work to two-dimensional details that pass through the entire part.

Plunge EDM is a slower and more complicated process, but can produce a more complex detail. The electrode is actually machined to the shape of the desired cut and then plunged vertically into the material. The detail of the cut is limited only by the ability to machine the electrode. Plunge EDM has a slower burn rate than a wire cut simply because there is significantly more material being removed at one time. Another difficulty with the vertical EDM process is the ability to remove debris as it burns away. With a wire cut there is a hole passing through the entire part allowing EDM fluid to flow through and remove debris. This is not always the case with plunge EDM causing it to be a slower process. If debris is not properly removed, the particles can become charged and cause additional burning.

Both the plunge and wire EDM processes were used to manufacture the cooling manifold passages in the blades and NGVs. All EDM work was performed on two-axis Computer Numerical Control (CNC) machines by Johnson Precision Inc.

3.3.2 Blade Manifold Channels

The blade cooling manifold channels proved to be challenging to fabricate. Figure 3-5 shows a cross section of these passages. The forward manifold was cut using plunge EDM while the rear was a wire cut.

The forward passage required two vertical EDM plunges; one cut at an angle from the

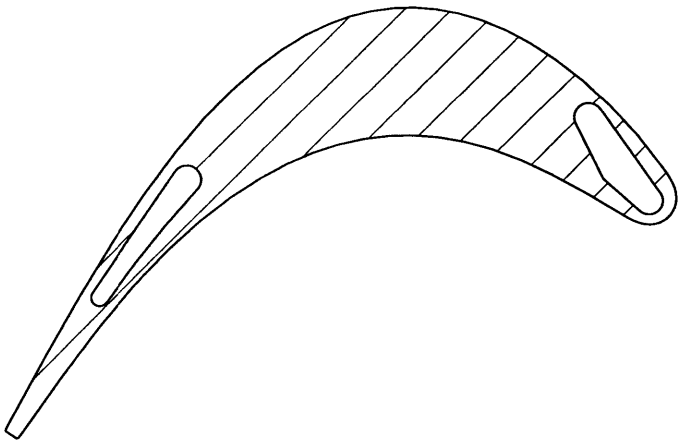

Figure 3-5: Blade cooling manifold passages.

top of the part and another from the bottom. This was done to follow the contour of the leading edge which can be seen in Figure 3-1. An approximately constant wall thickness of 0.050" was maintained. However, this process required a high degree of accuracy so that the two plunges would mate correctly inside the blade. To achieve this, a complex fixture was designed to hold each blade in the identical position. The fixture and blade can be seen in Figure 3-6.

The rear channel was produced with a simple wire cut directly through the blade. A vertical plunge was not possible for this channel due to the slender geometry. An electrode with this geometry would actually burn itself away before passing through the part. The tolerances of this channel also required a high degree of precision, therefore the same fixture was used.

The blade material also caused a problem with the EDM process. The parts were originally fabricated out of an aluminum casting alloy; AL-2618. This particular alloy contained sporadic impurities, or inclusions. When the electrode encountered these inclusions, the impurity would burn away creating a hole through the piece. As a result, several blades were destroyed in the EDM process.

3.3.3 Nozzle Guide Vane Manifold Channels

The NGV manifold passages were not as difficult to machine as the blade. A cross-section of these passages is shown in Figure 3-7. The relative ease of machining these details was a result of using only the wire EDM process. Again, precision cuts were required to maintain

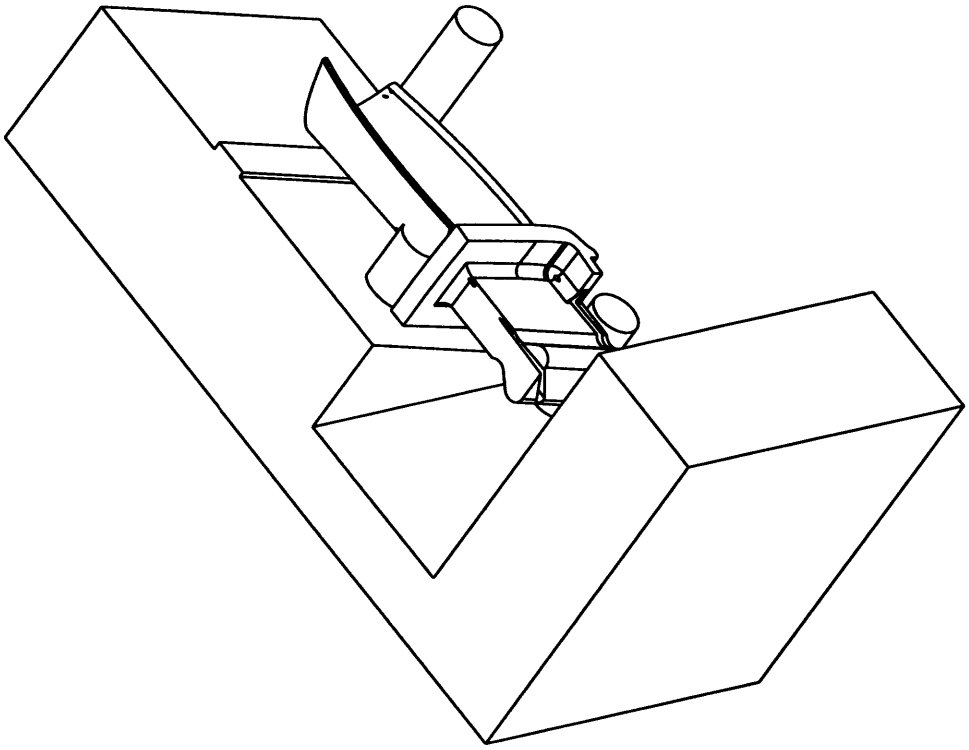

Figure 3-6: Blade fixture for EDM.

a relatively constant wall thickness and a custom designed fixture was required. This is shown in Figure 3-8.

3.4 Laser Drilling

3.4.1 Introduction

Laser drilling was chosen to fabricate the film cooling holes due to its speed, precision, and ability to drill extremely small, deep holes. No other method was found to fabricate the 1/4 scale (0.008" diameter) ABB cooling holes. However, even the laser was not capable of drilling some of the holes in the scaled geometry. This was due to their large length-to-diameter ratios (L/D) and shallow angles. The laser was able to handle an L/D up to approximately 15. The limitations of the laser and contingency procedures for difficult holes will be discussed in later sections. The machines used for this work were of the 5-axis CNC type and all work was performed by Laser Services Inc.

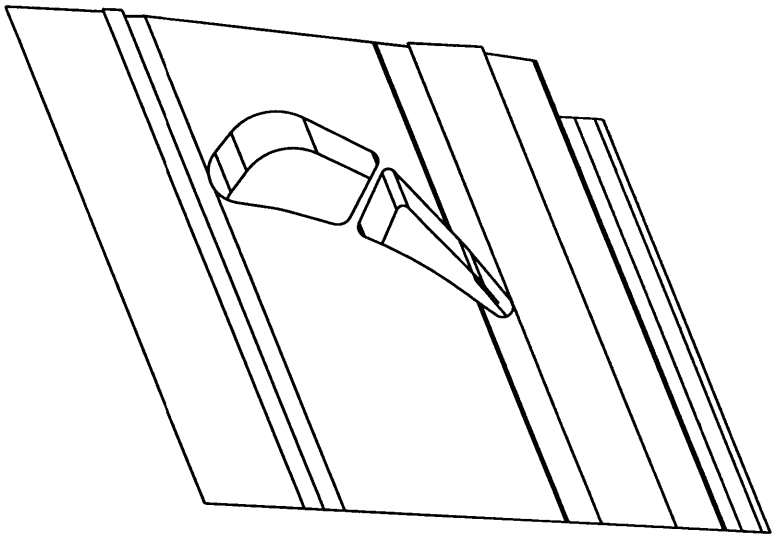

Figure 3-7: NGV cooling manifold passages.

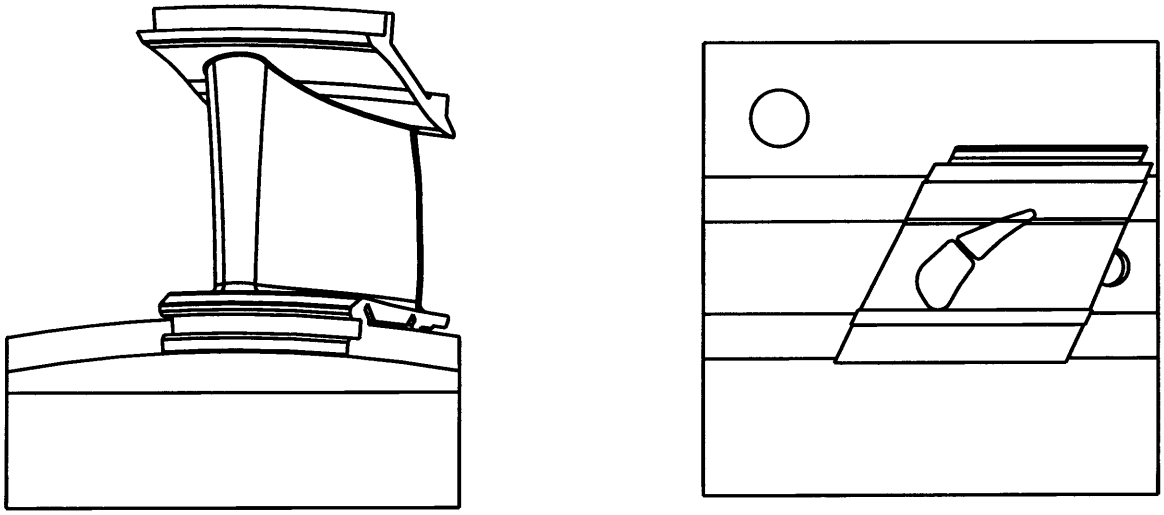

Figure 3-8: NGV fixture for EDM.

Laser drilling consists of using a high power, finely focused, beam of light to cut holes in various materials. There are several types of lasers used for cutting and drilling material. For this application a YAg (Yttrium-Silver) laser was used. There are several parameters which can affect the size, shape, and depth of the holes being drilled. These include:

1. Power: The power output (Watts) by the laser significantly affects the holes being drilled. The higher the power, the deeper and larger the hole.

2. Pulse: The laser is not run continuously, but instead is pulsed. The duration of each pulse and the number of pulses can be controlled to achieve the desired hole geometry. By pulsing the laser, the material is effectively "chipped" away. If the laser were to run continuously, the material would begin to melt.

3. Focus: By changing the focal point of the laser, the point of highest power density can be moved. Moving the focus can help to create a sharper, smaller hole.

4. Assist Gas: A nozzle flowing gas (oxygen for this application) onto the point were the laser is cutting is used as a kind of catalyst. The gas aids in the cutting of the material. By adjusting the type and flow rate of assist gas, a more precise cut can be made.

There are also several typical problems which are encountered when using a laser for small hole drilling. Some of these problems are:

1. Flare: The holes tend to be larger where the beam enters the material than where it exits. As the material is chipped away, its only path is back out through the initial opening.

2. Re-cast layer: As the molten material is chipped away from the part it tends to spray out onto the surface. It can re-adhere itself to the piece and even plug nearby holes. This re-cast layer must be removed. This problem varies with material. The harder the material, the less re-cast and the more clean the hole. The AL-2618 alloy used in this application was very soft and poor for laser drilling. The re-cast layer became a serious problem and its removal will be discussed.

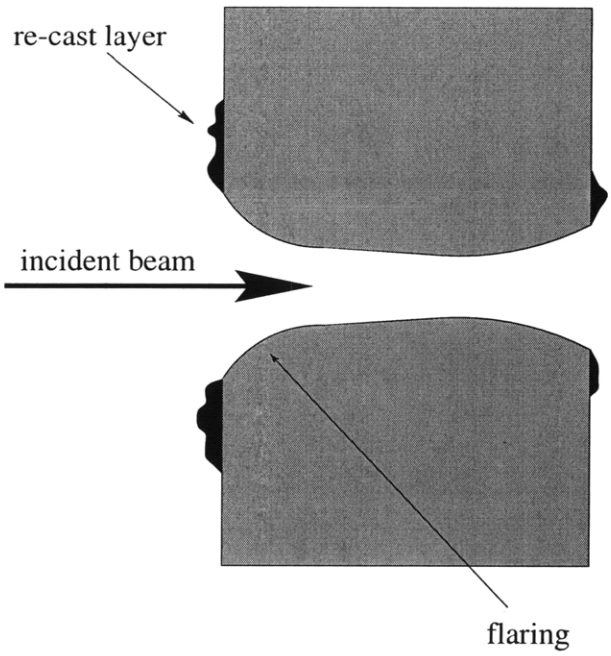

Figure 3-9: Typical laser drilled hole cross section.

3. Back-striking: This problem occurs when a high powered beam breaks through a part and strikes another region of the piece. This occurred when drilling holes into the cooling manifold channels. The beam would break through the first wall where it was intended and then proceed to strike the wall on the opposite side of the channel.

4. Bouncing: If the incidence angle of the beam is to shallow, it will scratch the piece and bounce off without actually drilling a hole. For this application the smallest allowable angle between the beam and the material was approximately 40^o.

A cross section of a typical laser drilled hole is shown in Figure 3-9. The flare and re-cast layer can be seen. The severity of the flare and re-cast layer increased with increasing L/D and decreasing incident beam angle.

3.4.2 Blade Cooling Holes

The laser drilling of the blade film-cooling holes proved to be challenging. The hole geometry is shown in Figure 3-3. The two leading edge rows of holes were difficult to fabricate due to their compound angles and close spacing. Small, yet complex movements of the 5-axis

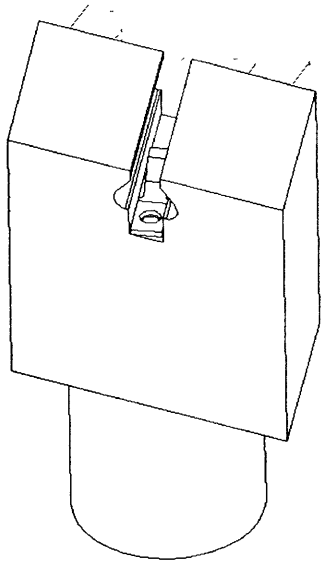

Figure 3-10: Blade fixture for laser drilling.

machinery were required to drill at these difficult angles. The close spacing of the holes caused problems with the re-cast layer. The debris from the drilling tended to fill nearby holes. This problem was overcome by a thorough cleaning post-process.

The suction surface row did not cause any difficulties due to the relatively large hole spacing and reasonable incidence angles. A back-striking problem was encountered when drilling the pressure surface holes. Due to the thin geometry of the rear manifold passage, the laser beam tended to cut through the entire blade rather than just the one desired wall. To overcome this, the inside of the channel was lined with copper tape which reflects the beam.

The trailing edge holes were not manufacturable. The design called for 69 holes with 0.008" diameter and a spacing of approximately 0.012" center-to-center. In addition to this, the L/D of these holes was on the order of 30. Due to these constraints, the trailing edge holes were eliminated from the design.

A new fixture was designed to provide better access to the blade for drilling. It can be seen in Figure 3-10.

3.4.3 Nozzle Guide Vane Cooling Holes

The laser machining of the NGV film cooling holes was more difficult than those drilled into the blade. The large number of holes and variety of compound angles made this an arduous task. Figure 3-4 shows the complexity of the geometry. Every possible problem described in the above sections was encountered when drilling the NGV cooling holes.

The leading edge holes were numerous and closely spaced. This led to the development of a significant re-cast layer which later had to be removed. Difficulties were encountered with the incidence angles of the suction surface and pressure surface holes. Many of the original angles were shallow enough to cause the beam to bounce off of the NGV without burning a hole. As a result, these angles were simply changed to the smallest allowable angle for a quality hole. Back-striking was also common but overcome with the use of copper lining.

Like the blade, the trailing edge holes proved to be the most difficult. These holes required an L/D of approximately 25 which was not possible with the YAg laser technology. However, these holes could not be eliminated as on the blade trailing edge. They accounted for a substantial portion of the total NGV cooling flow and without them, the part could not be considered a reasonable scaled model of the ABB NGV. As a result, the holes were scaled up to 0.028" and reduced in number to 15. This allowed for the same coolant flow but was more manufacturable. With this change, the trailing edge holes were conventionally drilled.

The upper and lower platform holes called for both difficult angles and large L/D ratios. Angles which caused the beam to bounce off of the surface were altered to eliminate this problem. To reduce L/D ratios, the non-flow sides of the platforms were machined to reduce the thickness of the material. In addition to this, channels were cut in certain locations to aid in this same fashion. Figure 3-11 shows these modifications.

3.4.4 Tip Casing Cooling Holes

The tip casing cooling holes were not as difficult to fabricate. The tip casing ring was fixed so that the laser head lay on its interior. The ring was then rotated to drill two rows of cooling holes. A significant re-cast layer developed and was later removed by cleaning procedures which will be described in the next section.

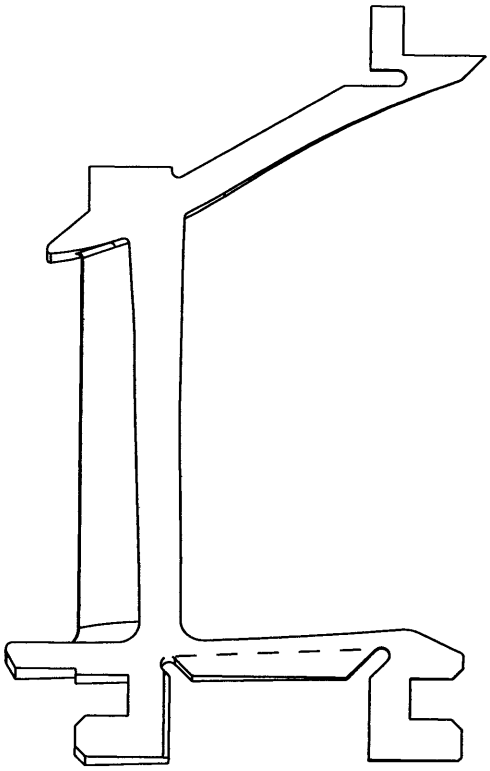

Figure 3-11: NGV platform modifications for laser drilling.

3.4.5 Cleaning Procedures

The laser drilled cooling holes required a substantial amount of cleaning. A significant re-cast layer developed on many of the parts and there were deposits of debris within the holes themselves. Ultrasonic cleaning was used to remove all loose debris within the holes or on the surface of the parts. This consists of submerging the blades and NGVs in ultrasonic cleaning fluid (a type of oil) which is inside the cleaning mechanism itself. A high frequency sound wave propagates through the fluid causing any loose particles to be flushed away. After this procedure was completed, the holes were cleaned by hand with 0.006" wire.

These procedures adequately cleaned the blades, however, a re-cast layer still remained on the NGVs. These parts were then cleaned with an aluminum oxide blasting process. Small aluminum oxide particles were mixed with water and sprayed over the NGVs. This was successful in removing the remaining re-cast layer without causing a significant change in the surface finish of the part.

3.5 Laser Welding

The blade manifold channels pass through the entire part and must be capped off on the blade's free end. The process of laser welding was selected to perform this task. Laser welding utilizes a beam similar to that used in the drilling and cutting processes. However, the beam melts the metal and is capable of welding two pieces together rather than cutting the material.

Small aluminum end-caps were cut to the approximate cross sectional shape of the blade cooling passages. These pieces were then placed over the ends of the passages and laser welded to the blade. After some trial-and-error, the process worked well and all of the blades were fitted with laser welded end-caps.

To ensure that these end-caps could withstand the stresses induced by rotation and the pressure forces of the coolant, a simple experiment was performed. Sample pieces were welded and then pressurized to 450 psi to simulate operational loads. All of the samples remained intact under these conditions.

3.6 Summary

This chapter has presented the film-cooled turbine geometry and its fabrication. The conversion from the uncooled turbine was explained and the machining techniques used were reviewed. The advantages and problems associated with electro-discharge machining and laser drilling were discussed. Modifications to the scaled turbine design due to machining limitations were presented. Finally, the laser welding process was briefly described.

Chapter 4

Film-Cooling Hole Discharge Coefficient Calibration

4.1 Introduction

Discharge coefficient, C_d, can be defined as the ratio of the true and theoretical flow rate for an orifice or passage. In symbolic form:

$$C_d = \frac{\dot{m}_{true}}{\dot{m}_{theoretical}} \tag{4.1}$$

For a thick, square edged, smooth walled orifice, C_d is on the order of 0.85. This indicates that the orifice passes 85% of the ideal through flow. The losses are a result of separation at the leading edge which leads to a vena-contracta inside the channel. A schematic of this is shown in Figure 4-1. There is an effective orifice area which is a function of C_d and geometric area:

$$A_{effective} = C_d A_{geometric} \tag{4.2}$$

Discharge coefficient can also be considered a non-dimensional effective area of holes of various geometry and quality.

This is an important parameter for turbine film-cooling holes. It helps to quantify the quality and repeatability of the holes. In addition to this, knowledge of the C_d is required to determine the actual mass flow passed through the cooling holes and is critical for any modeling or CFD efforts.

In the case of the ABB turbine, a calibration of the film-cooling hole discharge coefficients

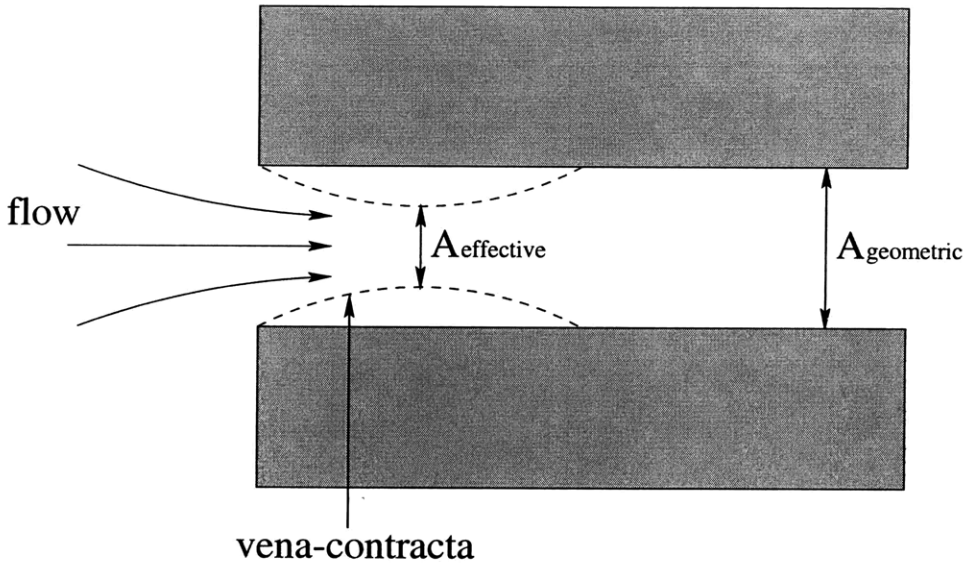

Figure 4-1: Losses in an orifice.

is necessary for all of the afore mentioned reasons. As described in Chapter 3, the cross sectional geometry of the laser drilled holes is not well known; nor is there any reason to believe that they are smooth. A measure of the discharge coefficient of these holes will give an indication of the quality and repeatability of the laser drilling process. An estimate of the C_d is also necessary because a subsequent modeling effort is planned. However, calibrating every hole is not practical. Therefore, two calibrations were performed: a global calibration of the entire blade or NGV, and a discrete row calibration of every row of holes on a blade or NGV. A summary of turbine cooling hole discharge coefficient literature can be found in reference [11].

4.2 Reynolds Number Effects

There can be significant Reynolds Number effects involved in calculating film-cooling hole discharge coefficients. Andrews and Mkpadi[12] have shown, for orifices with L/D ratios of 2-10, there is a significant change in C_d with Reynolds Number. For Reynolds Numbers less than 10^4 these effects are most noticeable. However, for higher values, on the order of 10^5 and larger, C_d is relatively constant. Osnaghi, Perdichizzi, Savini, Harasgama, and Lutum[13] measured the discharge coefficients of the film cooling holes in a model turbine NGV. It was shown that C_d tends to rise with Mach Number. There was no data presented

on the effect of Reynolds Number.

With knowledge of the static pressure distribution along the ABB blade and NGV airfoils, the approximate Reynolds Number for each row of cooling holes can be obtained. The static pressure distributions were generated by a CFD code. With this information, the pressure differential across the holes and the hole exit velocities could be calculated. Combining this with knowledge of the gas properties and hole diameter, Reynolds Number can then be computed. Estimates for the flow through the ABB cooling holes showed that Reynolds Number varied between 10^4 and 10^6. Although these Reynolds Numbers are large, it could not be concluded that the effects are negligible. Therefore, any device which was designed to measure cooling hole C_d should be capable of simulating a range of Reynolds Numbers.

4.3 Calibration Apparatus

A schematic of the calibration apparatus can be seen in Figure 4-2. The device consists of the following:

1. A compressed CO_2 cylinder for providing the test gas.
2. A heat exchanger to warm the expanding CO_2 to a known temperature.
3. A series of rotameter flow tubes for measuring volume flow rate.
4. A pressure gauge for measuring inlet pressure.
5. A high pressure test chamber.
6. A fixture to hold and seal the blade or NGV.
7. A pressure gauge for measuring the pressure in the test chamber.

This device was intended to provide the ability to vary hole Mach Number and Reynolds Number. By removing the dome of the test chamber and exposing the holes to atmospheric back-pressure, Mach Number effects could be easily explored. By varying the inlet pressure, the hole Mach Number can be changed. In this simpler configuration, performing a global calibration of the blades and NGVs would be trivial. A single inlet pressure could be applied

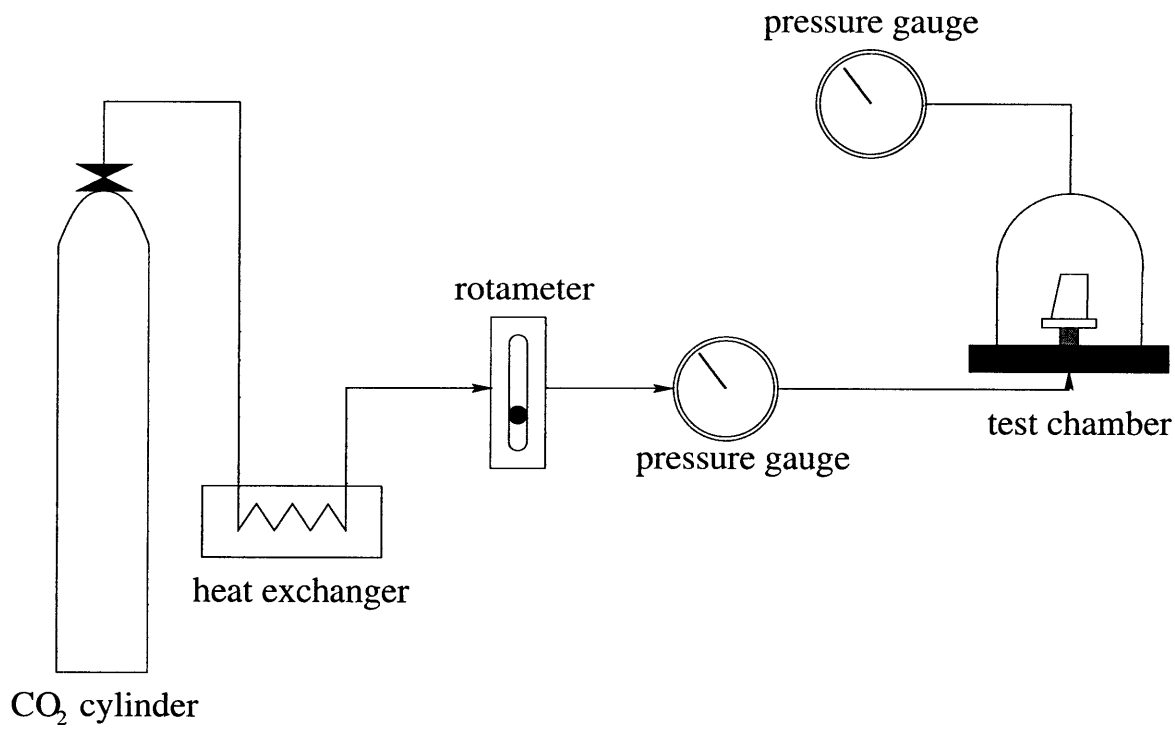

Figure 4-2: Schematic of discharge coefficient calibration apparatus.

to all of the blades or NGVs individually. An overall C_d could be measured and part-to-part consistency quantified. By varying both the inlet pressure and the chamber back-pressure, density, viscosity, and exit velocity could be matched; thus Reynolds Number could be simulated.

4.4 Discharge Coefficient Calibrations

4.4.1 Theory and Procedures

To obtain the discharge coefficients of the film-cooling holes, the actual mass flow passed through the holes must be ratioed with the calculated ideal mass flow as shown in Equation 4.1. The actual mass flow rate is measured with the previously described apparatus. The temperature of the CO_2 is set by the heat exchanger and the pressure is set by the bottle regulator. This is measured by the inlet pressure gauge. The volume flow rate in Standard Cubic Feet per Minute (SCFM) of air is measured by the rotameter flow tubes. This can

be converted to a volume flow rate of CO_2 by applying the relation

$$Q_{CO_2} = Q_{air}\sqrt{\frac{T_{CO_2}}{T_0} \cdot \frac{P_0}{P_{CO_2}} \cdot \frac{R_{CO_2}}{R_{air}}} \tag{4.3}$$

where P_0 and T_0 are temperature and pressure at standard conditions. The true mass flow rate can then be calculated from

$$\dot{m}_{true} = Q_{CO_2}\rho_{CO_2} \tag{4.4}$$

where ρ is density. This can be obtained from the ideal gas law

$$\rho = \frac{P}{RT} \tag{4.5}$$

The ideal mass flow rate can be calculated from the definition of corrected flow

$$W_c = \frac{\dot{m}_{ideal}\sqrt{RT}}{PA} \tag{4.6}$$

where A is an estimate of the cross sectional through flow area. All quantities in this relation are known except for ideal mass flow rate and corrected flow. Corrected flow can also be written as a function of Mach Number, M, and ratio of specific heat, γ:

$$W_c = \frac{M\sqrt{\gamma}}{\left[1 + \frac{\gamma-1}{2}M^2\right]^{\frac{\gamma+1}{2(\gamma-1)}}} \tag{4.7}$$

Mach Number can be calculated from the isentropic relation:

$$M = \sqrt{\left[\left(\frac{P}{P_0}\right)^{\frac{\gamma-1}{\gamma}} - 1\right]\frac{2}{\gamma-1}} \tag{4.8}$$

Thus, corrected flow can be obtained leaving ideal mass flow rate as the only unknown. This is then extracted from Equation 4.6 and discharge coefficient can be determined via Equation 4.1. However, the geometric area of the laser drilled holes is not well known. Therefore, only the effective area, C_dA can actually be computed.

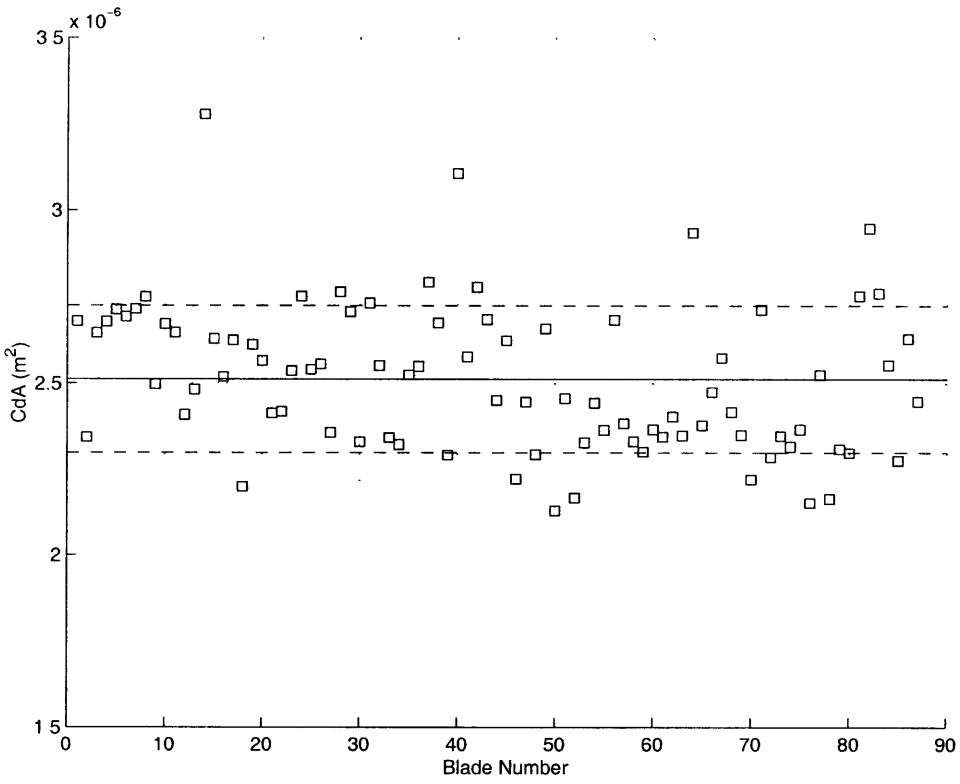

Figure 4-3: Turbine blade C_dA.

4.4.2 Global Blade Cooling Hole Effective Area

The overall C_dA for the scaled blades were measured. Each blade was pressurized while exposed to atmospheric back-pressure and volume flow rate was measured. True mass flow rate and effective area were calculated. Figure 4-3 shows a plot of blade number vs. measured C_dA. A total of 90 blades were tested and the average C_dA is indicated by the mean-line at 2.51×10^{-6} m^2. One standard deviation is shown by the dashed line and is $\pm0.212\times10^{-6}$. These data indicate that for most of the blades, overall C_dA is in the range of 2.3-2.7$\times10^{-6}$ m^2. This shows reasonable consistency in the manufacturing process. However, a small number of the parts exhibit either unusually large or small effective area. This would imply an imperfection in the part and these blades were eliminated from use in the blowdown experiment.

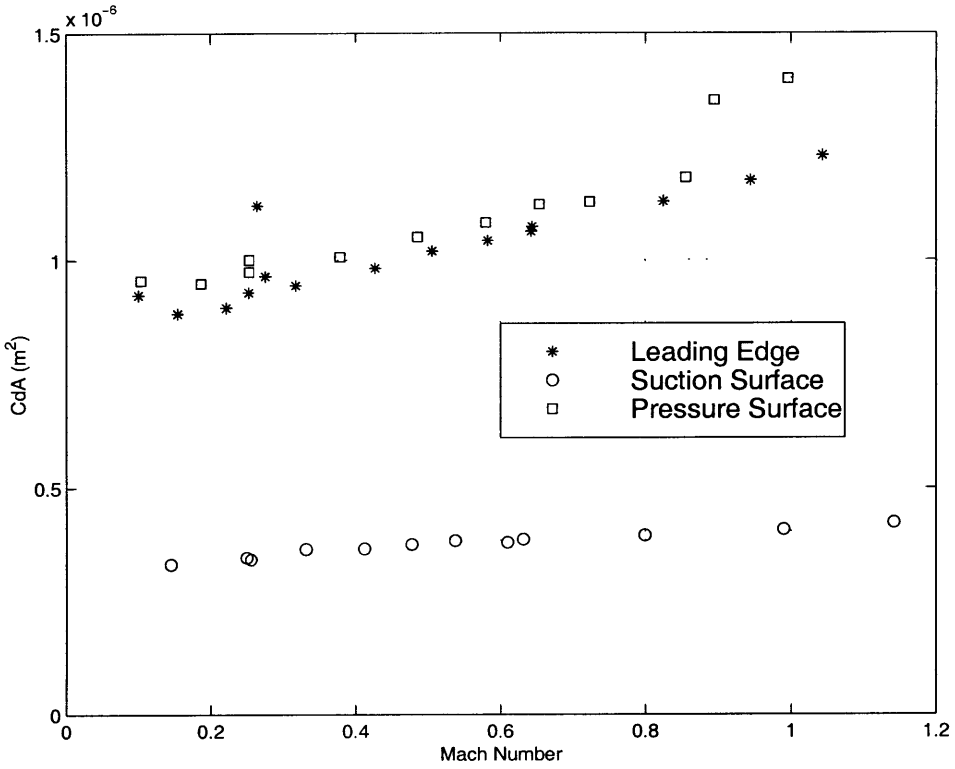

Figure 4-4: Discrete blade row C_dA.

4.4.3 Discrete Blade Row Effective Area

The individual rows of cooling holes on ten of the turbine blades were calibrated. Ten blades whose overall C_dA lay near the mean-line were selected. The characteristics (L/D, hole quality, angle, etc.) of each row differ significantly; therefore each must be calibrated individually. To accomplish this, all rows except for that being tested, were blocked with aluminum tape. The two leading edge rows were calibrated together due to their close spacing. The blade was exposed to atmospheric back-pressure and the inlet pressure was adjusted over a range of values. Figure 4-4 shows effective area vs. hole Mach Number for one of the blades. The C_dA tends to rise with Mach Number. This is the same trend which was observed by Osnaghi, Perdichizzi, Savini, Harasgama, and Lutum[13].

Figure 4-5 shows effective area for the leading edge row of ten blades. The same variation with Mach Number can be seen in all cases. However, a relatively large amount of scatter can be seen in these data. This indicates that the laser drilling process was actually not very consistent. Internal geometries and diameters of individual holes may vary significantly.

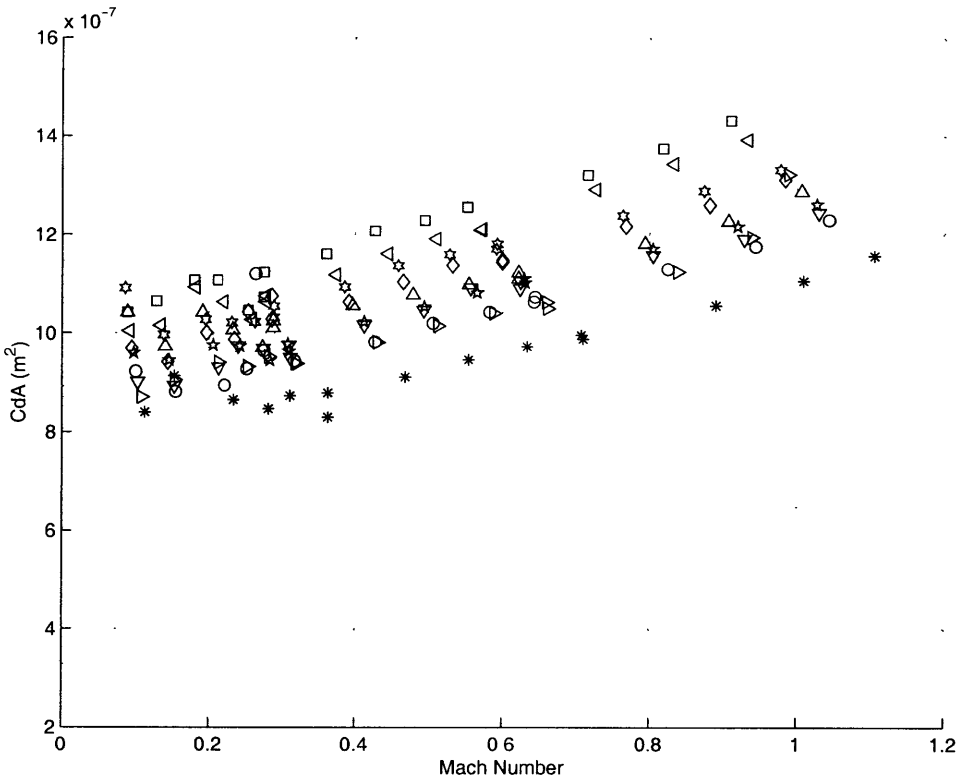

Figure 4-5: Leading edge row C_dA for ten blades.

Data for C_dA on 12 blades can be seen in Appendix A.

Reynolds Number effects were not explored due to practical limitations of the apparatus. Completely blocking off and sealing the holes was difficult and with the pressurized chamber in place, there is no means of ensuring that the part is well sealed. Similar complications were encountered when testing the NGV cooling holes. This is a limitation which can be overcome with some modifications to the facility.

4.5 Conclusions

The film cooling hole discharge coefficient calibrations have established blade-to-blade consistency. Any parts which showed significant deviation from the mean-line C_dA were removed from use in the experiment. The trend of increasing C_dA with Mach Number was also shown. Discrete row effective area for the turbine blades were obtained for use in later studies of the experimental data and for physics-based modeling.

4.6 Summary

This chapter has discussed the use of discharge coefficient as a measure of the quality and consistency of the laser drilled film cooling holes. An apparatus for measuring C_dA was constructed and presented. The theory and procedures involved were discussed. The overall effective area for the turbine blades were measured and the data showed blade-to-blade consistency. Discrete row C_dA was also measured and a variation due to Mach Number was shown. Limitations imposed by the apparatus prevented the testing of Reynolds Number effects.

Chapter 5
Coolant Flow Metering

5.1 Introduction

In a gas turbine engine, film-coolant flow is typically bled from the latter stages of the compressor and fed into the turbine. This involves feeding the coolant through a series of manifolds and into the blades, NGVs, and tip casing. The blades and NGVs also contain a set of serpentine passages for internal convective cooling which occurs prior to the coolant passing through the film-cooling holes. To simulate this coolant flow for aerodynamic performance testing, the coolant-to-mainstream mass flow ratio and momentum flux ratio must be matched.

5.2 Coolant Feed System

The coolant feed system was designed to impose a controlled and known coolant mass flow to the blades, NGVs, and tip casing independently. Figure 5-1 shows a schematic of the system.

The system operates in a blowdown mode similar to that of the main flow. The coolant supply tank is insulated and lined with a jacket through which liquid nitrogen and compressed air are passed to cool the stored gas to the desired temperature. The coolant tank is equipped with a fast-acting ball valve. After pressurizing the tank and actuating the valve, the coolant flows to a manifold and is split into three components: blade, NGV, and tip casing coolant. This manifold is shown in figure 5-1. The blade coolant is fed directly into the facility, while the NGV and tip casing coolants are again split. They are fed into

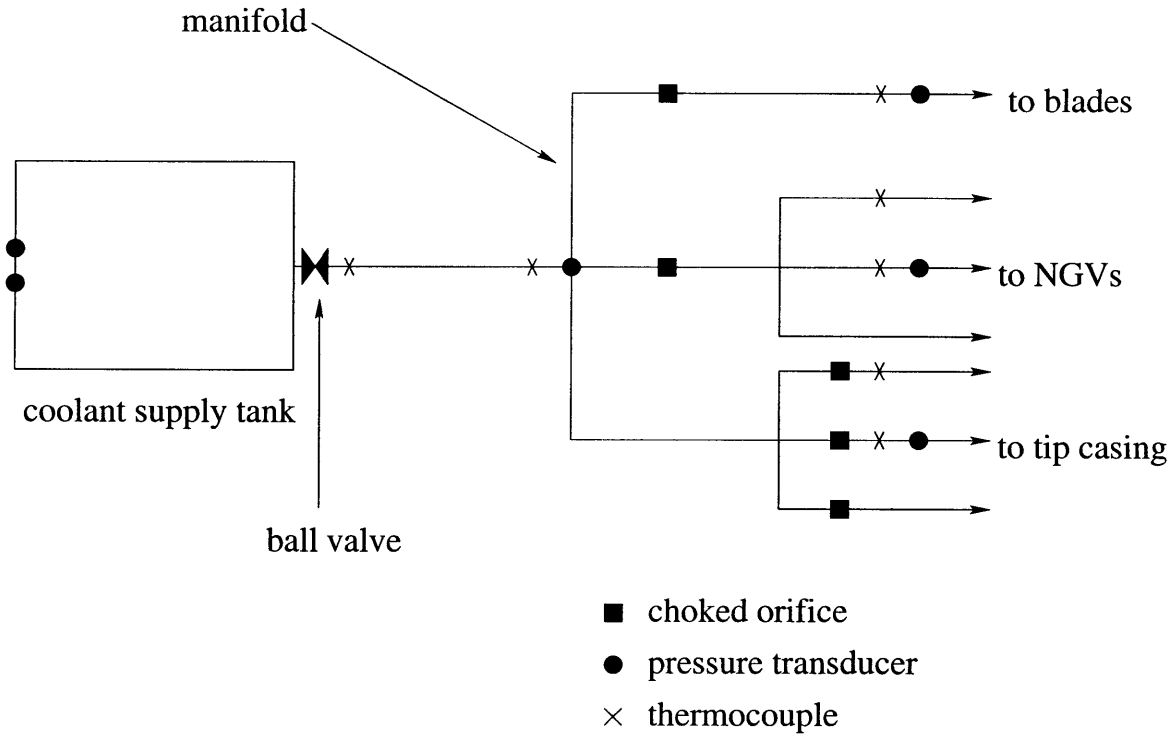

Figure 5-1: Coolant feed system schematic.

the facility in three locations to minimize losses.

The flow to each component is individually metered and controlled by thick walled, squared edged, choked orifices. This flow metering method is useful because it imposes a mass flow independent of downstream conditions. An L/D ratio of 1-6 was used for these orifices because at these values, the discharge coefficient is well known[14]. The locations of these devices are shown in the schematic. A single orifice was used to meter the blade and NGV flows. The casing flow was metered by three orifices near the locations where the coolant enters the facility. The casing flow rate is relatively small and had it been metered farther upstream with a single orifice, the time constant associated with this flow would not match the rest of the facility. The tip casing flow would not coincide with the blade, NGV, and main flows.

The blowdown of the coolant must also be timed correctly. The coolant flow must be ejected out of the turbine during the test window imposed by the main flow. To accomplish this, the flow time constant of the coolant system was compared to that of the primary facility. This time constant is a function of the system volume-to-choked area ratio and its derivation can be found in reference [4]. By comparing time constants and running verification tests,

it was found that opening the coolant ball valve and main valve simultaneously caused the two blowdowns to coincide.

The system is instrumented to measure the pressure and temperature upstream of the orifices. A Kulite differential pressure transducer is located in the coolant supply tank along with a 300 psig Sensotec Super TJE high accuracy transducer for calibration. A 0.003" thermocouple is mounted just downstream of the ball valve. In the manifold section, a 300 psig pressure transducer and another thermocouple, measure the pressure and temperature. There are also several 100 psig transducers and temperature sensors located downstream of the orifices.

The test gas selected for the coolant was CO_2. This was done primarily to keep a constant gas composition through the downstream critical flow venturi nozzle. However, the conditions of the coolant CO_2 flow in the choked orifices of the cooling system pose a problem with the afore mentioned metering method. The temperature of the flow at sonic conditions can be below the saturation temperature of CO_2. This results in one of two phenomena: a portion of the CO_2 liquefies and a condensation shock forms, or the flow becomes metastable or supersturated. In either case, it is not clear that the correct mass flow is being fed to the turbine.

5.3 Critical Flow Metering

5.3.1 Calculation Procedure

To calculate mass flow rate from a critical(choked) flow metering device (nozzle or orifice), the relation

$$\dot{m} = AC_dC_R\frac{P_0}{\sqrt{RT_0}} \tag{5.1}$$

is used. A is the throat area, C_d the discharge coefficient, C_R the critical flow coefficient, R the gas constant, and P_0 and T_0 are stagnation pressure and temperature respectively. The discharge coefficient is a weak function of Reynolds Number.

5.3.2 Critical Flow Coefficient

An important quantity in this calculation procedure is the critical flow coefficient, C_R. Critical flow coefficient can be defined as the normalized sonic mass flux for inviscid, one dimensional, steady, isentropic flow and is also referred to as corrected flow. It can be written as

$$C_R = (\rho^* u^* / P_0)\sqrt{RT_0} \tag{5.2}$$

where ρ^* and u* are the density and velocity at sonic conditions. For a perfect gas at choked conditions, this is a function of γ only.

$$C_{R,ideal} = \left[\gamma \left(\frac{2}{\gamma+1}\right)^{\frac{\gamma+1}{\gamma-1}}\right]^{1/2} \tag{5.3}$$

In the case of the coolant system, the gas is non-ideal. Real gas effects must be accounted for and the speed of sound is no longer equal to $\sqrt{\gamma RT}$. To determine the sonic flow state, the following equations must be satisfied.

$$h_0 - h^* = \frac{(u^*)^2}{2} \tag{5.4}$$

$$M = \frac{u^*}{a} = 1 \tag{5.5}$$

$$s_0 = s^* \tag{5.6}$$

Equation 5.4 is conservation of energy and it relates the stagnation and sonic enthalpy to the sonic velocity. Equation 5.5 satisfies the criteria that for critical flow the local maximum velocity must equal the local sonic velocity and equation 5.6 satisfies the isentropic condition of constant entropy.

An iterative procedure for calculating this sonic condition is outlined in reference [15].

1. Calculate the stagnation quantities P_0, T_0, ρ_0, h_0, and s_0.

2. Estimate the sonic flow state (ρ^*, T*) using any reasonable approximation such as

$$\frac{T^*}{T_0} = \frac{2}{\gamma + 1} \tag{5.7}$$

$$\frac{\rho^*}{\rho_0} = \left(\frac{T^*}{T_0}\right)^{\frac{1}{(\gamma-1)}} \tag{5.8}$$

3. Compute s* and correct T* and ρ^* to satisfy equation 5.6.

4. Calculate the error in satisfying the energy equation 5.4 or the Mach Number constraint 5.5.

$$\epsilon = h_0 - h^* - \frac{(u^*)^2}{2} \tag{5.9}$$

$$\epsilon = M - 1 \tag{5.10}$$

   Correct T* and ρ^* based on this error.

5. Repeat the previous two steps until equations 5.4, 5.5, and 5.6 are satisfied.

Once this sonic state has converged, these condition are used in conjunction with equation 5.2 to obtain the critical flow coefficient. These coefficients are tabulated in many references[16].

However, this procedure is not applicable to metastable flows. The thermodynamic properties of the fluid are not known. For a typical gas flow, knowledge of the temperature and pressure is adequate for obtaining density, compressibility factor Z, viscosity, and other relevant quantities. These are tabulated or reside in a database[17]. For supersaturated conditions, these quantities are not readily available. This motivates the development of an experiment to measure the critical flow coefficients for metastable CO_2.

5.4 Coolant Flow Metering Experiment

5.4.1 Method

To measure the critical flow coefficients for supersaturated CO_2 the existing coolant tank could be used. If conditions in the tank were above the condensation point of CO_2 and the gas was exhausted through a nozzle through which it became metastable, it would be possible to obtain C_R. Mass flow rate can be expressed as

$$\dot{m} = -V\frac{\partial \rho}{\partial t} \tag{5.11}$$

where V is the volume of the tank. Time-resolved density can be obtained from a measurement of temperature and pressure combined with the real gas tables. Differentiating with respect to time would result in the $\partial\rho/\partial t$ term. If the tank volume is known, the mass flow rate can then be computed. This value can be used in conjunction with equation 5.1 to calculate the critical flow coefficient.

However, the volume is not accurately known and must be measured. To accomplish this, a similar blowdown procedure can be used. A test gas with a relatively constant C_R over a large range of conditions, such as argon, should be used. If it is exhausted through a nozzle at conditions far from its condensation point, equation 5.1 can be used to find $\dot{m}$ directly. Again, a temperature and pressure measurement would yield $\partial\rho/\partial t$. Tank volume can then be calculated from equation 5.11. The volume would then be used to calculate the unknown critical flow coefficients for metastable CO_2.

5.4.2 Experimental Configuration

A schematic of the experimental configuration can be seen in Figure 5-2. The gas in the coolant tank is exhausted through a toroidal throat critical flow venturi nozzle which was designed to conform to the specifications put forth in the ASME/ANSI standard[15]. This was done to ensure that a well known discharge coefficient could be used in the calculations. A cross section of this nozzle is shown in Figure 5-3.

The tank was instrumented with two pressure transducers. A fast time response, differen-

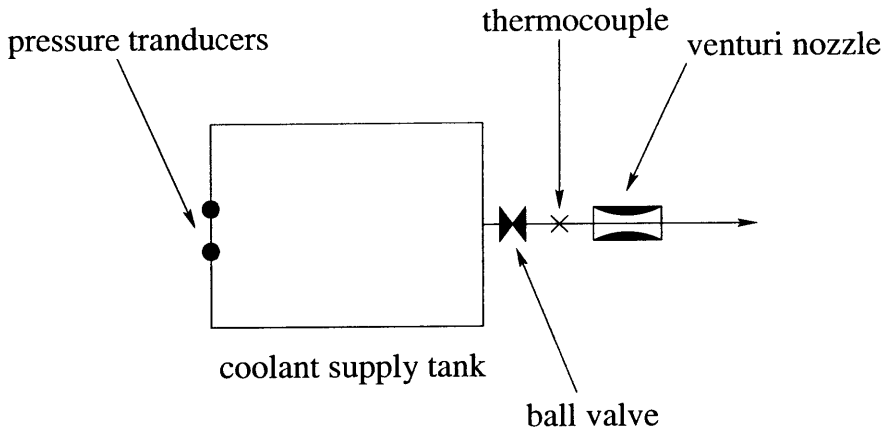

Figure 5-2: Schematic of coolant flow experimental configuration.

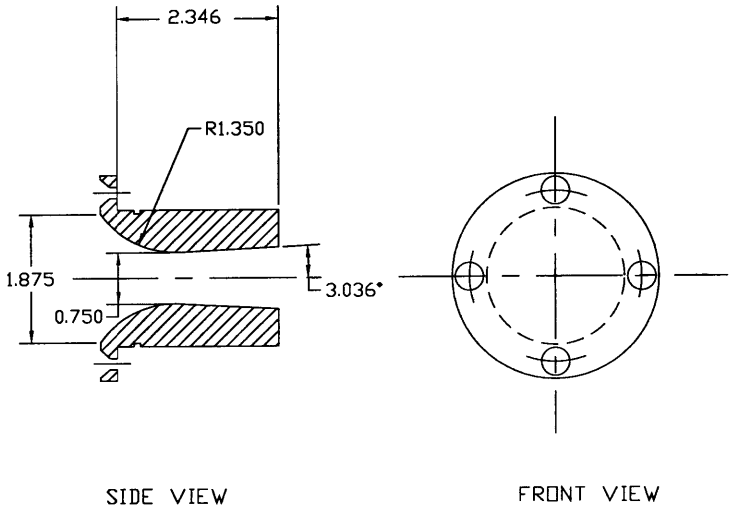

Figure 5-3: Toroidal throat critical flow venturi nozzle for coolant flow experiments. Dimensions in inches.

tial Kulite pressure transducer was used for time-resolved measurements. It was calibrated against a Sensotec Super TJE transducer with an accuracy of 0.1%. The calibration procedures were identical to those described in section 2.5.5. Just upstream of the nozzle, a temperature probe with a 0.003" junction was used to measure time-resolved temperature.

5.4.3 Test Matrix

Selecting the proper test points for the experiment is critical. The flow through the nozzle should reach the metastable condition while the gas in the tank is unsaturated. To aid in selecting test points, a control volume model of the experiment was utilized. The pressure and temperature of both the nozzle flow and the tank conditions were estimated and compared to the saturation line. Initial tank conditions for the CO_2 tests were selected so that the sonic flow was below the condensation limits while the tank conditions were not. Argon was used as the test gas for the volume measurement. Conditions for these tests were kept well outside of the condensation limits. Table 5.1 shows the test matrix which was selected.

Table 5.1: Test matrix for coolant flow experiments.

Test Number	Gas	$T_{initial}$(°F)	$P_{initial}$(psia)
001	Argon	90	50
002	Argon	90	150
003	Argon	90	250
004	CO_2	90	150
005	CO_2	90	250
006	CO_2	90	200
007	CO_2	50	250
008	CO_2	50	150
009	CO_2	30	250
010	CO_2	30	150
011	CO_2	15	250
012	CO_2	15	150
013	CO_2	5	250
014	CO_2	5	150

5.5 Results

5.5.1 Volume Calibration

Figures 5-4, 5-5, and 5-6 show pressure, temperature, and mass flow rate traces for test number 002. The initial conditions for this test were 90°F and 150 psia and the test gas was argon. Tank volume was calculated using the afore mentioned method. Table 5.2 summarizes the results of these calculations for the three argon experiments. The mean of these three values is 0.1121 ft^3 and they vary by 0.9%. This average value will be considered the actual tank volume to be used in the calculation of CO_2 critical flow coefficients.

Table 5.2: Summary of tank volume measurements.

Test Number	Volume (ft^3)
001	0.1115
002	0.1125
003	0.1123

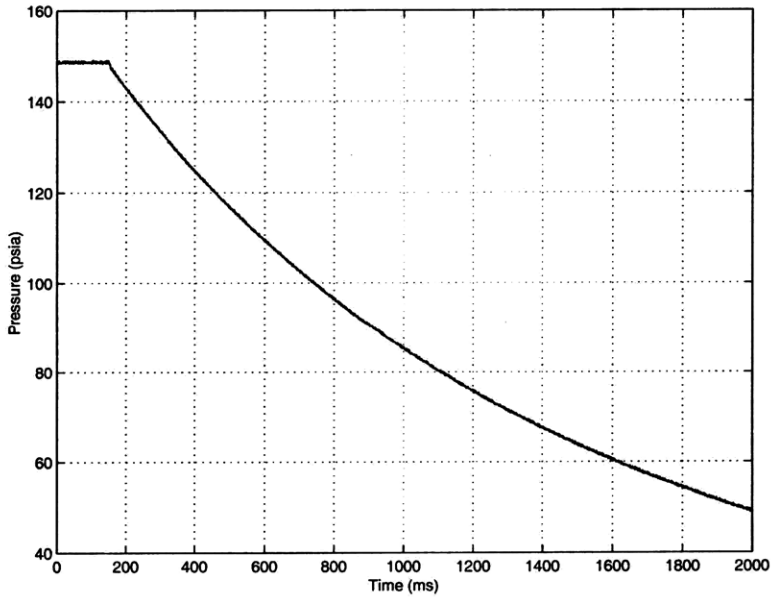

Figure 5-4: Coolant tank pressure for argon.

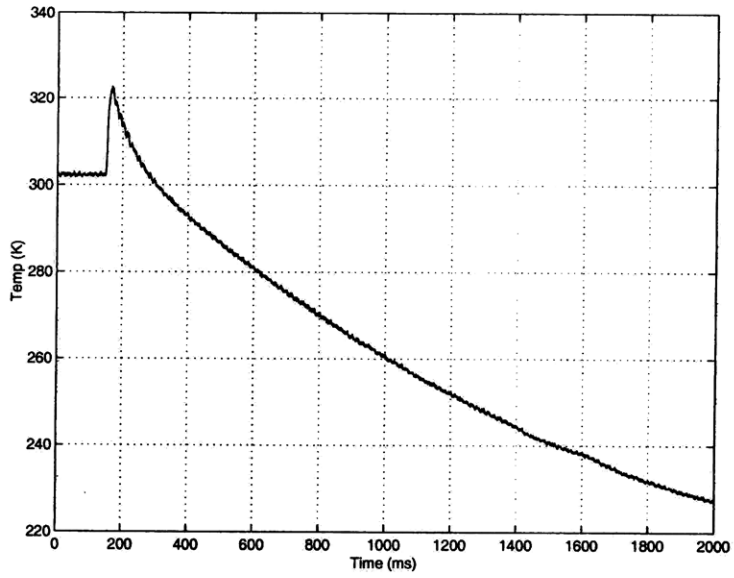

Figure 5-5: Coolant tank temperature for argon.

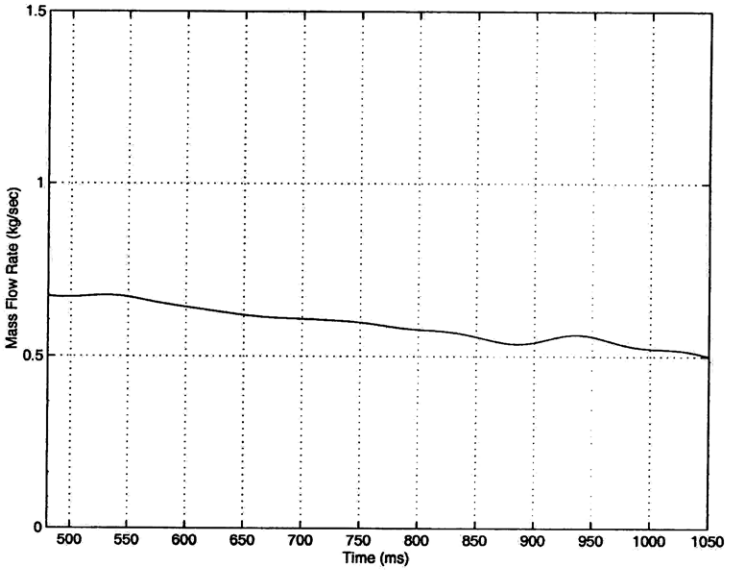

Figure 5-6: Argon mass flow rate.

5.5.2 Critical Flow Coefficients for Supersaturated CO_2

The pressure, temperature, and mass flow rate traces for the CO_2 tests are similar to those shown for argon. Figure 5-7 shows the measured CO_2 critical flow coefficient for conditions which are not in the supersaturated realm. The initial conditions were 250 psia and 90°F. The calculated value of 0.66 can be compared to the tabulated value of 0.685. There is a difference of 3.6%.

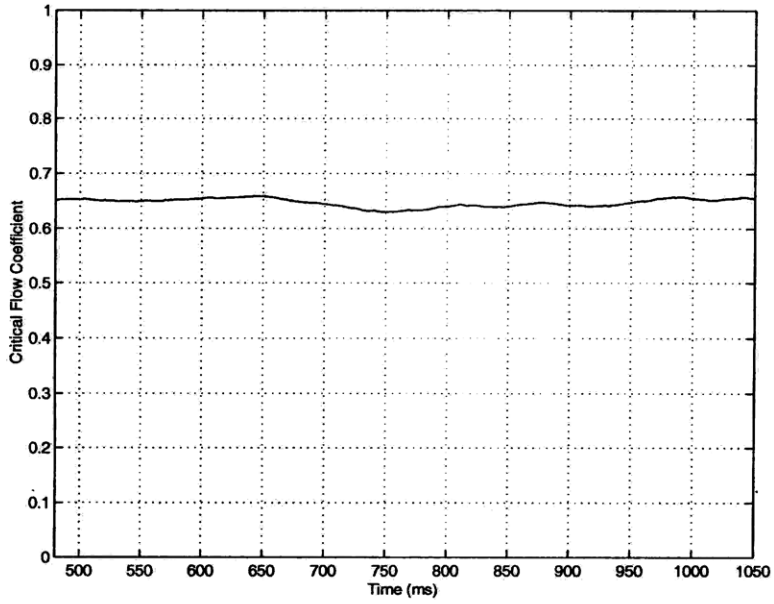

Figure 5-7: CO_2 Critical Flow Coefficient for unsaturated conditions.

This difference was typical for all coolant experiments with conditions which lay outside the supersaturated region. It can be reasonably assumed that this trend will continue for the critical flow calculations of the metastable CO_2. In several tests, the nozzle throat conditions lay outside the saturation line initially and dropped below this limit over the course of the test. There was no noticeable change in critical flow coefficient when this transition occurred.

Figure 5-8 shows C_R for test number 011 where the throat conditions fell well below the condensation limits of CO_2 during the blowdown. Initial conditions for this test were 250 psia and 15°F. The critical flow coefficient is approximately 0.66. There are no tabulated values of C_R for comparison. Data for the entire test matrix can be found in Appendix B.

5.6 Conclusions

The measured critical flow coefficients for supersaturated CO_2 lie in the same ranges as those for normal conditions. This indicates that critical flow orifices and nozzles can be used to meter metastable flows. In addition to this, the data did not indicate that any condensation shocks formed. It is believed that the flow transitions back to conventional conditions too rapidly for this to occur. The tests described above measured C_R for unsaturated conditions

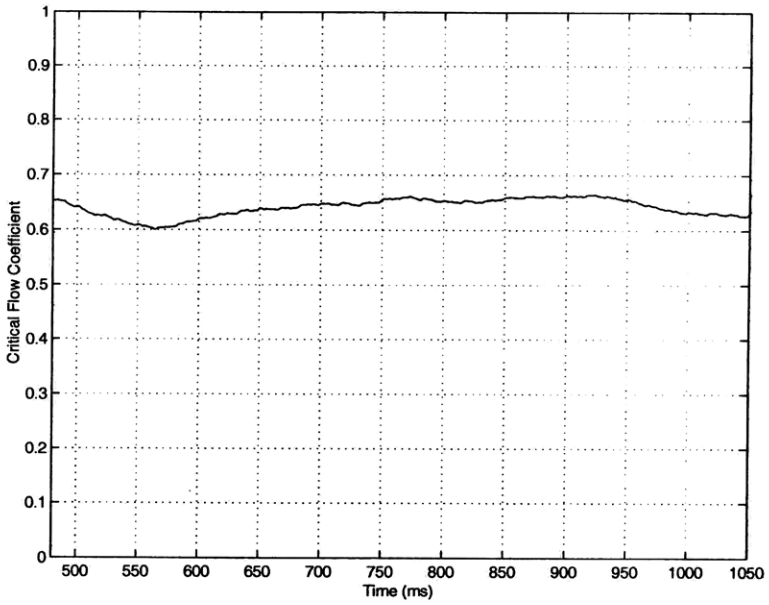

Figure 5-8: CO_2 Critical Flow Coefficient for supersaturated conditions.

to within 5% of the tabulated values. This same error can be expected in the measurements for the metastable flow regime.

5.7 Summary

This chapter presents the Blowdown Turbine coolant feed system. The problem of metering supersaturated CO_2 flow with a square edged, thick walled, choked orifice is discussed. Flow metering theory was reviewed and the critical flow coefficient was identified as the metric by which flow regimes could be compared. An experiment was devised to measure the C_R for various conditions. Critical flow coefficients for these metastable conditions compared well with those for unsaturated flows.

Chapter 6

Uncooled Turbine Performance Testing

6.1 Introduction

Prior to the cooled turbine testing, an uncooled turbine of identical blade and NGV geometry was tested in the Blowdown Turbine facility. This was done to provide a baseline for comparison to the cooled tests. This test series will be reviewed here.

The efficiency measurement method developed by Keogh[8] was used. This consists of using the eddy current brake torque meter to measure shaft torque and the downstream critical flow venturi nozzle to measure tunnel mass flow. The turbine operating design point was used as a baseline test and several off-design conditions were simulated. Variations in pressure ratio, corrected speed, and rotor tip clearance were studied. These tests were first analyzed by Jacobs[10] where a more complete discussion of these data is presented.

6.2 Efficiency Calculation

6.2.1 Mechanical Efficiency

Efficiency for a turbine can be defined as the actual power produced by the machine, normalized by the ideal power.

$$\eta = \frac{\mathcal{P}_{actual}}{\mathcal{P}_{ideal}} \tag{6.1}$$

The method of calculating efficiency which was utilized in these tests is referred to as the mechanical efficiency method because it requires a measurement of shaft torque. The real

gas model was used for calculating enthalpy drop across the turbine because the test gas, nominally CO_2, is non-ideal. Turbine mechanical efficiency can then be defined as

$$\eta_{mech} = \frac{\mathcal{T} \cdot \omega}{\dot{m}(h(P_1, T_1) - h(P_2, T_2))} \tag{6.2}$$

where $\mathcal{T}$ is shaft torque, ω is speed, $\dot{m}$ is mass flow rate, and h is the upstream and downstream enthalpy as a function of temperature and pressure.

However, expression 6.2 does not account for the transient effects of the blowdown environment. Its assumptions include constant rotational speed, constant tunnel through flow, and no heat transfer. Corrections for these effects must be incorporated.

6.2.2 Transient Corrections

Power Correction

In equation 6.2 actual turbine power is expressed as the product of torque and speed, neglecting rotor acceleration. To correct for this transient effect, a second term must be added and actual turbine power becomes

$$\mathcal{P} = \mathcal{T} \cdot \omega + I \cdot \frac{d\omega}{dt} \cdot \omega \tag{6.3}$$

I is the moment of inertia of the rotating components including the turbine blades, rotor discs, shaft, and brake drum. This quantity was measured experimentally by Keogh[8]. The rotor was spun and the brake actuated in a vacuum. Thus, the turbine produced no power and the moment of inertia could be calculated from equation 6.3. For the rotating system in the MIT Blowdown Turbine, the moment of inertia was found to be 1.8085 kg·m^2 with a standard deviation of 0.13%[8]. Figure 6-1 shows both the raw and corrected power for a typical uncooled turbine experiment.

Mass Storage Correction

The critical flow venturi nozzle measures the mass flow rate through it's throat. However, this is not necessarily the mass flow rate through the turbine which is located upstream of

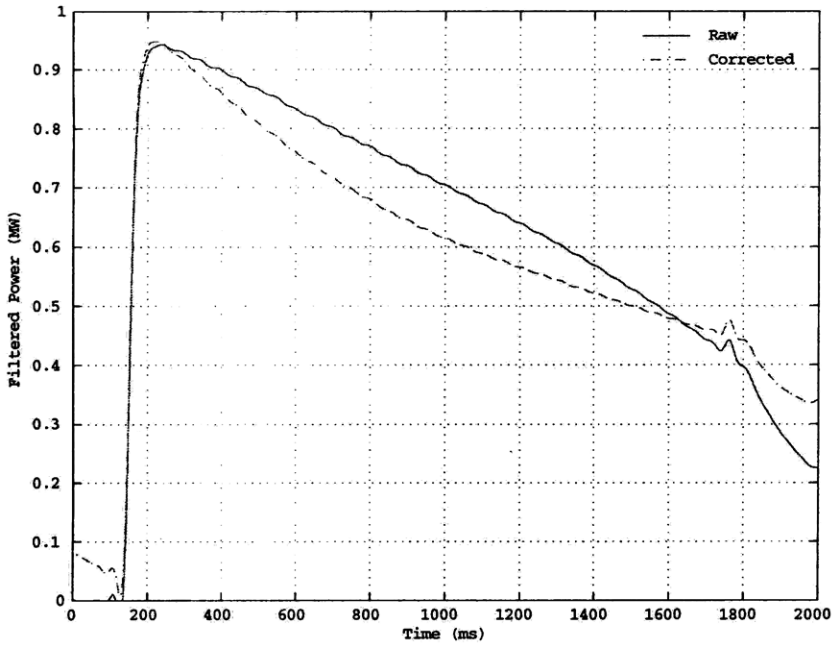

Figure 6-1: Typical uncooled turbine raw and corrected power.

the nozzle. This quantity is required for equation 6.2. Due to the volume separating the turbine from the venturi throat, there can be significant mass storage throughout the facility. This must be accounted for to obtain an accurate measure of the turbine through-flow.

Turbine and venturi nozzle mass flows can be related by

$$\dot{m}_{turb} = \dot{m}_{noz} + \dot{m}_{stored} \tag{6.4}$$

where $\dot{m}_{stored}$ is mass flow stored in volumes throughout the facility. To estimate stored mass flow, the equation of state can be written in terms of mass as

$$m_{stored} = \frac{PV}{TRZ} \tag{6.5}$$

with compressibility factor Z. This can be differentiated in time to give an expression for stored mass flow rate

$$\dot{m}_{stored} = \frac{V}{RZ}\left(\frac{1}{T}\right)\frac{\partial P}{\partial t} - \frac{V}{RZ}\left(\frac{P}{T^2}\right)\frac{\partial T}{\partial t} \tag{6.6}$$

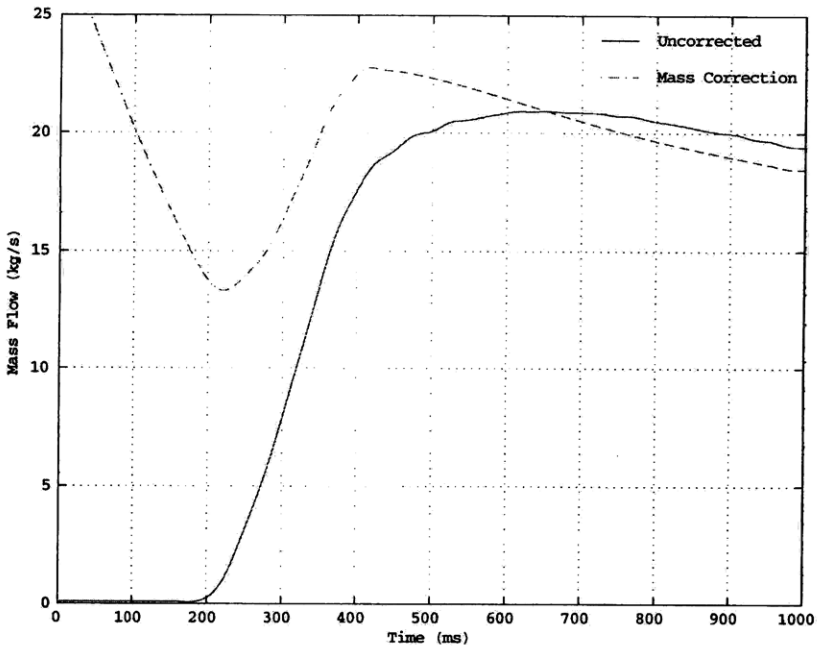

Figure 6-2: Typical uncooled turbine uncorrected and corrected mass flow rate.

This expression can be evaluated in time for each volume in the facility which is properly instrumented with temperature and pressure sensors.

There are many small chambers throughout the facility that are not instrumented. To account for these volumes, a transient model of the blowdown turbine facility was developed and applied to this problem. It provides an estimate of the flow properties in regions of the tunnel which are inaccessible. A full description of the model and subsequent calculations can be found in reference [8]. The results of this model combined with equation 6.6 correct the mass flow measurement for tunnel mass storage. Figure 6-2 show uncorrected and corrected turbine mass flow rate for a typical blowdown experiment.

Heat Transfer Correction

Due to the transient nature of the testing environment, the turbine does not reach thermal equilibrium. As a result, heat transfer occurs during the blowdown and the process can not

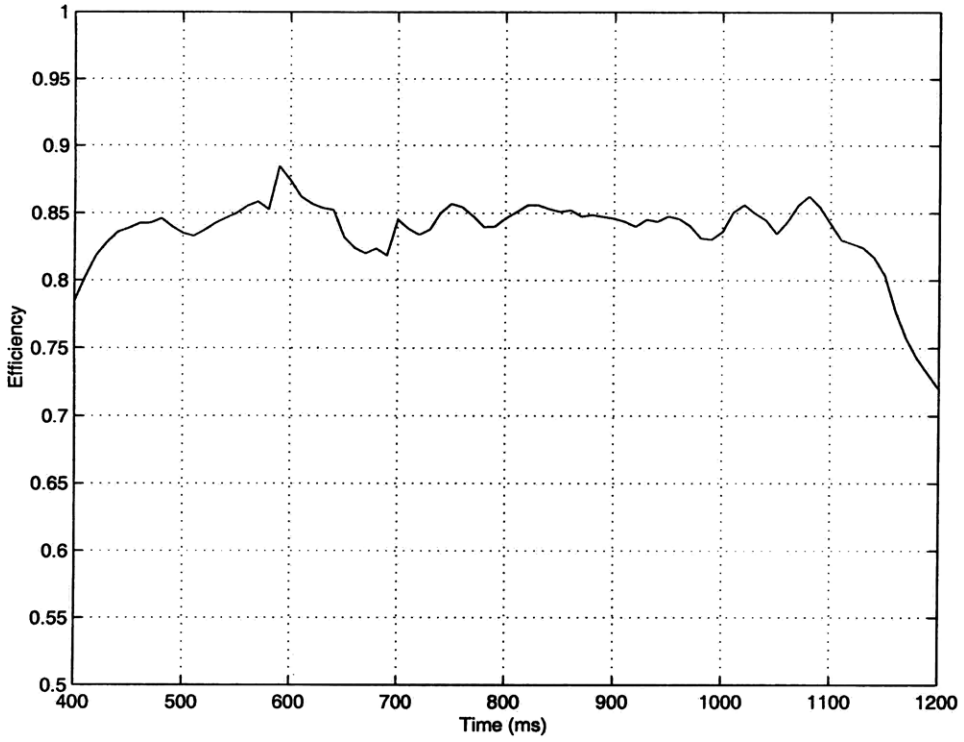

Figure 6-3: Typical uncooled turbine mechanical efficiency.

be considered adiabatic. An expression to account for this effect was derived by Keogh[8]

$$\eta_{mech,ad} = \eta_{mech} + \frac{Q}{h(P_1,T_1) - h(P_2,T_2)} \left(1 - \frac{T_2}{T^*}\right) \tag{6.7}$$

It is assumed that all heat transfer from the flow to the metal occurs at an equivalent temperature T*. Jacobs[10] applied this correction to the uncooled data set and found the adjustment to be on the order of 0.2%.

6.2.3 Corrected Mechanical Efficiency

After correcting turbine power and mass flow rate to account for transient effects, mechanical efficiency can be written as

$$\eta_{mech} = \frac{\mathcal{T} \cdot \omega + I \cdot \frac{d\omega}{dt} \cdot \omega}{(\dot{m}_{noz} + \dot{m}_{stored})\,(h(P_1,T_1) - h(P_2,T_2))} \tag{6.8}$$

Heat transfer effects are small and can be accounted for in subsequent calculations. Figure 6-3 show the mechanical efficiency calculated for a typical uncooled turbine experiment.

6.3 Test Matrix

Several parameters were varied for the uncooled test series. These include pressure ratio, corrected speed, and rotor tip gap. These off-design cases were compared to a baseline which is described in table 6.1.

Table 6.1: Uncooled turbine baseline test conditions.

Parameter	Value
Working Fluid	CO_2
Specific Heat Ratio γ	1.28
Reynolds Number	100% of full scale
Pressure Ratio π	2.0
Corrected Speed N_{cor}	100%
Rotor Tip Gap	1.5% blade span

Table 6.2: Uncooled turbine test matrix.

Test	Fluid	Re	γ	π	N_{cor}	Tip Gap
001	CO_2	100%	1.28	1.7	100%	1.5%
002	CO_2	100%	1.28	1.8	100%	1.5%
003	CO_2	100%	1.28	1.9	100%	1.5%
004	CO_2	100%	1.28	2.0	100%	1.5%
005	CO_2	100%	1.28	2.1	100%	1.5%
006	CO_2	100%	1.28	2.2	100%	1.5%
007	CO_2	100%	1.28	2.3	100%	1.5%
008	CO_2	100%	1.28	2.0	95%	1.5%
009	CO_2	100%	1.28	2.0	105%	1.5%
010	CO_2	100%	1.28	2.0	110%	1.5%
011	CO_2	100%	1.28	1.7	100%	3.0%
012	CO_2	100%	1.28	1.8	100%	3.0%
013	CO_2	100%	1.28	1.9	100%	3.0%
014	CO_2	100%	1.28	2.0	100%	3.0%
015	CO_2	100%	1.28	2.1	100%	3.0%
016	CO_2	100%	1.28	2.2	100%	3.0%
017	CO_2	100%	1.28	2.3	100%	3.0%
018	CO_2	100%	1.28	2.0	95%	3.0%
019	CO_2	100%	1.28	2.0	105%	3.0%
020	CO_2	100%	1.28	2.0	110%	3.0%

Table 6.2 shows the test matrix for the uncooled experiments.

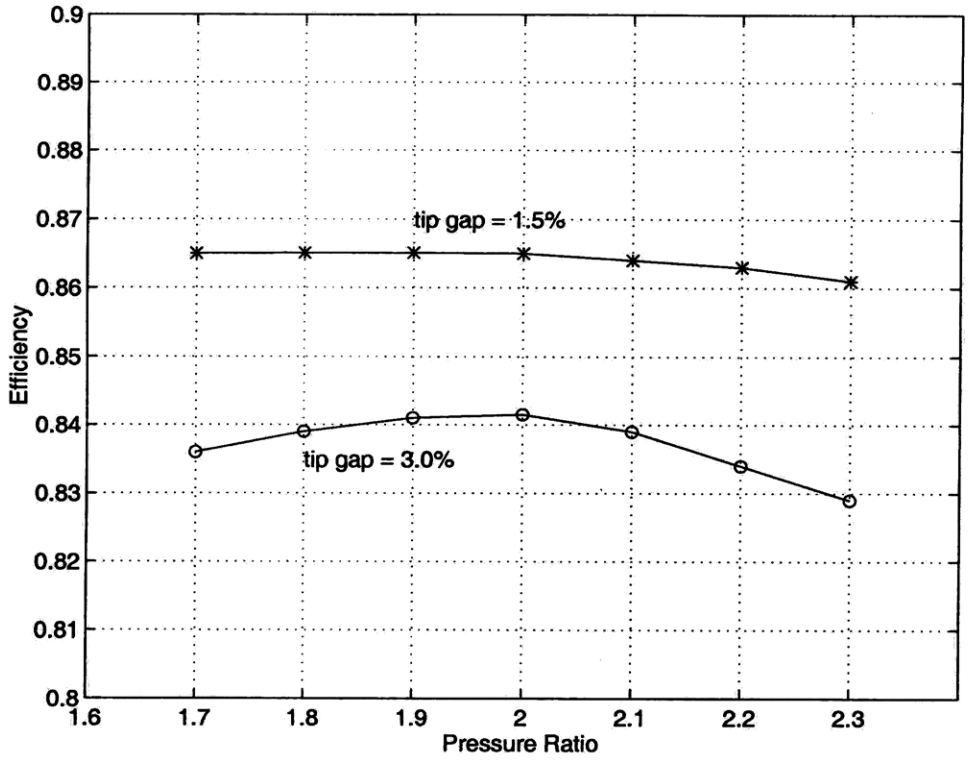

Figure 6-4: Uncooled turbine efficiency vs. pressure ratio for two rotor tip gaps.

6.4 Results

Figure 6-4 shows the results of the pressure ratio tests for two different rotor tip gaps. The smaller tip gap exhibited an efficiency approximately 2-3% greater than that of the large tip gap. The larger gap causes increased secondary flows and thus, increased losses. The variation in efficiency with pressure ratio is minimal in the case of the smaller tip gap. For the larger gap, the efficiency is maximum at $\pi \approx 1.95$ which is near the baseline condition.

Figure 6-5 shows the results of the corrected speed tests for the to tip gaps. Again, a difference of approximately 2-3% can be seen between the two gaps. The plot also shows that as speed is increased, efficiency tends to rise. However, as speed exceeds 105% the efficiency increase slows. This efficiency rise is explained by the change in blade loading with variation in speed. As rotor speed is increased, rotor relative inlet angle is decreased. Therefore, the blade angle-of-attack is reduced and blade loading decreases. With lower loading there is higher efficiency.

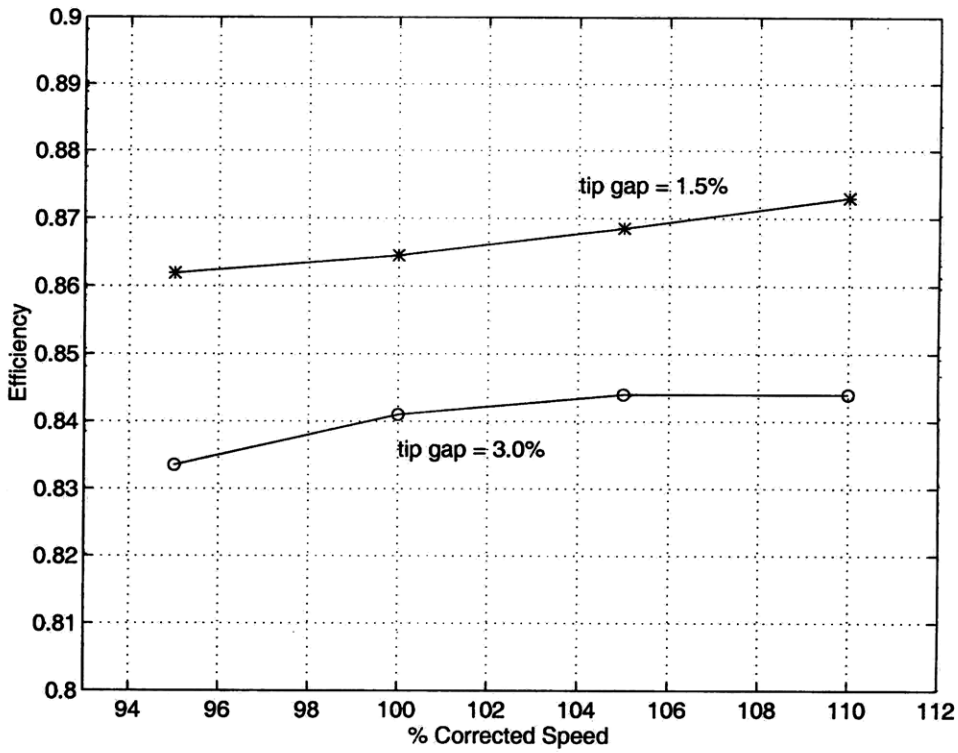

Figure 6-5: Uncooled turbine efficiency vs. corrected speed for two rotor tip gaps.

6.5 Conclusions

The uncooled turbine testing has provided a unique data set over a range of operating conditions as a baseline for comparison to cooled turbine performance. A 2-3% drop in efficiency for a two-fold increase in rotor tip gap was shown. A map of turbine performance over a significant range of pressure ratios was obtained. A corresponding map for corrected speed was also generated. The corrected speed tests confirmed that efficiency varies inversely with blade loading. Relative uncertainty of these measurements has been shown to be 0.16% by Jacobs[10].

6.6 Summary

This chapter has reviewed the uncooled turbine test program. The mechanical efficiency calculation and its associated transient corrections were described. The matrix of test conditions was presented. Turbine pressure ratio, corrected speed, and rotor tip gap were varied. Results from these tests were briefly discussed. The turbine exhibited changes in

performance due to blade loading and increased tip gap. Finally, it was concluded that these data would be useful as a comparison to cooled turbine performance tests.

Chapter 7

Film-Cooled Turbine Performance Testing

7.1 Introduction

After fabrication of the film-cooled turbine and installation of the coolant feed system, a cooled performance testing series was conducted. The mechanical efficiency calculation described in Chapter 6 was modified to account for the coolant flow injection. As in the uncooled tests, a baseline condition was selected and off-design performance was simulated. Pressure ratio, corrected speed, and coolant mass flow were varied parametrically throughout the test series. In addition, a preliminary comparison to the uncooled data will be shown.

7.2 Cooled Turbine Mechanical Efficiency Calculation

To compute efficiency for a film-cooled turbine, several modifications to the mechanical efficiency calculation described in the previous chapter must be made. Turbine efficiency can still be defined as the ratio of actual power produced by the machine to ideal power as shown in equation 6.1. The actual power is measured in the Blowdown Turbine facility and is still calculated via equation 6.3. Again, this accounts for transient effects in the blowdown environment. However, the ideal power of the turbine will not remain the same as that shown in the denominator of equation 6.8. Ideal power for a film-cooled turbine can be estimated via several methods. For the purposes of this study, the modifications to the turbine efficiency calculation found in reference [18] were used.

The injection of coolant flow into the mainstream must be factored into the ideal turbine

power. The ideal power due to the coolant flow alone is

$$\mathcal{P}_{cool,ideal} = \dot{m}(h(P_c, T_c) - h(P_2, T_2)) \tag{7.1}$$

where h is the coolant and downstream enthalpy. This definition assumes that the downstream flow is fully mixed. The ideal power due to coolant flow can be broken down further to account for the NGV, blade, and tip casing flows individually.

$$\mathcal{P}_{cool,ideal} = \mathcal{P}_{NGV,ideal} + \mathcal{P}_{bl,ideal} + \mathcal{P}_{casing,ideal} \tag{7.2}$$

Each individual component of equation 7.2 follows the form of equation 7.1.

The coolant mass flow which is injected is mixed with the main flow and measured as part of the total turbine through-flow by the downstream critical flow venturi nozzle. The ideal power due to the main flow is only dependent upon the turbine inlet mass flow. As a result, the turbine through-flow is over-estimated and the coolant must be factored out. Ideal power due to the turbine inlet flow then becomes

$$\mathcal{P}_{main,ideal} = \Delta h(\dot{m}_{noz} - \dot{m}_{coolant}) \tag{7.3}$$

After accounting for the effects of the coolant on ideal power, the equation for mechanical efficiency is

$$\eta_{mech,cool} = \frac{\mathcal{T} \cdot \omega}{(\dot{m}_{noz} - \dot{m}_{cool})(h(P_1, T_1) - h(P_2, T_2)) + \mathcal{P}_{cool,ideal}} \tag{7.4}$$

A final expression which treats transient effects such as rotor acceleration and tunnel mass storage is

$$\eta_{mech,cool} = \frac{\mathcal{T} \cdot \omega + I \cdot \frac{d\omega}{dt} \cdot \omega}{(\dot{m}_{noz} + \dot{m}_{stored} - \dot{m}_{cool})(h(P_1, T_1) - h(P_2, T_2)) + \mathcal{P}_{cool,ideal}} \tag{7.5}$$

7.3 Test Matrix

The baseline cooled turbine performance conditions for this test series are summarized in Table 7.1. The Reynolds Number is 72% of the design value and that which was used in

the uncooled tests. To achieve the desired coolant-to-mainstream temperature ratio, the main supply tank was heated to 400°F. To completely match Reynolds Number at this temperature, the tank pressure would have been greater than safety limits would permit. The cooled turbine test matrix is shown in Table 7.2. Variation in coolant mass flow rate,

Table 7.1: Cooled turbine baseline test conditions.

Parameter	Value
Working Fluid	CO_2
Reynolds Number	72% of full scale
Pressure Ratio π	2.0
Corrected Speed N_{cor}	100%
Rotor Tip Gap	3.0% blade span
T_{main}/T_{cool}	1.52
Coolant Mass Flow $\dot{m}_{cool}$	9.7% of main flow

Reynolds Number, corrected speed, and pressure ratio were tested. All tests were conducted with a tip gap of 3% of blade span.

Table 7.2: Cooled turbine test matrix.

Test	Fluid	Re	π	N_{cor}	$\dot{m}_{cool}$	T_{main}/T_{cool}	Run Record #
001	CO_2	72%	2.0	100%	5.0%	1.15	ABB110
002	CO_2	72%	2.0	100%	8.0%	1.15	ABB111
003	CO_2	72%	2.0	100%	9.7%	1.15	ABB113
004	CO_2	72%	2.0	100%	12.0%	1.15	ABB117
005	CO_2	72%	2.0	100%	9.7%	1.52	ABB118
006	CO_2	72%	2.0	90%	9.7%	1.52	ABB121
007	CO_2	72%	2.0	95%	9.7%	1.52	ABB120
008	CO_2	72%	2.0	110%	9.7%	1.52	ABB128
009	CO_2	72%	2.1	100%	9.7%	1.52	ABB123
010	CO_2	72%	1.9	100%	9.7%	1.52	ABB122

7.4 Results

7.4.1 Baseline Conditions

As a result of the coolant, it is more difficult to maintain constant conditions over the course of a blowdown experiment. Figure 7-1(a,b) shows the pressure ratio and corrected speed

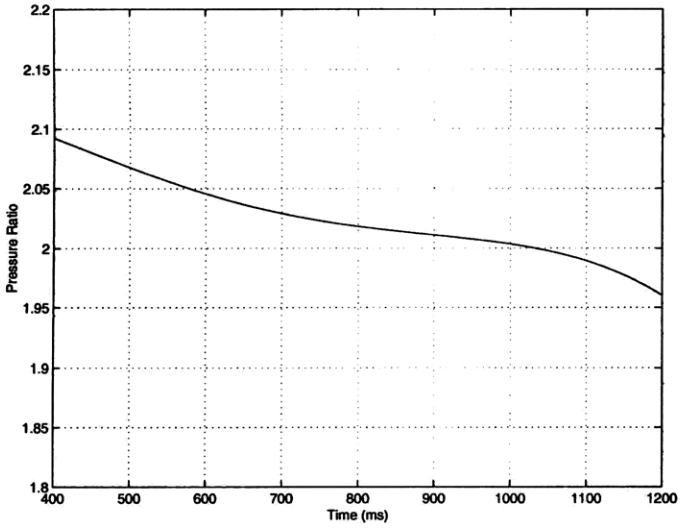

(a) Pressure ratio

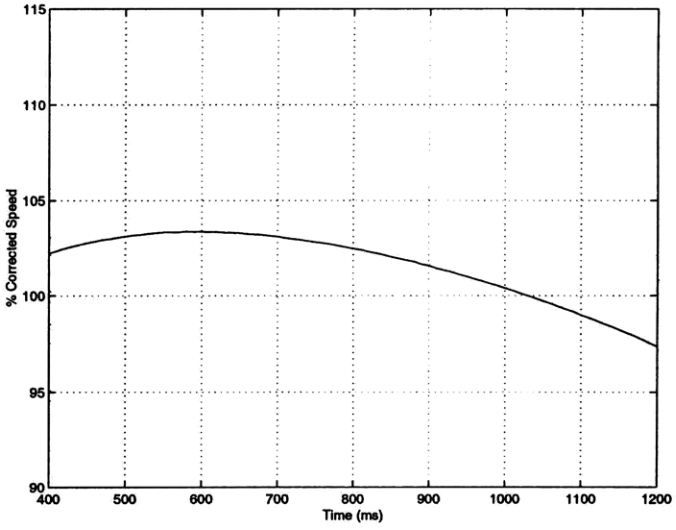

(b) Corrected speed

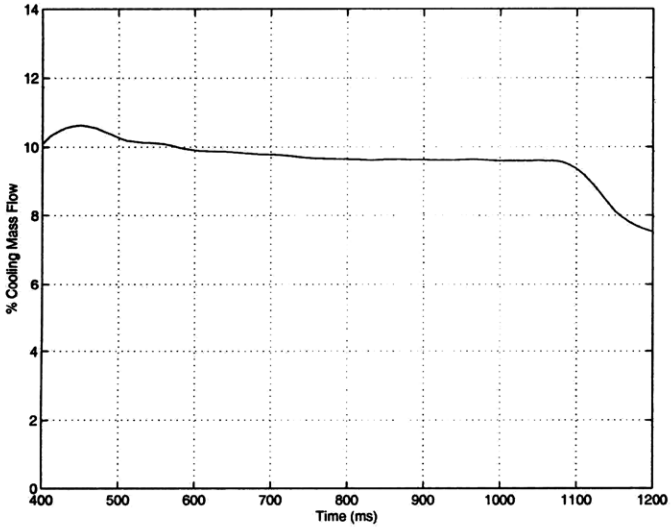

(c) Coolant mass flow

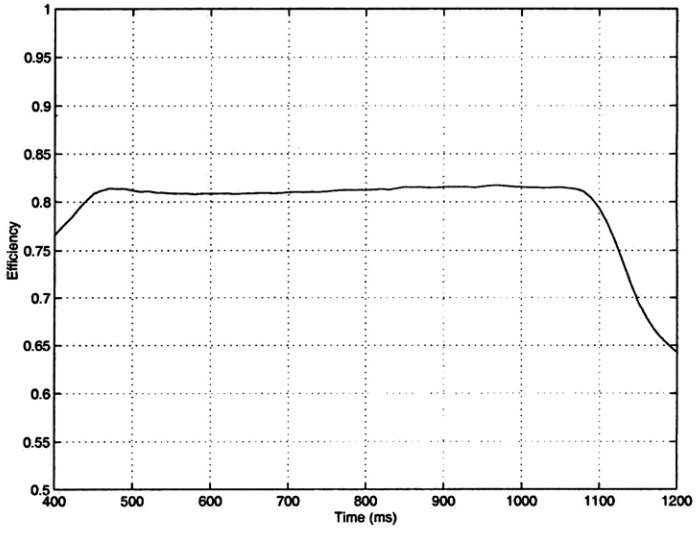

(d) Efficiency

Figure 7-1: Baseline cooled turbine experiment.

for the baseline test conditions. The figures indicate a larger variation in conditions over the test window than was seen in the uncooled experiments. Figures 7-1(c,d) are plots of coolant mass flow and efficiency. Coolant mass flow was relatively constant over the course of the test. This is expected due to the choked orifices' wide range of operating conditions. The efficiency is also relatively constant over the usable test window. Data for the entire test matrix can be found in Appendix C.

7.4.2 Variation in Coolant Flow

The effect of coolant mass flow on turbine performance was studied. Coolant mass flow was varied from approximately 5% of the main flow up to 12%. All other parameters were held constant between tests. It was observed that as coolant mass flow increased, turbine efficiency decreased. This is due to aerodynamic losses associated with coolant flow injection. Figure 7-2 shows the coolant mass flow as a function of time for four different experiments. Figure 7-3 plots the decrease in efficiency with increasing coolant mass flow. A 2% drop in efficiency can be seen for a two-fold increase in coolant mass flow. A data point from the uncooled turbine configuration is shown for reference. This point is not directly comparable because the cooling holes themselves may account for some aerodynamic loss.

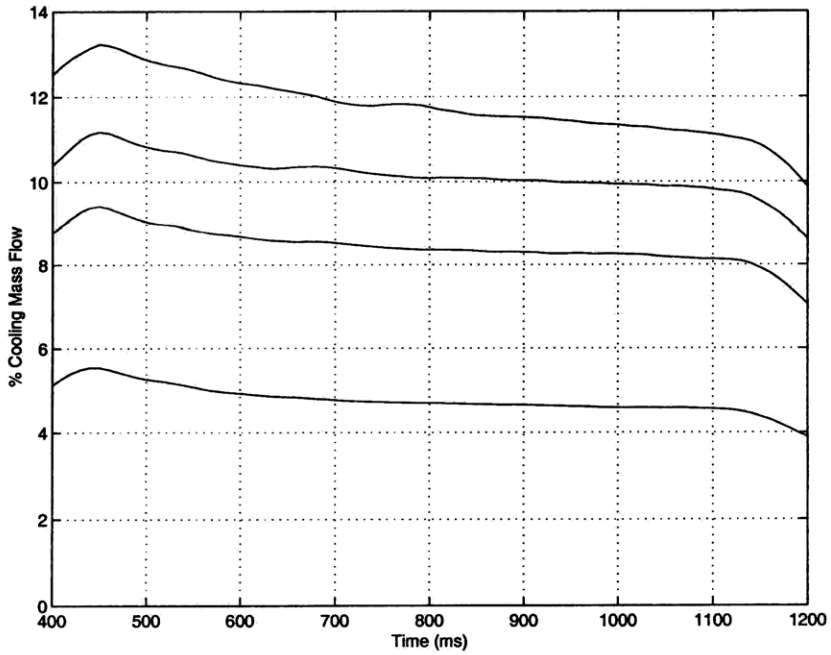

Figure 7-2: Coolant mass flow for four different tests.

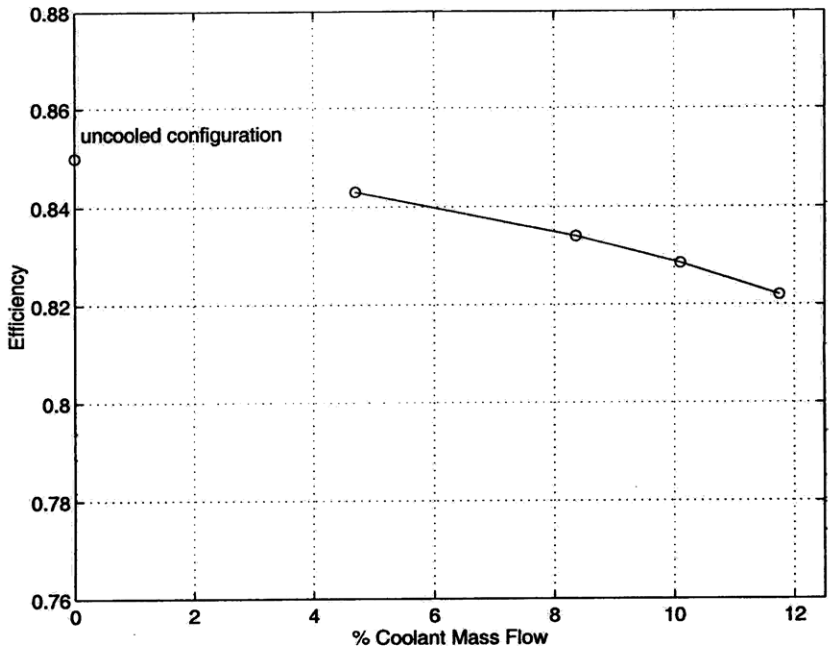

Figure 7-3: Turbine efficiency vs. coolant mass flow.

7.4.3 Variation in Pressure Ratio

As in the uncooled experiments, pressure ratio was varied while all other conditions were held constant. Figure 7-4 shows a plot of efficiency vs. pressure ratio. There is no distinct trend. This is similar to the results of the uncooled pressure ratio tests. These data can not be directly compared to the uncooled data because by testing at a higher temperature, the non-dimensional parameters such as Reynolds Number and gas-to-wall temperature ratio are not comparable.

7.4.4 Variation in Corrected Speed

Figure 7-5 shows a plot of efficiency vs. corrected speed. As in the pressure ratio and coolant mass flow tests, all other parameters were held constant. Like the uncooled experiments, efficiency increases with speed. Again, this is a result of a decrease in flow incidence angle and a decrease in blade loading. Like the pressure ratio tests, these experiments are not directly comparable to the uncooled experiments.

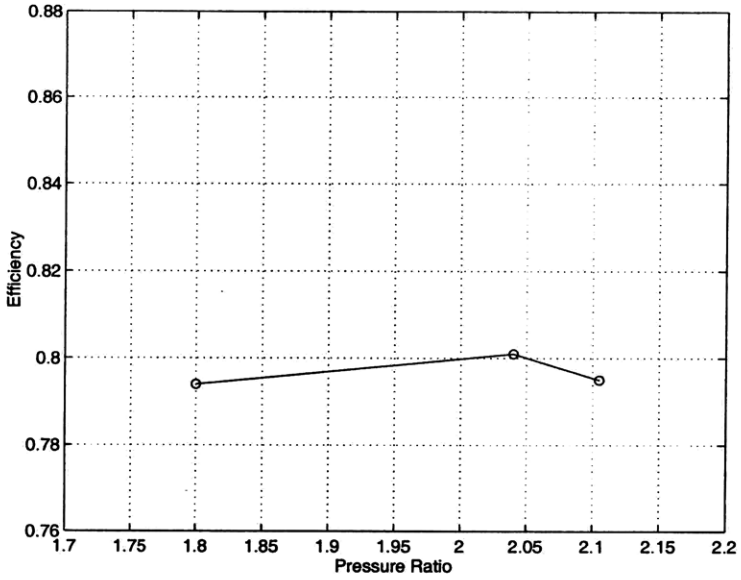

Figure 7-4: Cooled turbine efficiency vs. pressure ratio.

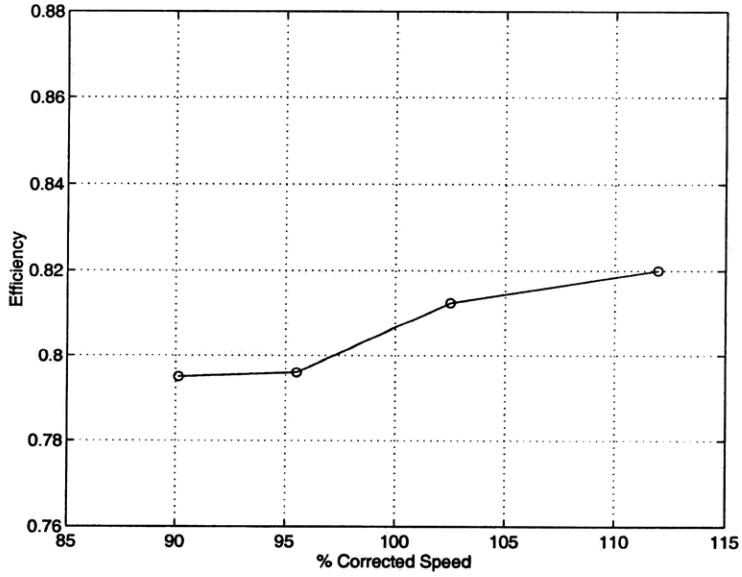

Figure 7-5: Cooled turbine efficiency vs. corrected speed.

7.4.5 Comparison to Uncooled Turbine Tests

Cooled test #004 was run at conditions very similar to those used in the uncooled test series. Figure 7-6 shows efficiency for this test plotted on the same axes as efficiency for an uncooled test. The tip gaps in the two experiments were the same. The coolant flow in the cooled experiment was 11.75% of the main flow. An efficiency drop of approximately 2.0% is shown and can be attributed to aerodynamic losses due to coolant flow injection.

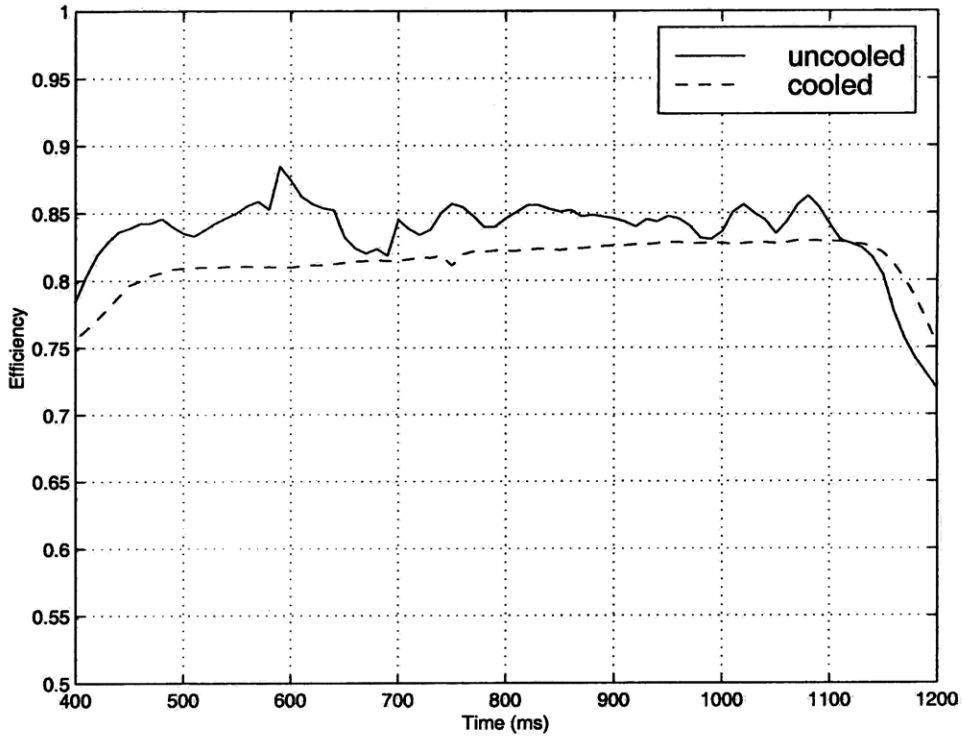

Figure 7-6: Efficiency for comparable uncooled and cooled turbine tests.

7.5 Conclusions

Aerodynamic performance of a film-cooled turbine was measured in the Blowdown Turbine test facility. Efficiency consistently decreased with an increase in coolant mass flow rate. Trends similar to the uncooled tests were observed when pressure ratio and corrected speed were varied. A preliminary comparison of the cooled and uncooled data shows that turbine efficiency drops significantly with coolant flow injection. Only tests with similar non-dimensional parameters were compared.

7.6 Summary

This chapter presents the modifications to the mechanical efficiency calculation to account for coolant flow injection. The film-cooled turbine test matrix is discussed and baseline conditions reviewed. Data for the baseline case is presented followed by the results of the coolant flow, pressure ratio, and corrected speed tests. Finally, a preliminary comparison to the uncooled data is made.

CHAPTER 8
CONCLUSIONS

8.1 Review of Objectives

The primary objective of this work was to provide a detailed data set of film-cooled turbine performance. The Blowdown Turbine experimental facility was utilized for this task and a scaled ABB GT24 first stage low pressure turbine was the test article. Efficiency was measured using the mechanical approach outlined by Keogh[8] and was reviewed in Chapters 6 and 7.

To accomplish this goal several other objectives were met. A geometrically scaled, film-cooled turbine was required for testing. An uncooled version of the ABB turbine had to be modified for these purposes. Once complete, knowledge of the discharge coefficients of the cooling holes was needed. The facility itself required modifications to allow for independent control of turbine coolant to the NGVs, blades, and tip casing. This led to a host of other questions regarding the flow of metastable CO_2 through a flow metering device.

Ultimately, a scaled, film-cooled turbine was tested and a detailed data set acquired. These data were reviewed for simple trends and compared to uncooled data in Chapter 7 of this work. Subsequent modeling and CFD efforts will use these data as a baseline for comparison.

8.2 Summary of the Work

A fully scaled, film-cooled turbine was fabricated from an uncooled blade and NGV set. The uncooled components were modified via electro-discharge machining, laser drilling, and laser welding. This proved to be a difficult task. Acceptable tolerances were extremely small and

the film-cooling holes themselves were 0.25 scale. As a result, modifications to the design were made for manufacturing purposes. Custom made fixtures were designed and used for all machining.

Characterization of the cooling hole quality and effective area was then required. A measurement of the C_dA of each row of cooling holes was necessary. This, coupled with estimates of the static pressure distribution along the blades and NGVs, would provide information regarding the mass flow passed through each set of cooling holes for a given test. A calibration apparatus was constructed to obtain this C_dA.

The Blowdown Turbine facility was modified to feed coolant to the blades, NGVs, and tip casing. To independently control this flow, coolant was routed separately to each of the afore mentioned components and thick, squared edged, choked orifices were used as metering devices. However, by utilizing sonic flow metering methods, the test gas (nominally CO_2) became supersaturated. To account for this, an experiment to determine its effect on the flow metering was devised. This involved several coolant flow blowdown-type experiments. It was found that metastable flow could be metered via existing methods.

A film-cooled turbine test series was successfully completed. The effects of coolant mass flow, pressure ratio, and corrected speed were studied. Aerodynamic losses due to increased coolant flow injection decreased efficiency. Trends similar to those shown in a previous uncooled test series were observed in the pressure ratio and corrected speed tests. There was no clear trend in turbine efficiency with changes in pressure ratio while efficiency increased with corrected speed. The latter of this two observations is believed to be due to a decrease in blade loading. Finally, a preliminary comparison of cooled and uncooled turbine data indicated a 2% drop in efficiency due to cooling.

8.3 Recommendations for Future Work

There are several near-term recommendations which can be made to improve upon the film-cooled turbine performance test series. Additional tests will provide much insight into turbine fluid physics. Total coolant flow was varied over a range of test conditions. However, independent component's flows were not. A large fraction of the total cooling flow passes

through the NGVs. This flow is then swept up into the rotor and will have a significant effect on aerodynamic performance. Therefore, varying the NGV coolant flow may provide some insight. Changes in coolant flow to the blades and tip casing may also prove interesting, but are secondary to the NGV flow.

Additional tests over a larger range of pressure ratios and speeds may also be warranted. No discernible trend was discovered in the pressure ratio testing and with more test points, this may no longer be the case. Additional speed tests would refine the trend already observed.

Also, additional analysis of the current uncooled and cooled data sets is necessary. More work is required to adequately compare the two. Because the conditions between the two test series vary significantly, direct comparison is not useful.

Long-term work may included a detailed study of the uncooled tip-gap experiments. Currently tip-gap models and CFD simulations are generally bench-marked against cascade experiments. With this unique data set of a fully rotating turbine stage, a study comparing these data to CFD codes is warranted. Significant improvements to the underlying models may be made.

Other suggested work would include a detailed study of the cooled data set and a modeling effort. Physics-based modeling of the fluid mechanics of the coolant/mainstream interactions would provide insight into the actual loss mechanisms in a turbine. The data set described here is ideal for validating such models. This could ultimately result in improved turbine designs and design tools. It may even be possible to use film-cooling as an aerodynamic advantage in a turbine. These questions could be answered by further study of these data and associated modeling.

Appendix A

Turbine Blade Discrete Row C_dA

A.1 Introduction

This appendix includes all measured cooling hole effective areas for the scaled ABB turbine blades. Each plot shows the C_dA for the leading edge, suction surface, and pressure surface rows on an individual blade, although, for some blades, not all rows were tested. All data are presented on the same scale for comparison. The calculations are discussed in Chapter 4.

A.2 Figures

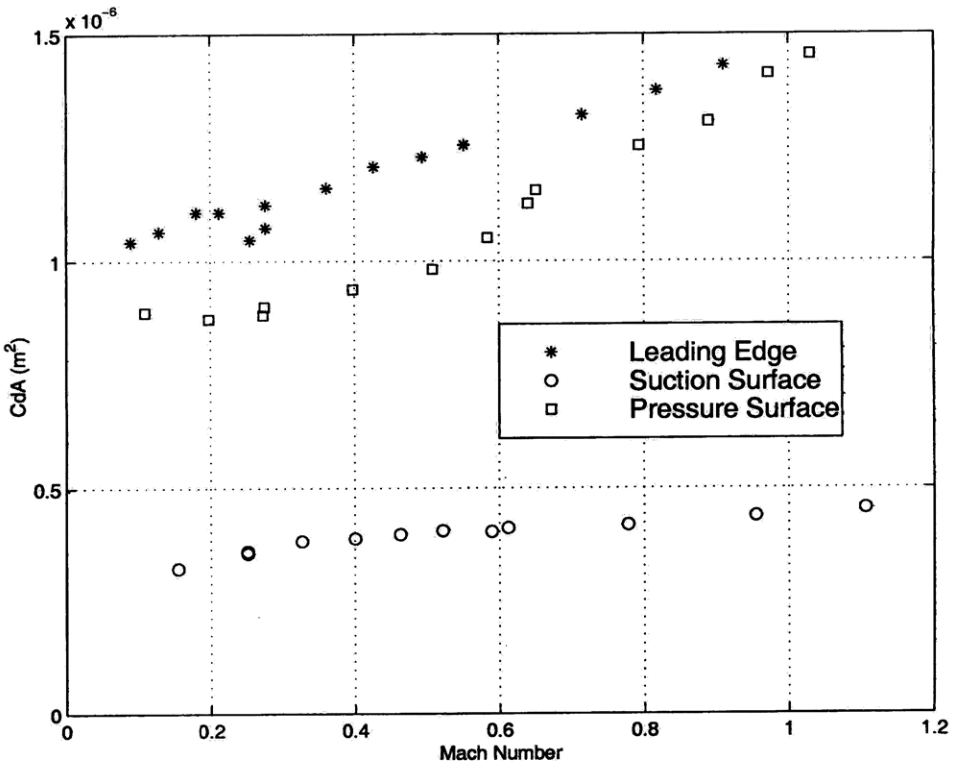

Figure A-1: Blade #054 cooling hole effective area.

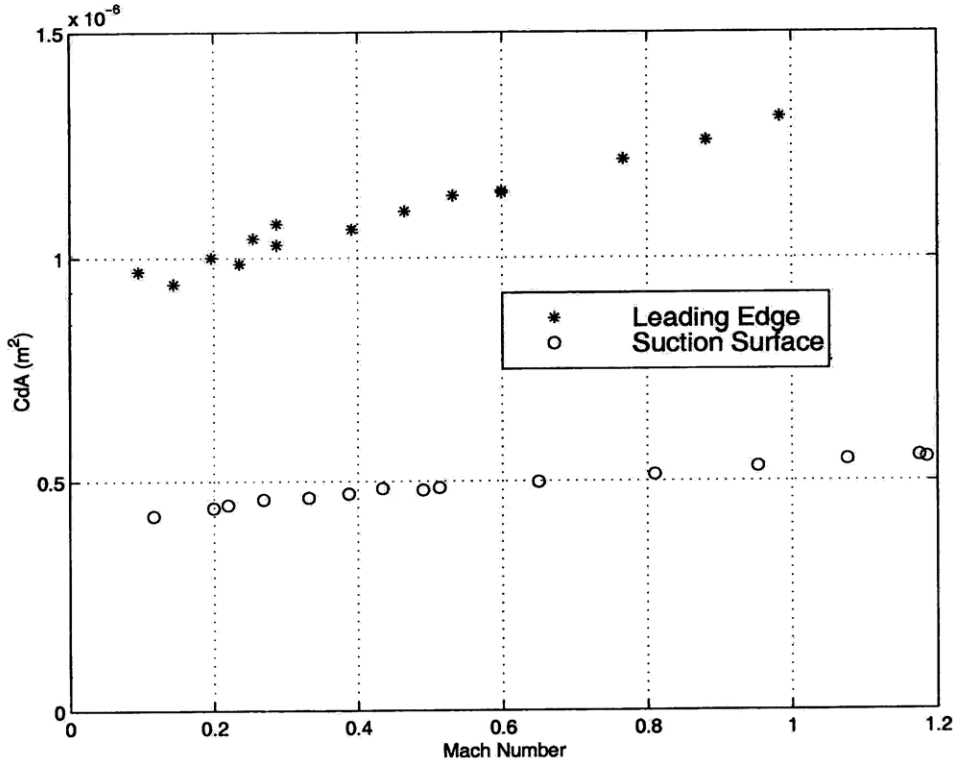

Figure A-2: Blade #011 cooling hole effective area.

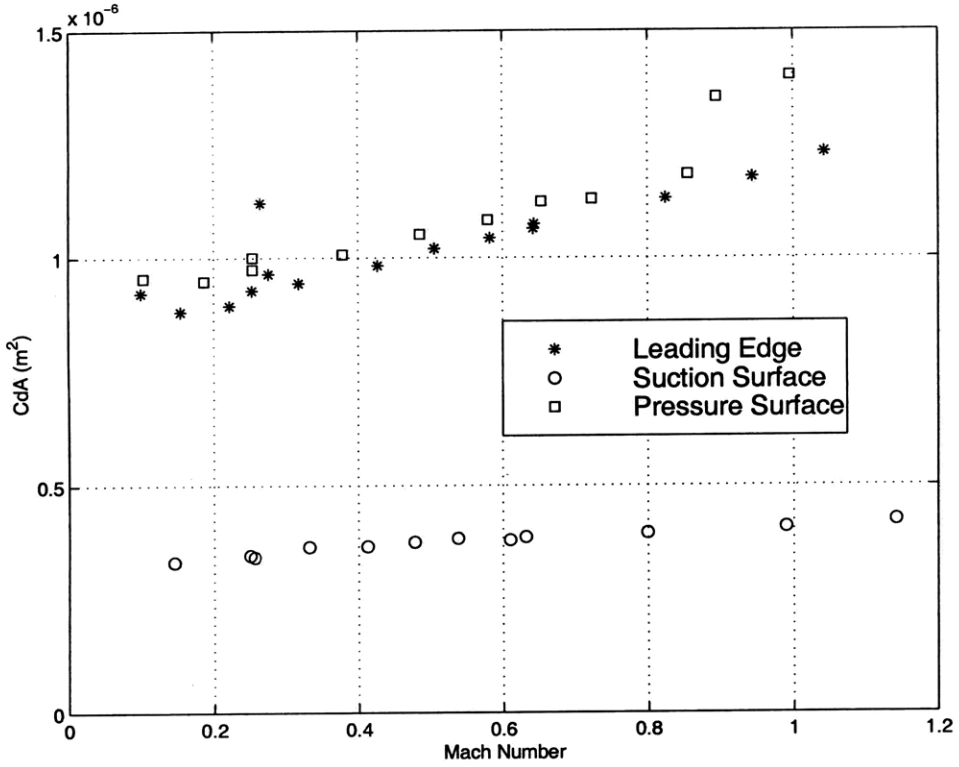

Figure A-3: Blade #077 cooling hole effective area.

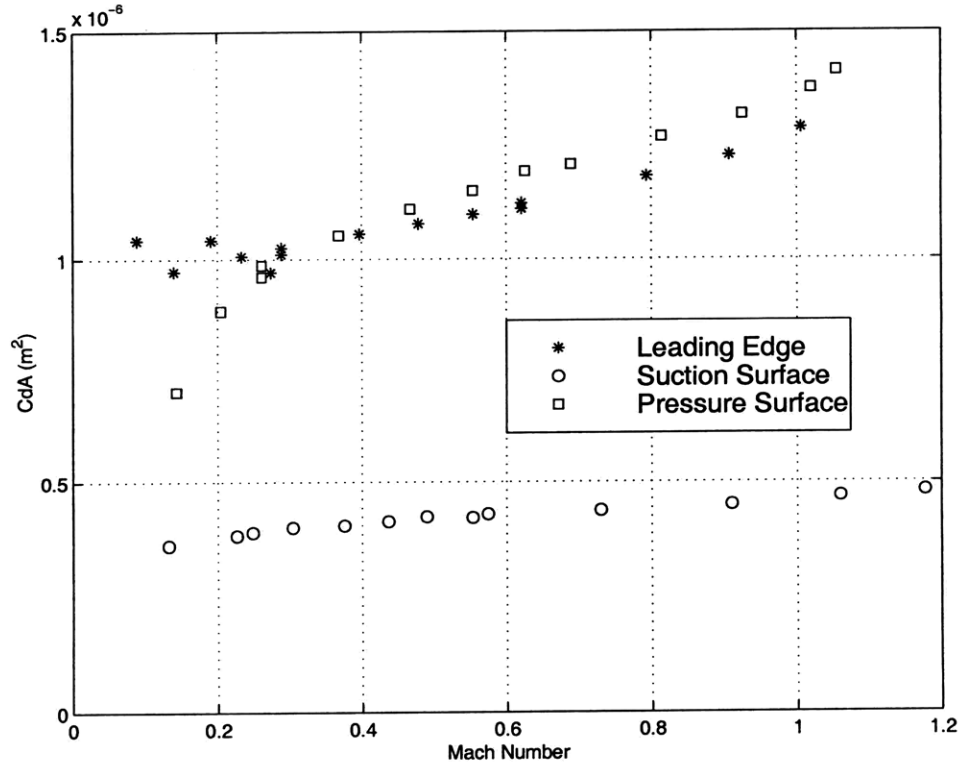

Figure A-4: Blade #023 cooling hole effective area.

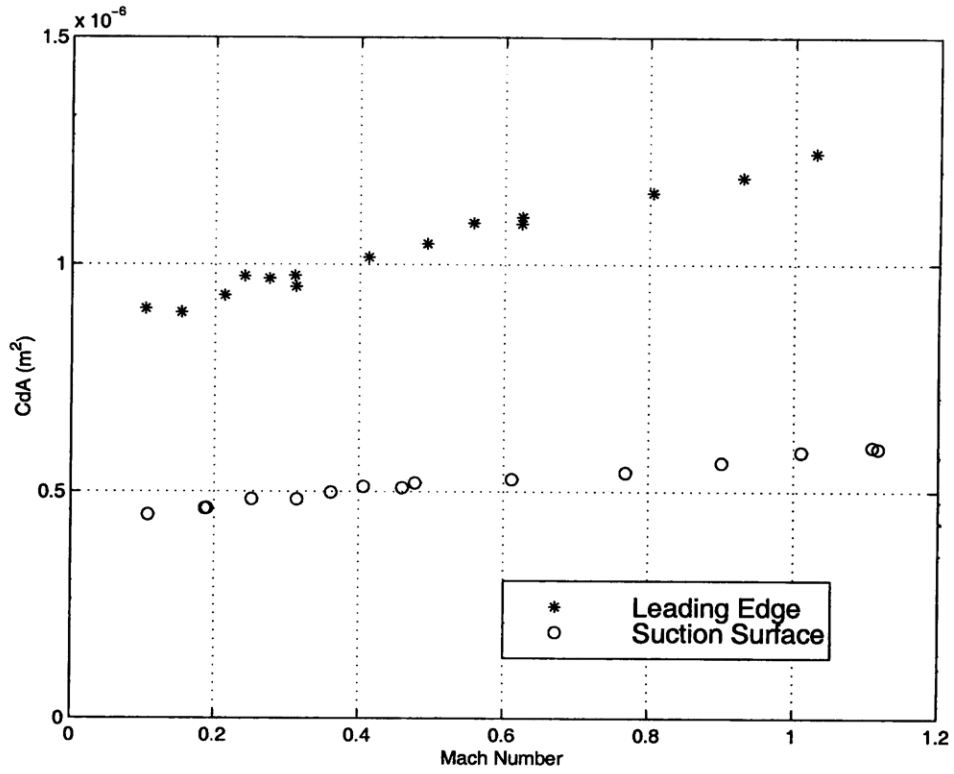

Figure A-5: Blade #048 cooling hole effective area.

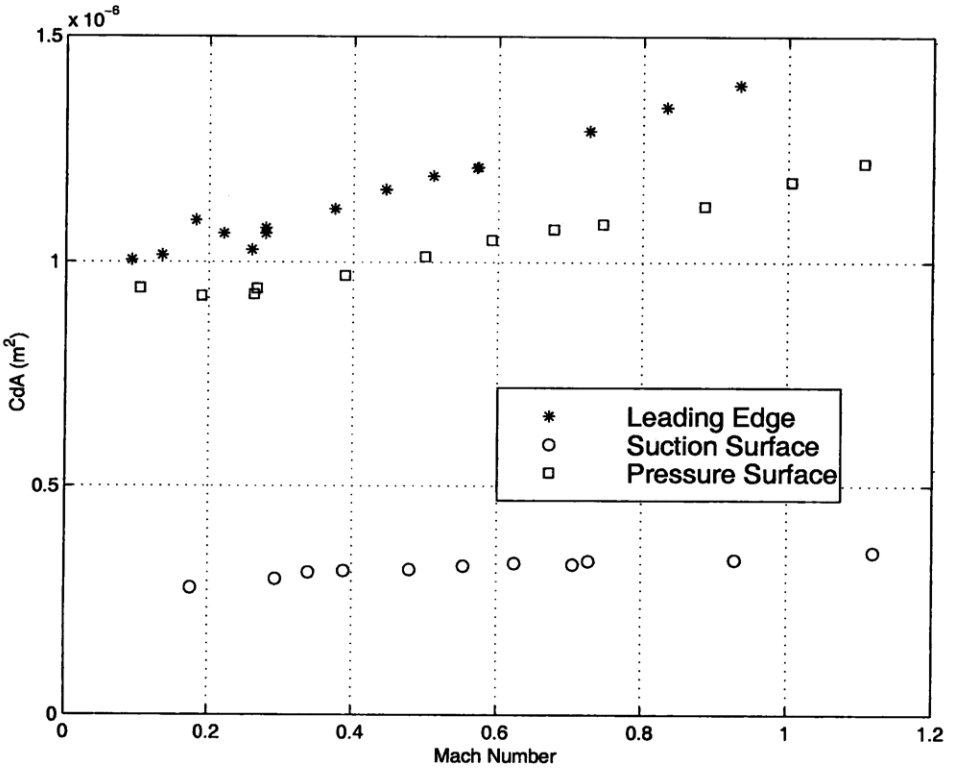

Figure A-6: Blade #017 cooling hole effective area.

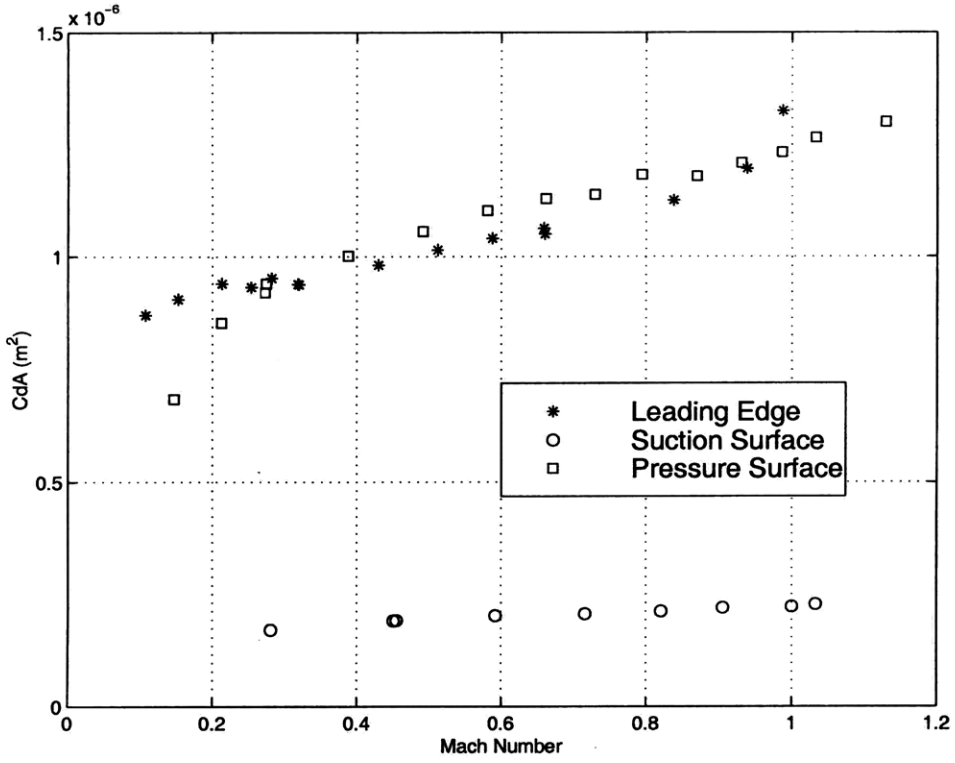

Figure A-7: Blade #052 cooling hole effective area.

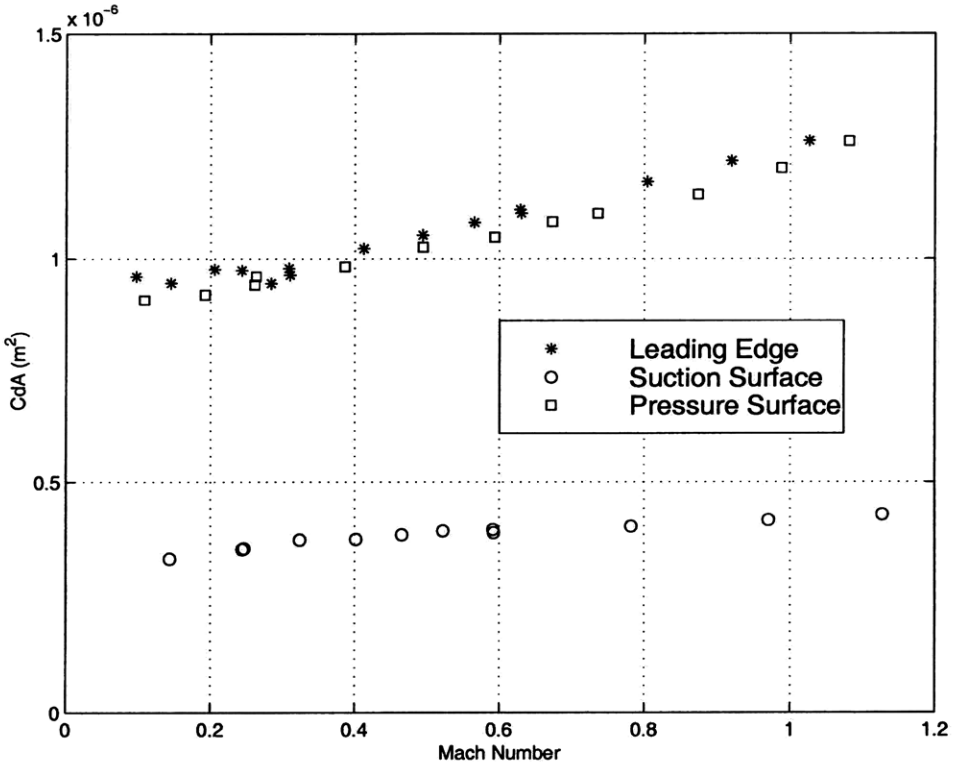

Figure A-8: Blade #092 cooling hole effective area.

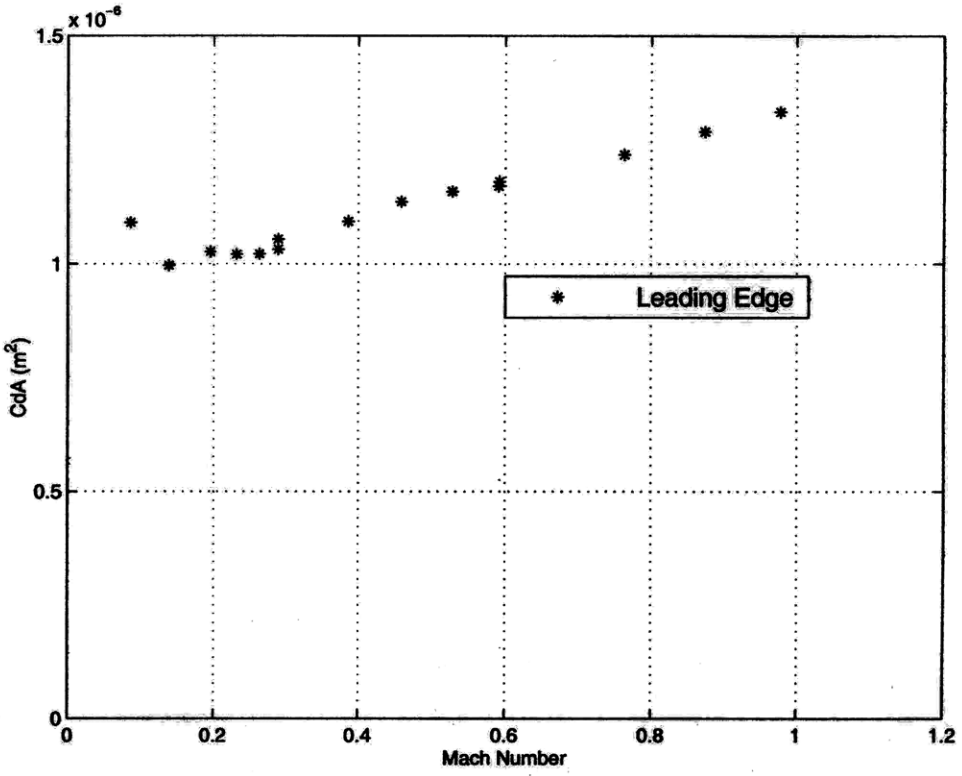

Figure A-9: Blade #004 cooling hole effective area.

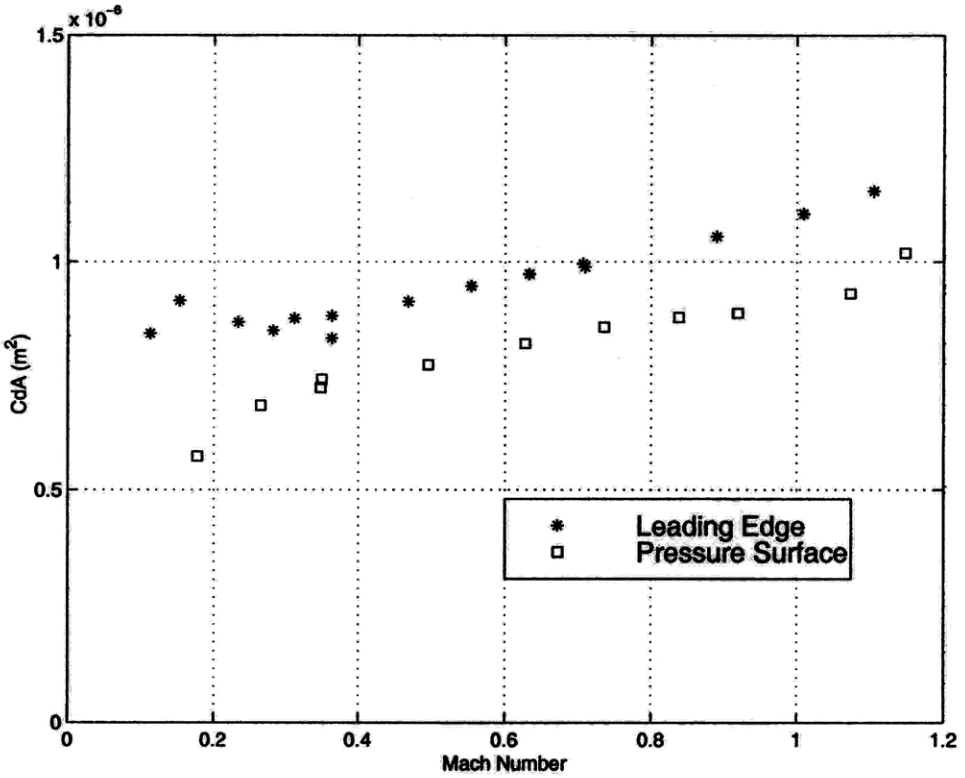

Figure A-10: Blade #062 cooling hole effective area.

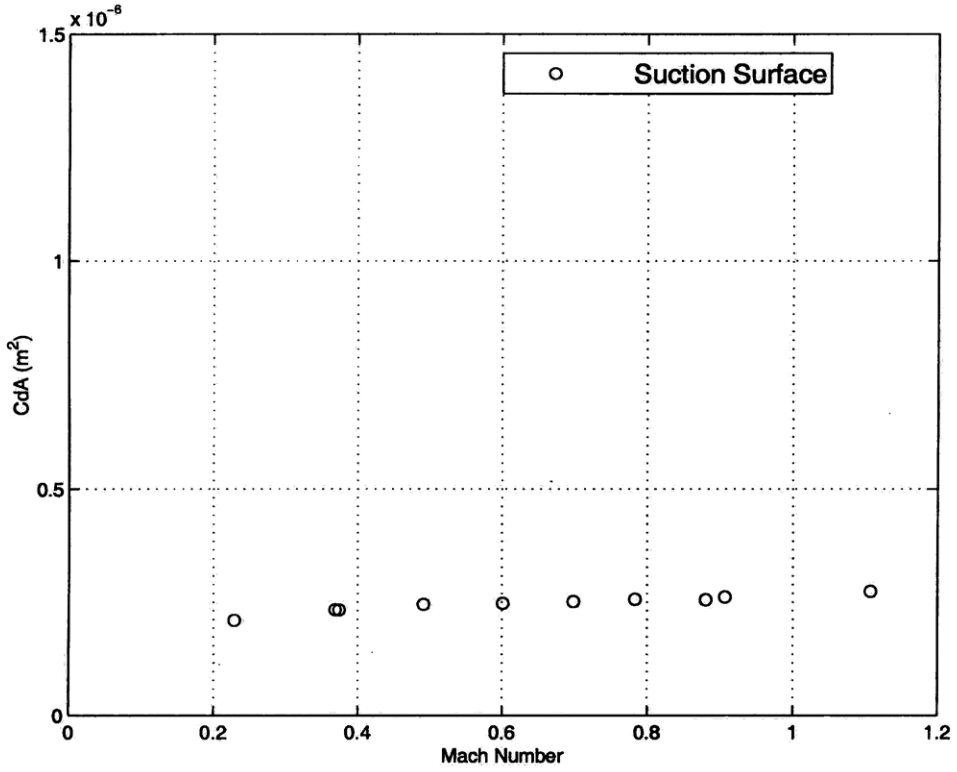

Figure A-11: Blade #056 cooling hole effective area.

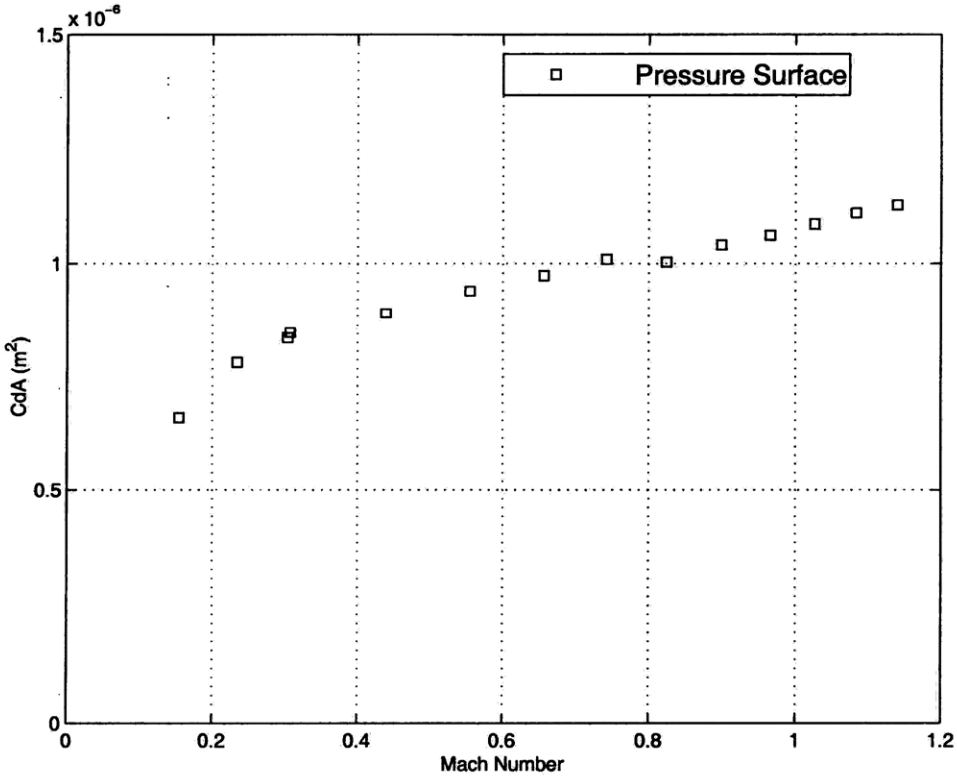

Figure A-12: Blade #064 cooling hole effective area.

Appendix B
Coolant Flow Metering Experimental Data

B.1 Introduction

This appendix includes pressure, temperature, and mass flow rate data for the experiments described in Chapter 5. Also presented are critical flow coefficients as a function of time for various conditions of CO_2. The mass flow rate and C_R traces are plotted on the same scale for comparison.

B.2 Figures

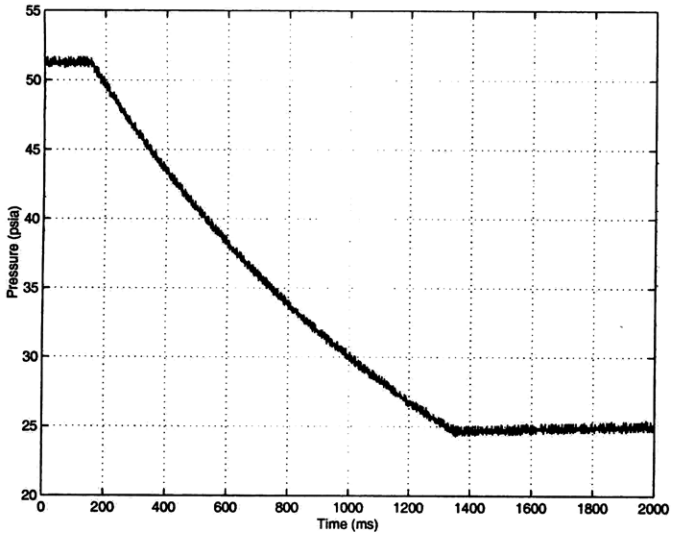

(a) Pressure

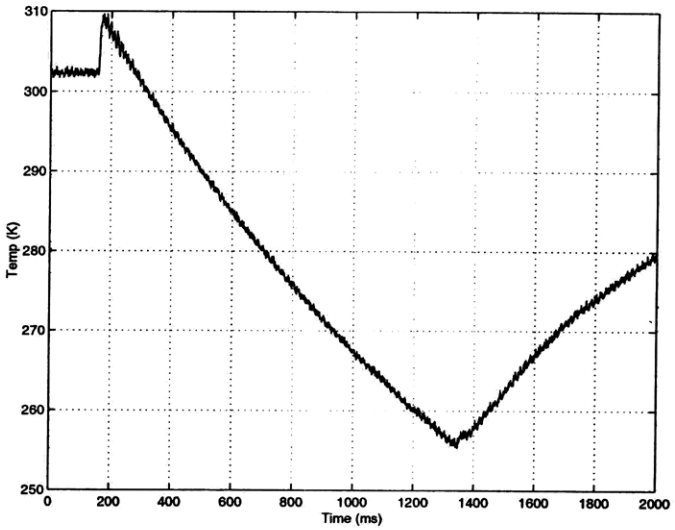

(b) Temperature

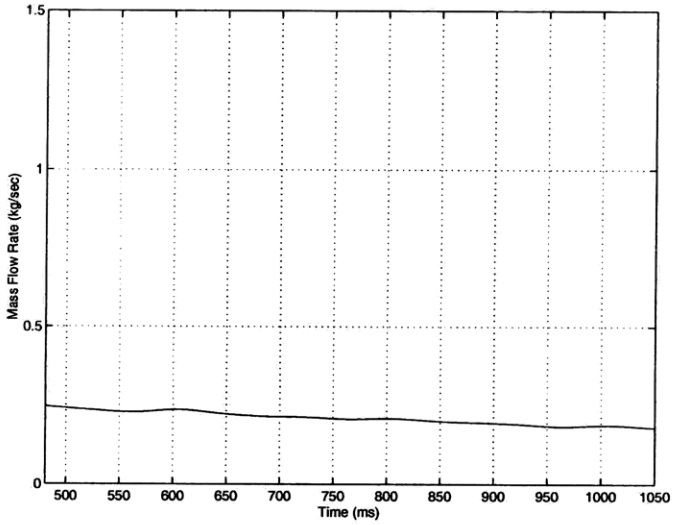

(c) $\dot{m}$

Figure B-1: Coolant flow test #001. Test gas: argon.

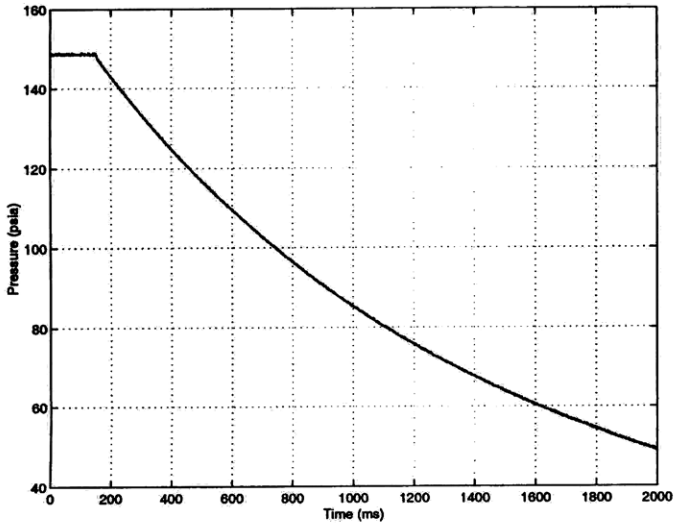

(a) Pressure

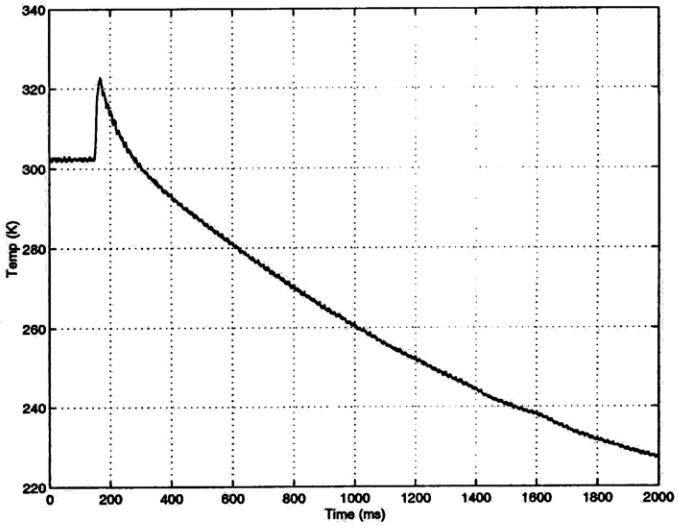

(b) Temperature

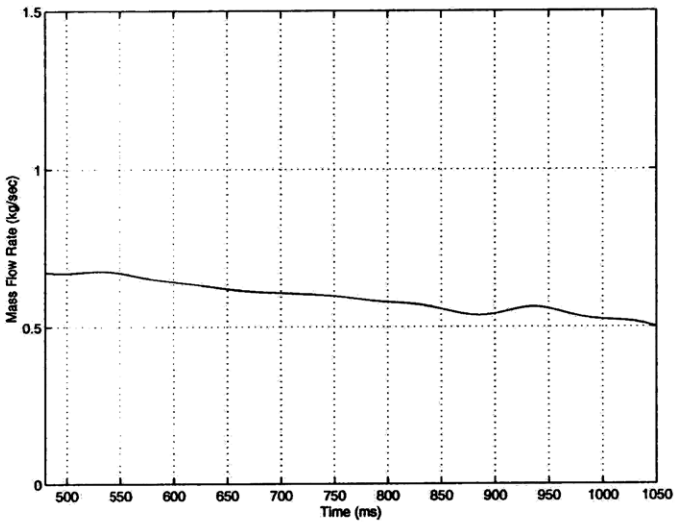

(c) $\dot{m}$

Figure B-2: Coolant flow test #002. Test gas: argon.

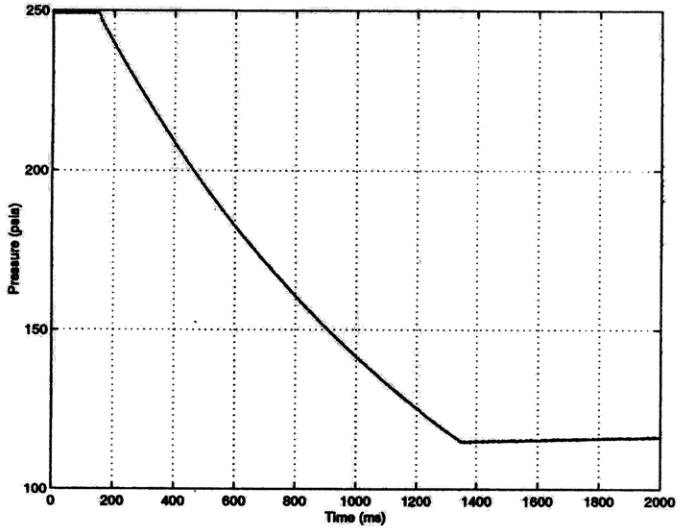

(a) Pressure

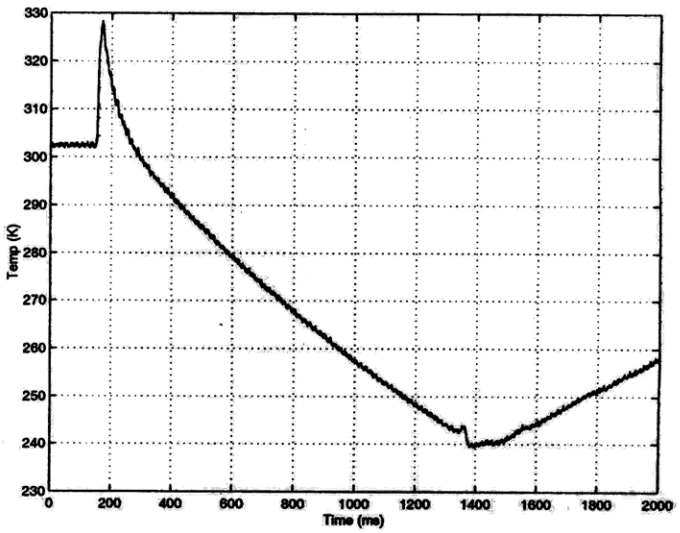

(b) Temperature

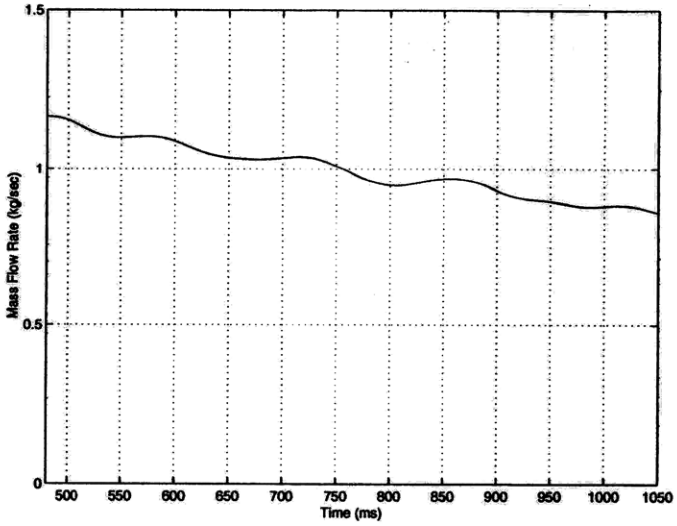

(c) $\dot{m}$

Figure B-3: Coolant flow test #003. Test gas: argon.

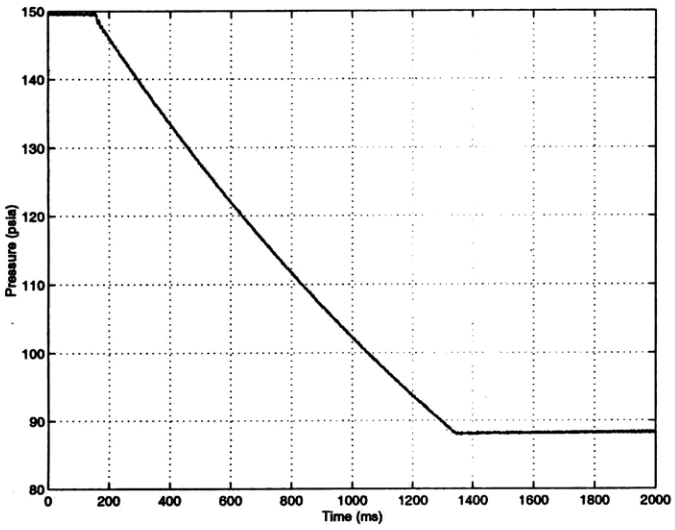

(a) Pressure

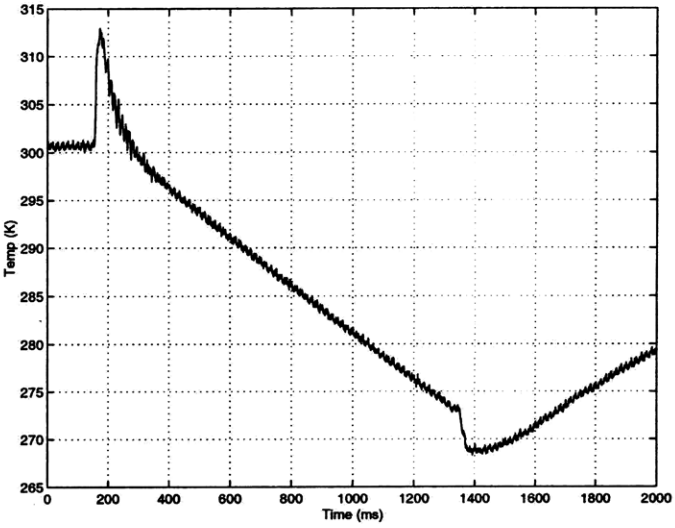

(b) Temperature

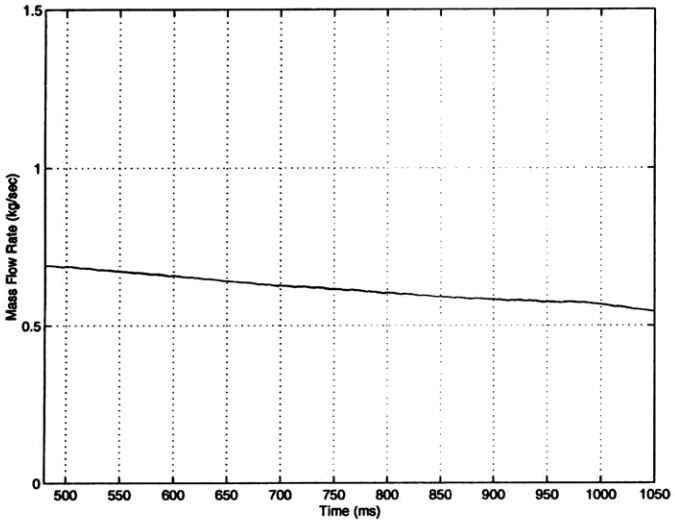

(c) $\dot{m}$

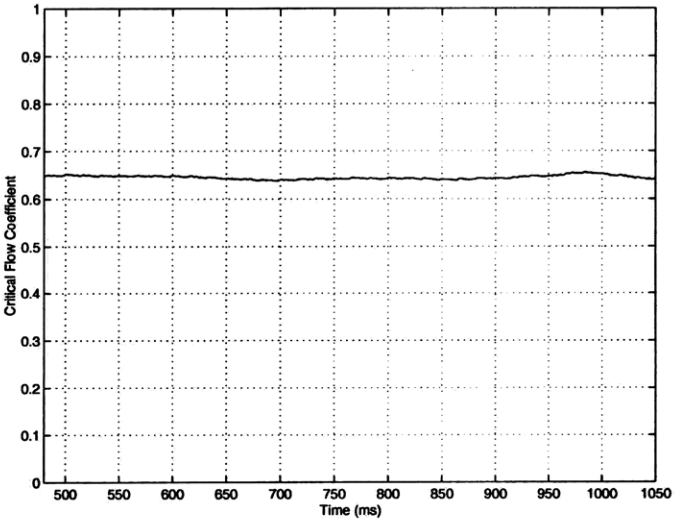

(d) C_R

Figure B-4: Coolant flow test #004. Test gas: CO_2.

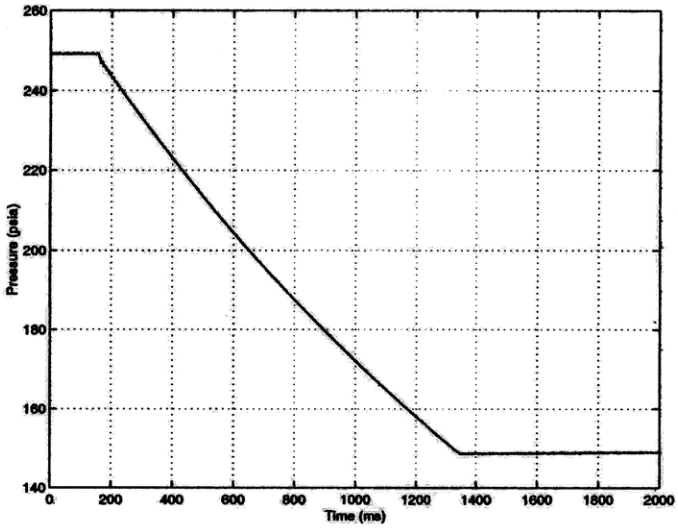

(a) Pressure

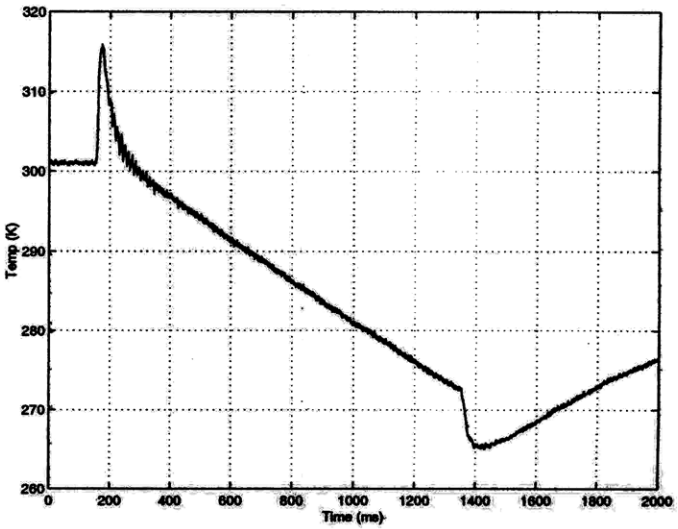

(b) Temperature

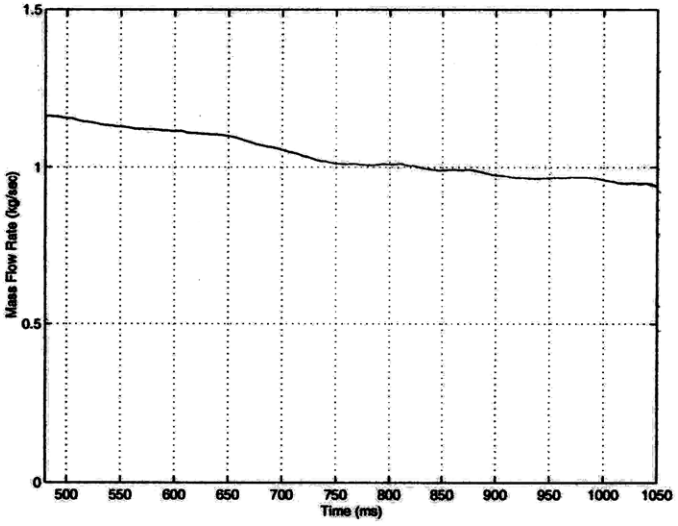

(c) $\dot{m}$

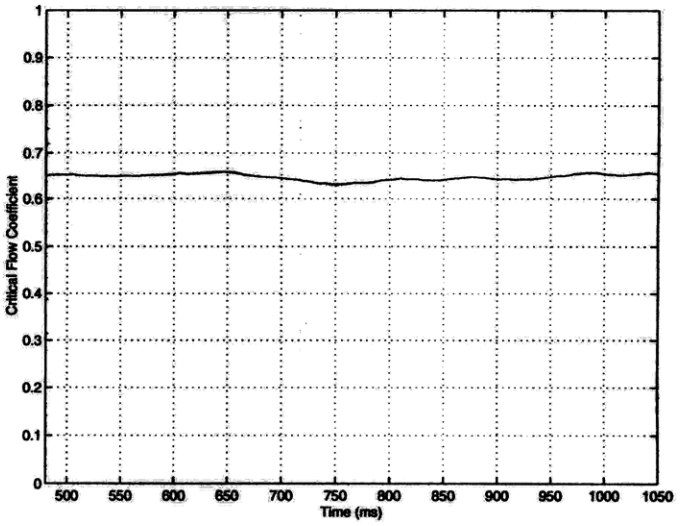

(d) C_R

Figure B-5: Coolant flow test #005. Test gas: CO_2.

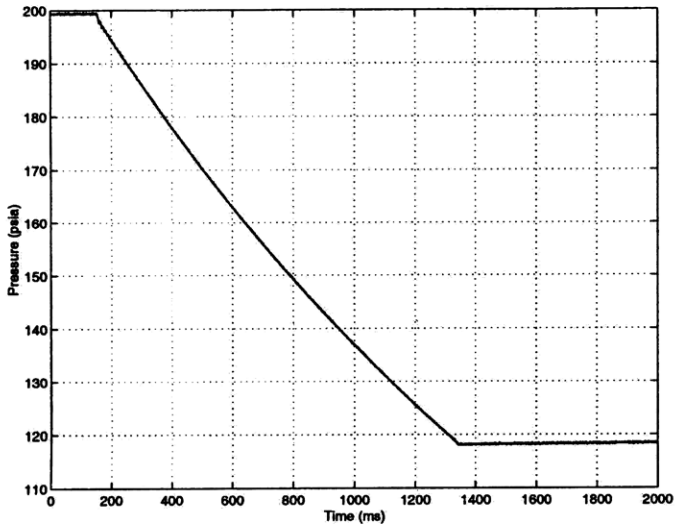

(a) Pressure

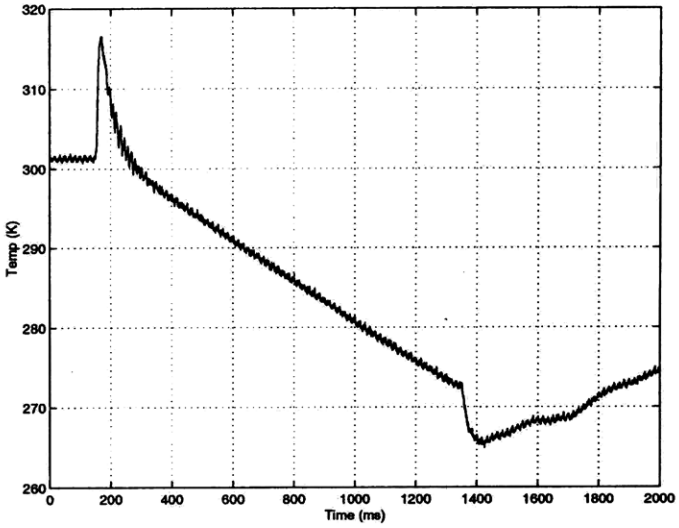

(b) Temperature

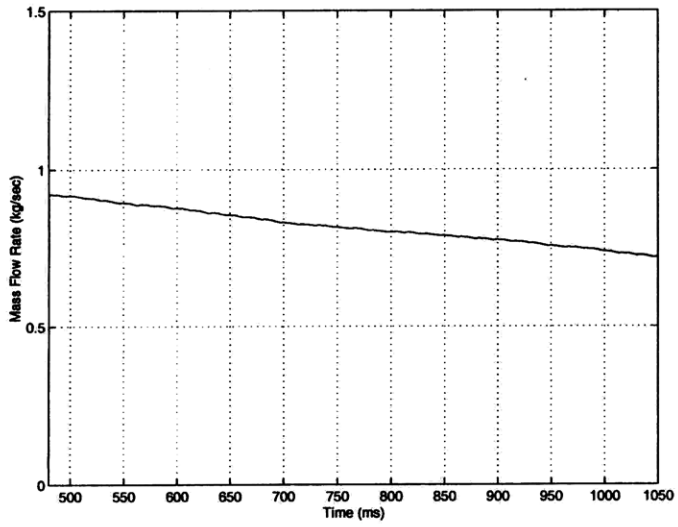

(c) $\dot{m}$

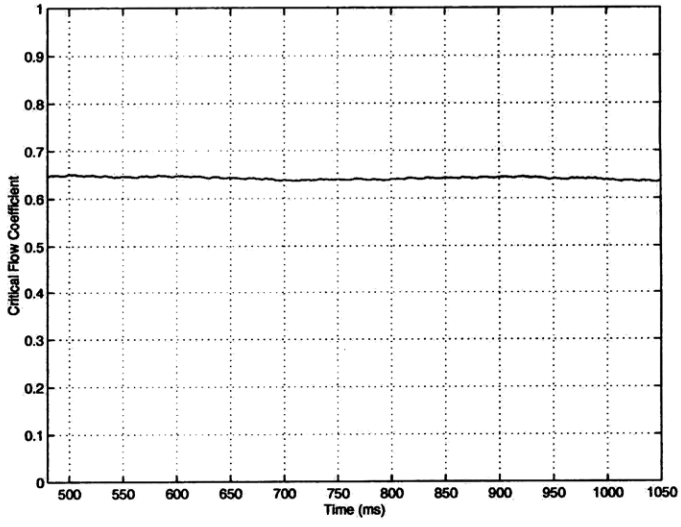

(d) C_R

Figure B-6: Coolant flow test #006. Test gas: CO_2.

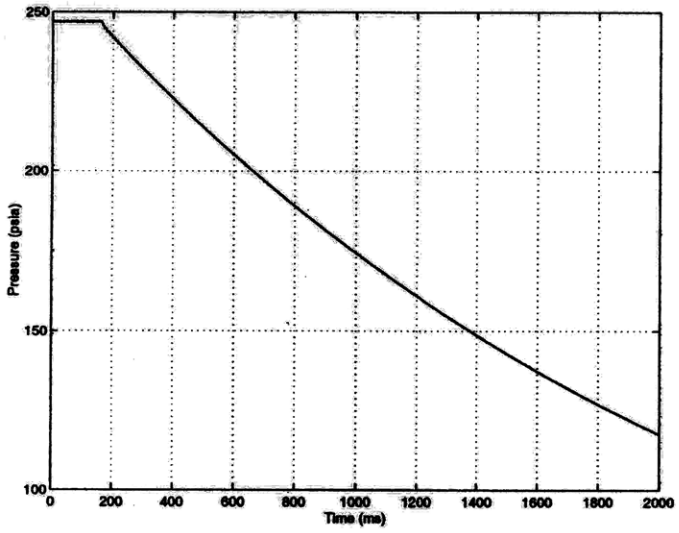

(a) Pressure

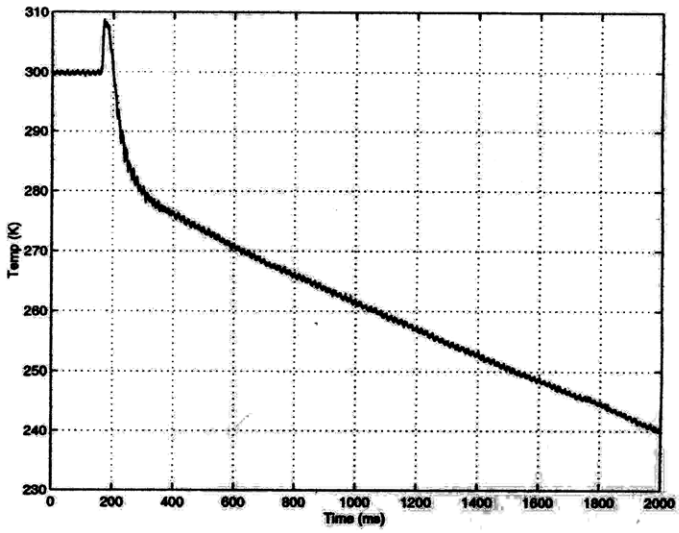

(b) Temperature

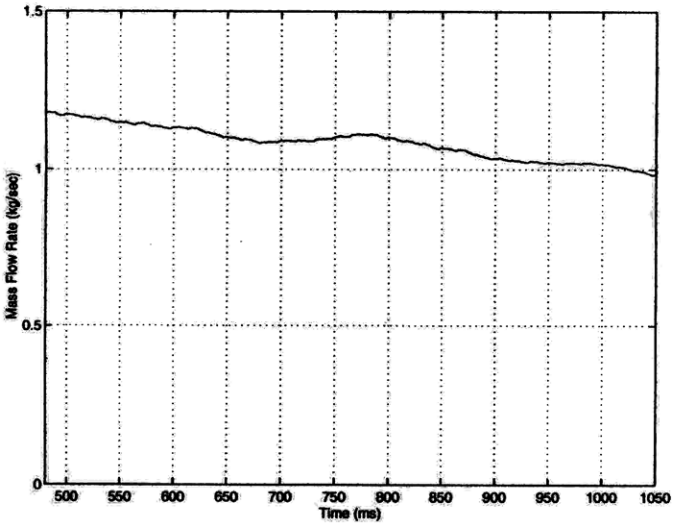

(c) $\dot{m}$

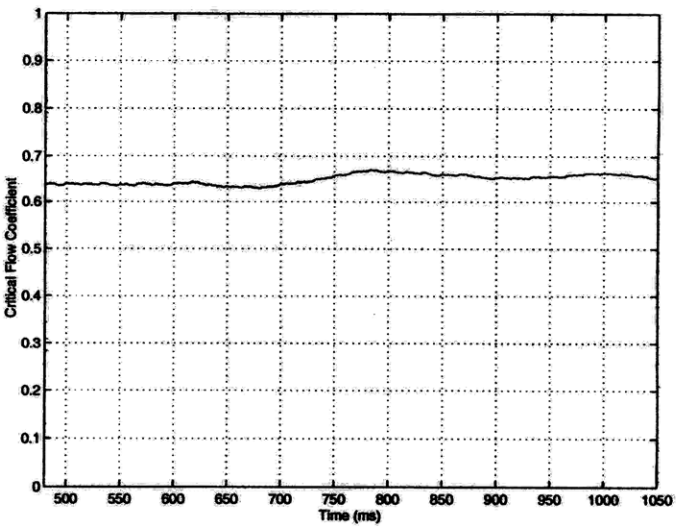

(d) C_R

Figure B-7: Coolant flow test #007. Test gas: CO_2.

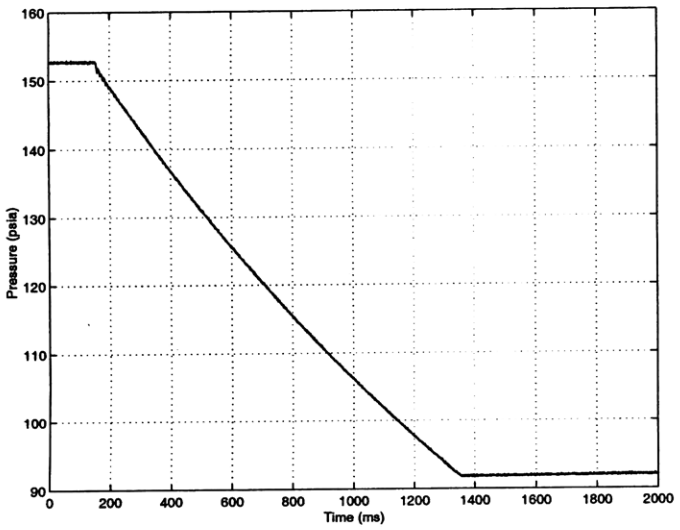

(a) Pressure

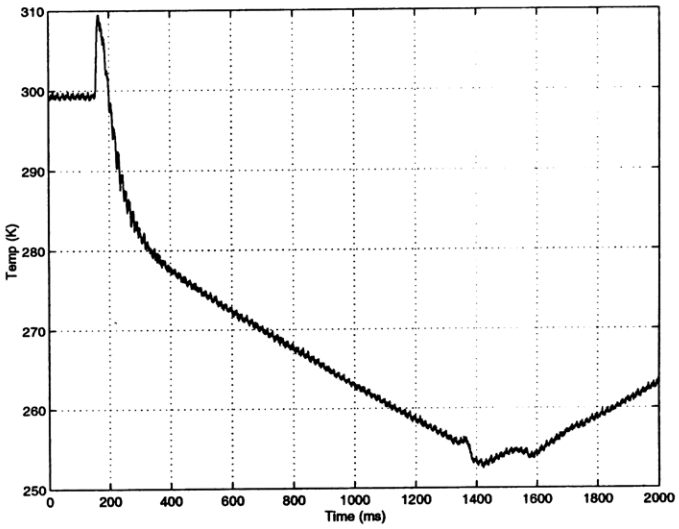

(b) Temperature

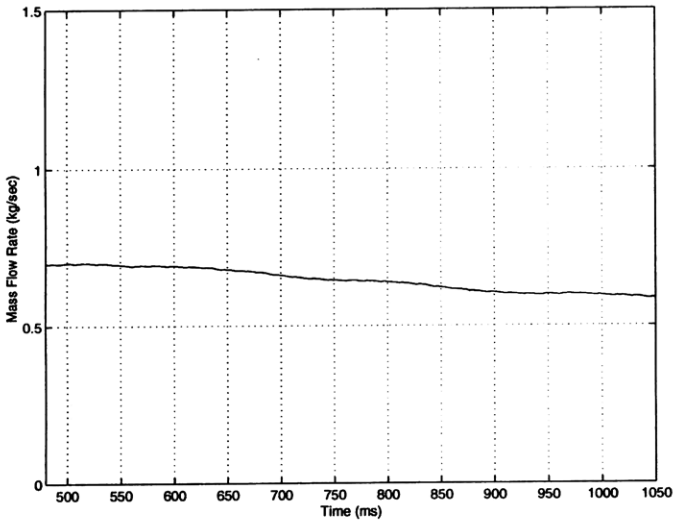

(c) $\dot{m}$

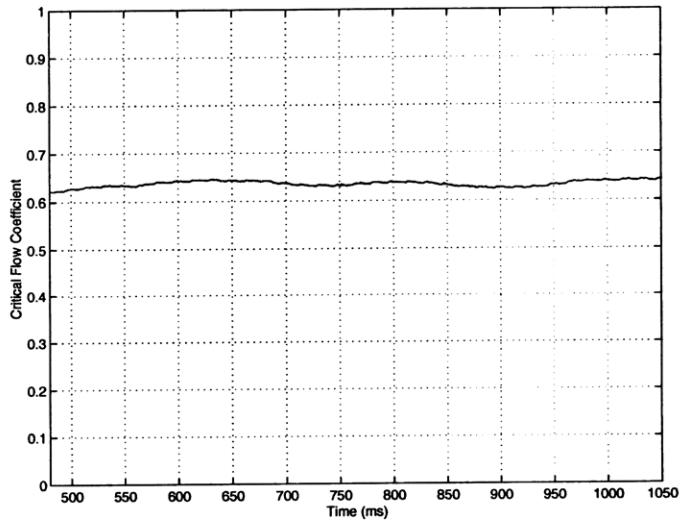

(d) C_R

Figure B-8: Coolant flow test #008. Test gas: CO_2.

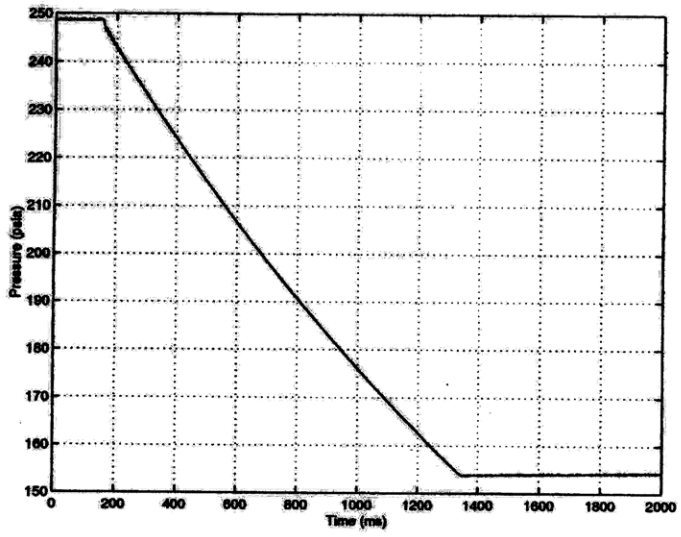

(a) Pressure

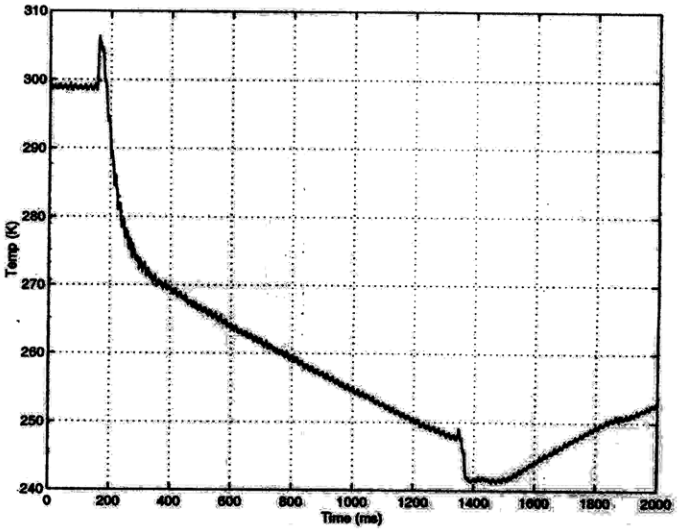

(b) Temperature

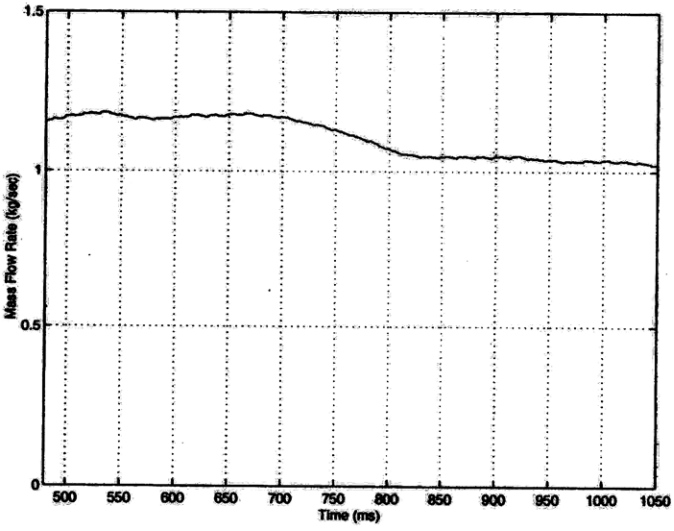

(c) $\dot{m}$

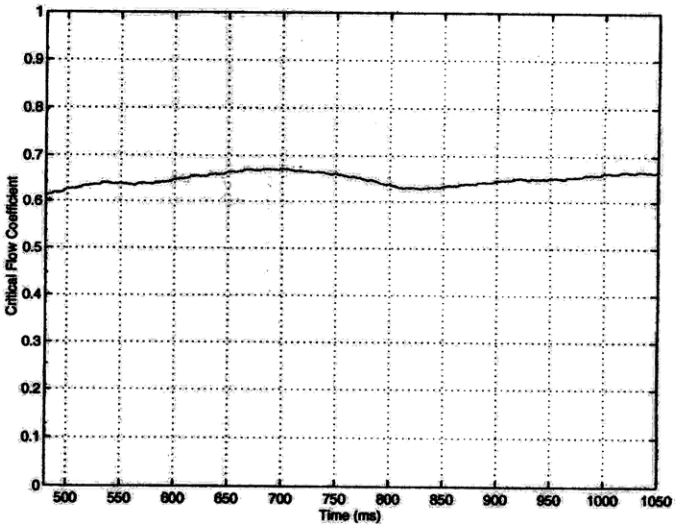

(d) C_R

Figure B-9: Coolant flow test #009. Test gas: CO_2.

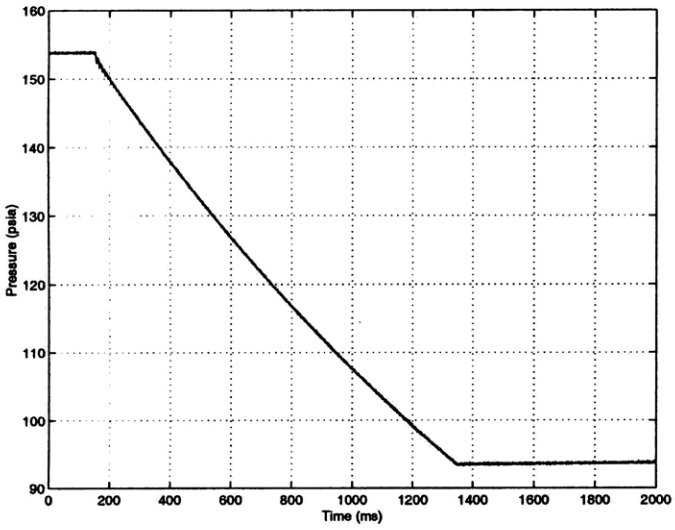

(a) Pressure

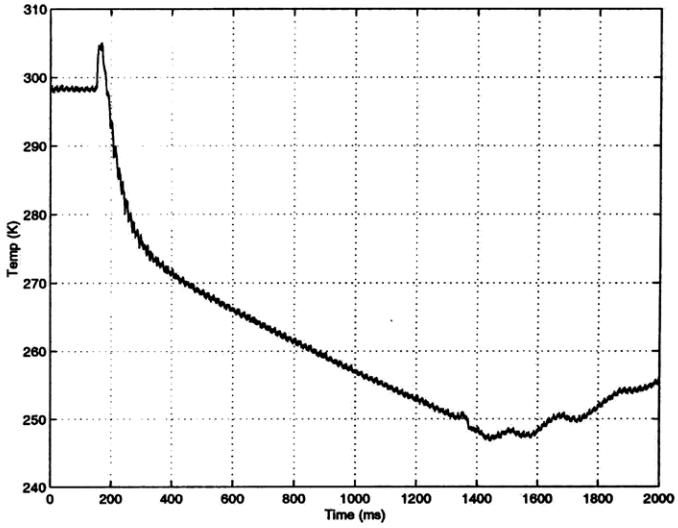

(b) Temperature

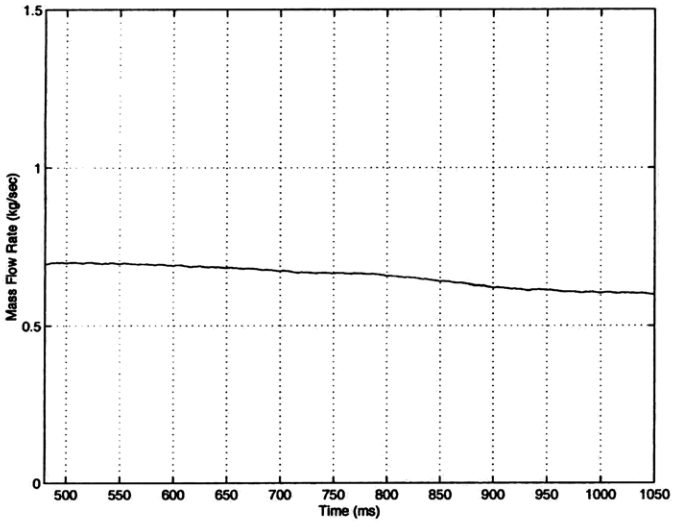

(c) $\dot{m}$

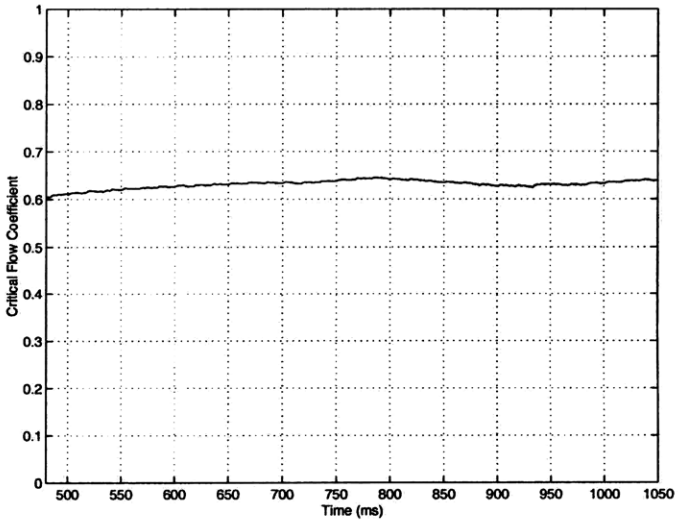

(d) C_R

Figure B-10: Coolant flow test #010. Test gas: CO_2.

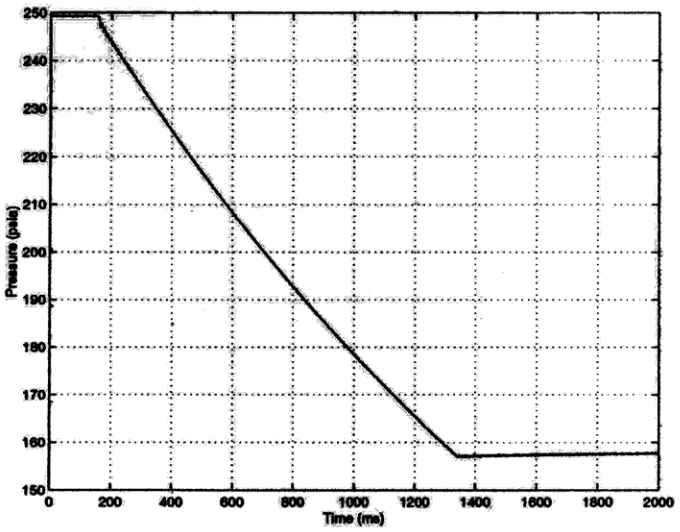

(a) Pressure

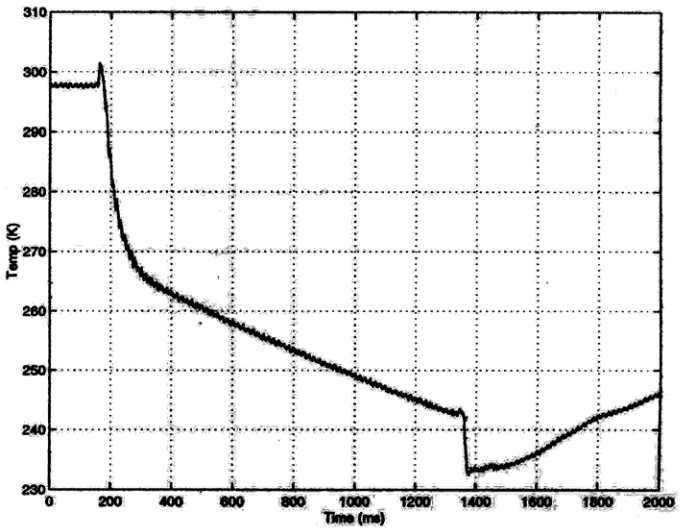

(b) Temperature

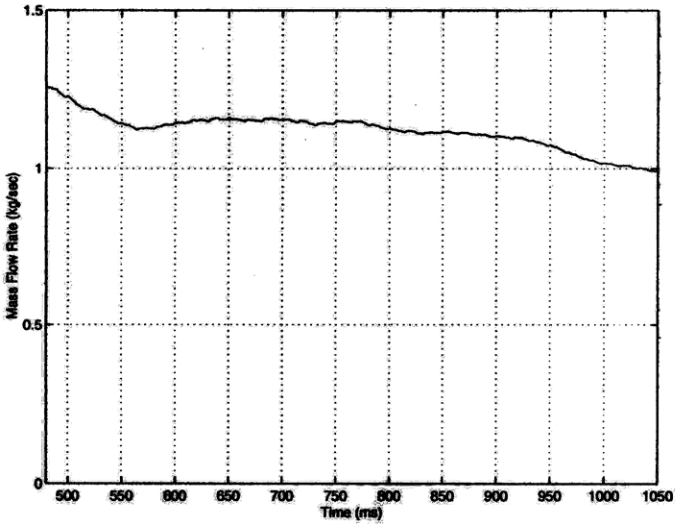

(c) $\dot{m}$

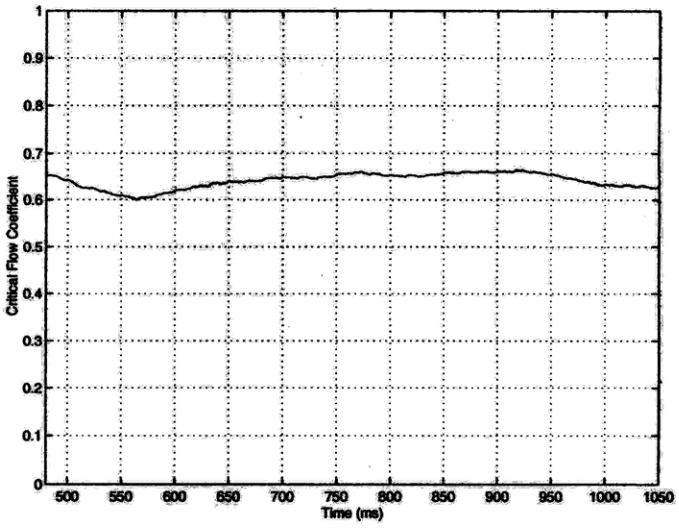

(d) C_R

Figure B-11: Coolant flow test #011. Test gas: CO_2.

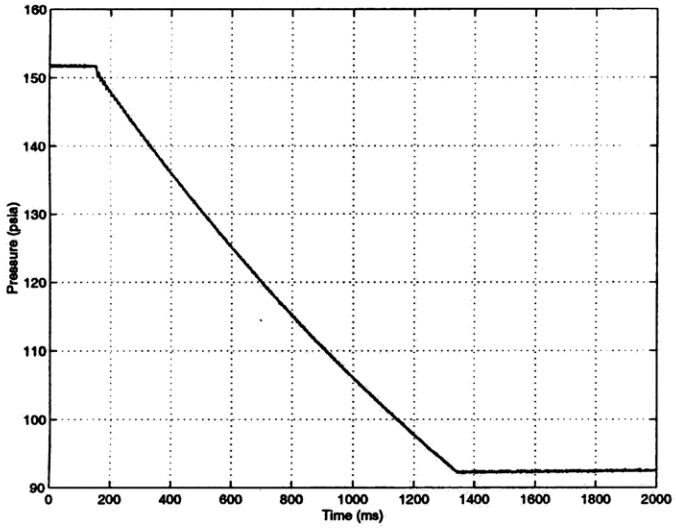

(a) Pressure

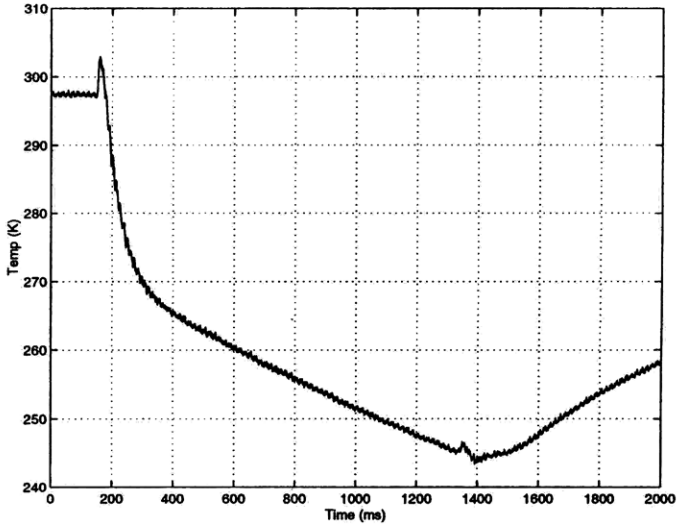

(b) Temperature

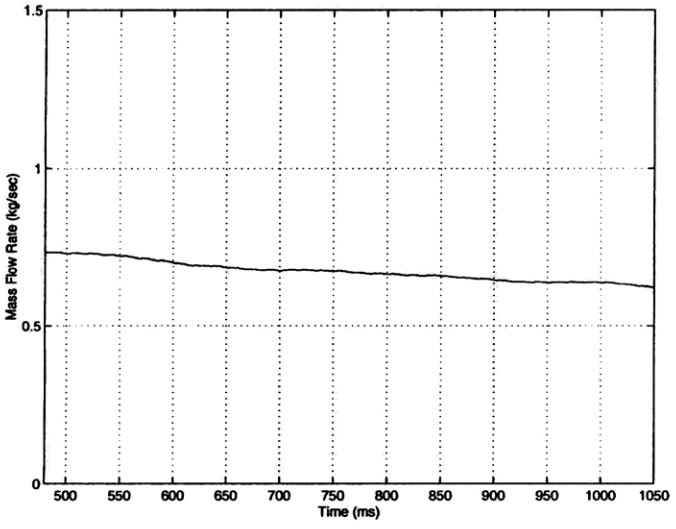

(c) $\dot{m}$

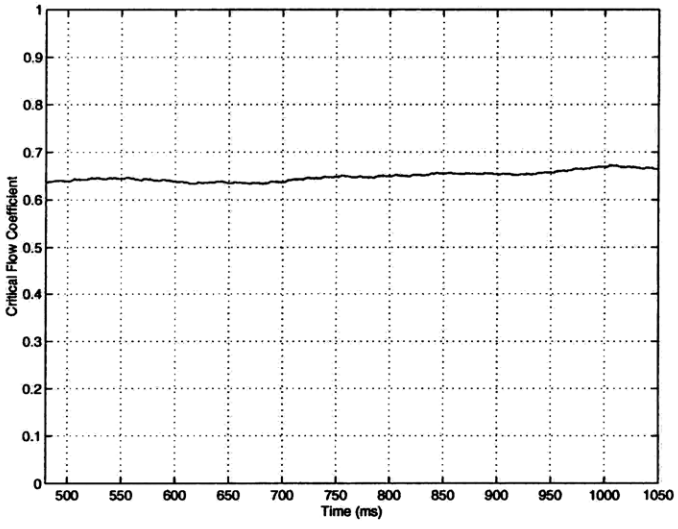

(d) C_R

Figure B-12: Coolant flow test #012. Test gas: CO_2.

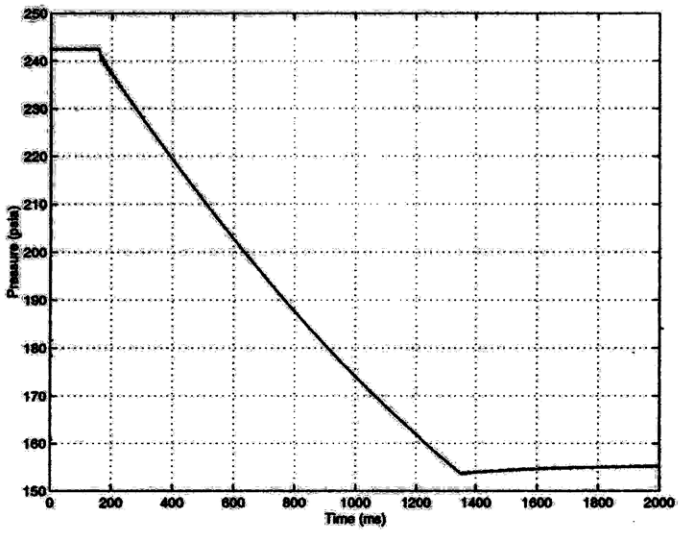

(a) Pressure

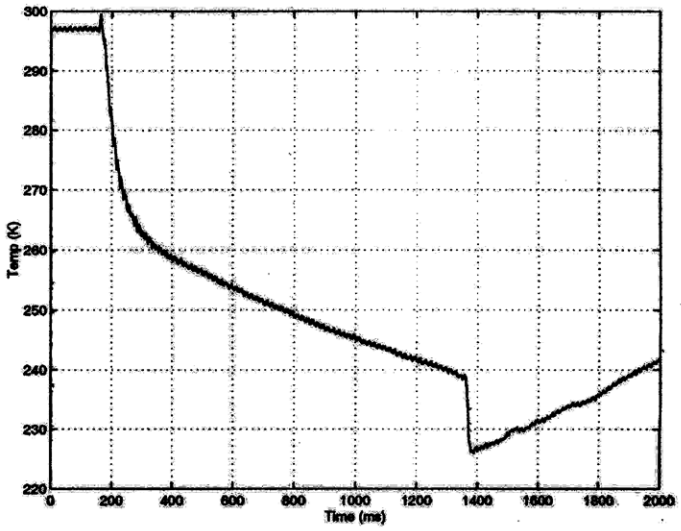

(b) Temperature

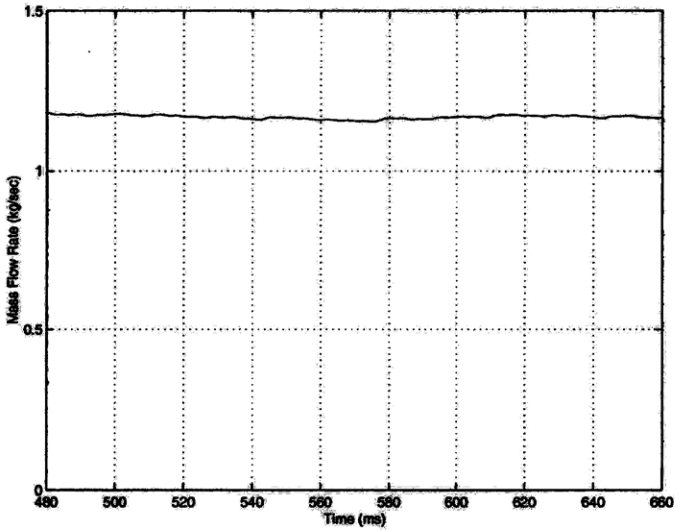

(c) $\dot{m}$

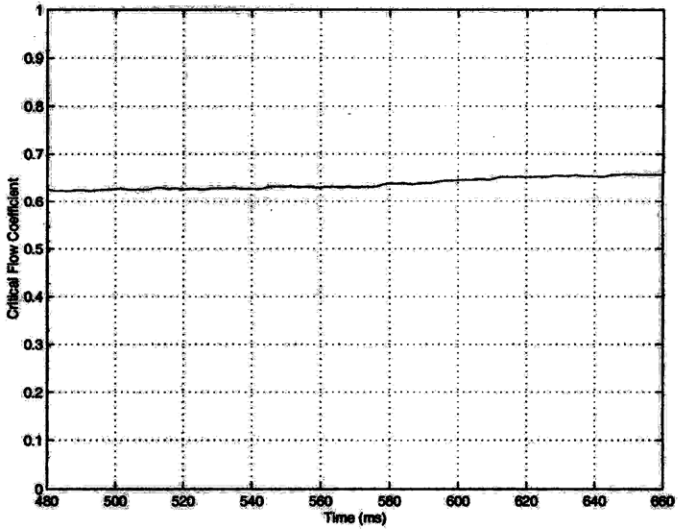

(d) C_R

Figure B-13: Coolant flow test #013. Test gas: CO_2. Data for a limited range of time is presented due to conditions in the coolant supply tank below the condensation limits.

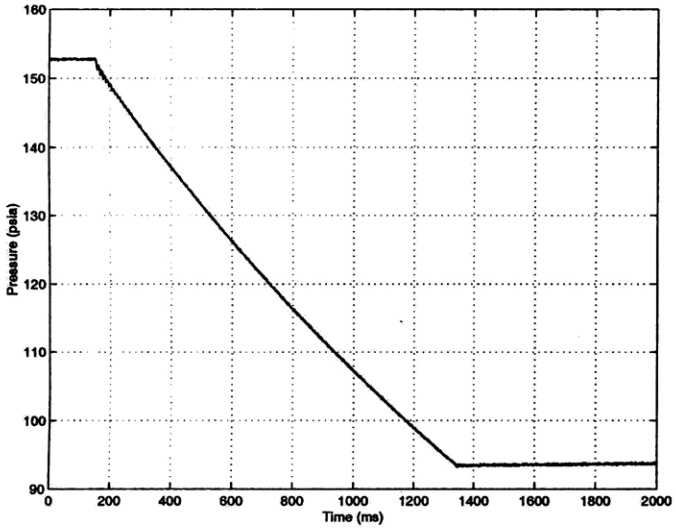

(a) Pressure

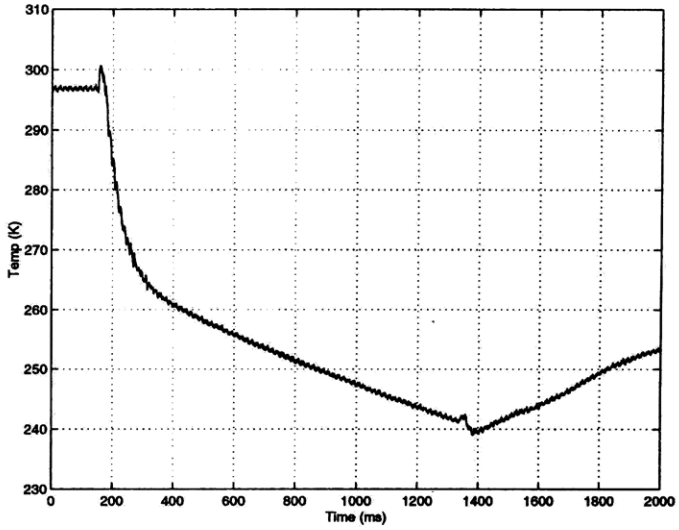

(b) Temperature

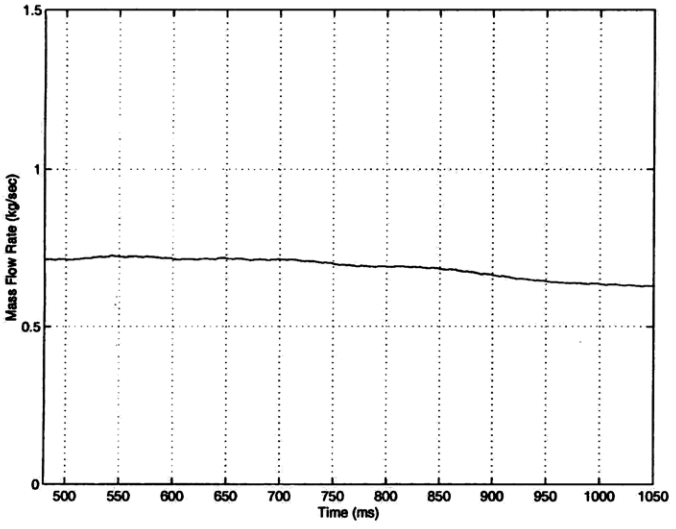

(c) $\dot{m}$

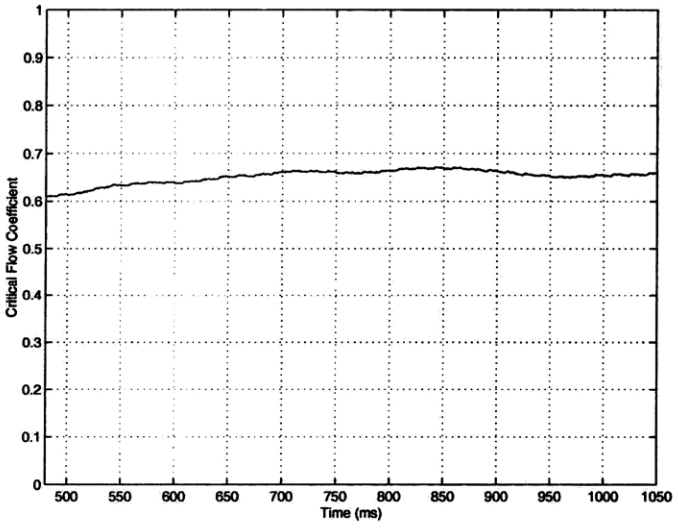

(d) C_R

Figure B-14: Coolant flow test #014. Test gas: CO_2.

Appendix C

Film-Cooled Turbine Experimental Data

C.1 Introduction

This appendix includes the experimental data for the cooled turbine performance testing described in Chapter 7. Plots of pressure ratio, corrected speed, coolant mass flow, and efficiency are presented for all cases. Efficiency for different tests is shown on the same scale for comparison.

C.2 Figures

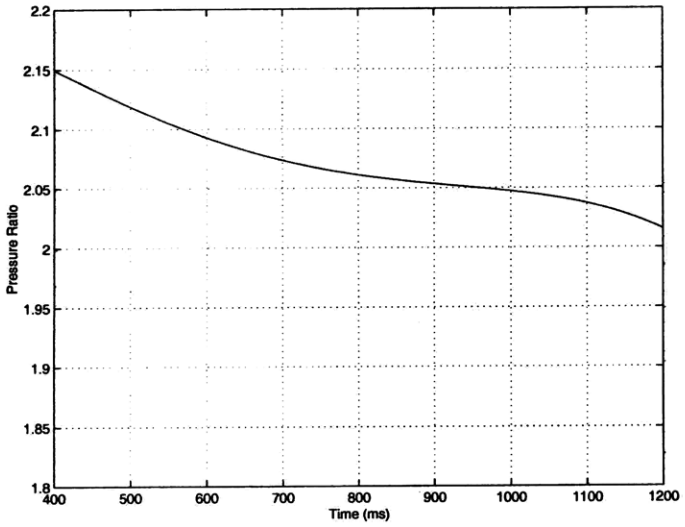

(a) Pressure ratio

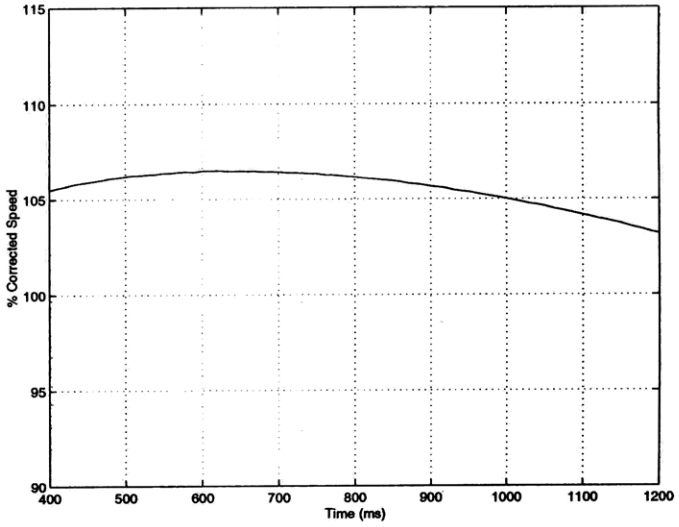

(b) Corrected speed

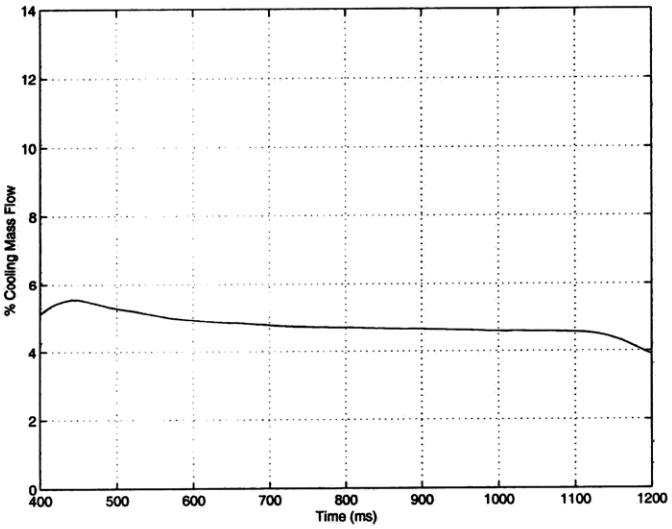

(c) Coolant mass flow

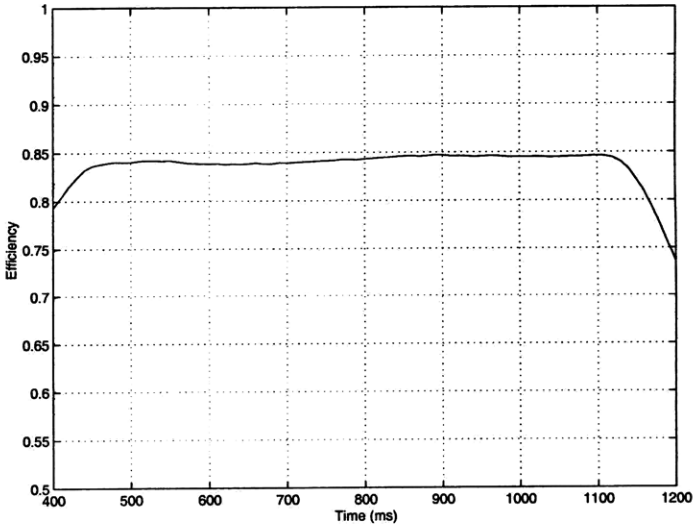

(d) Efficiency

Figure C-1: Film-cooled turbine test #001.

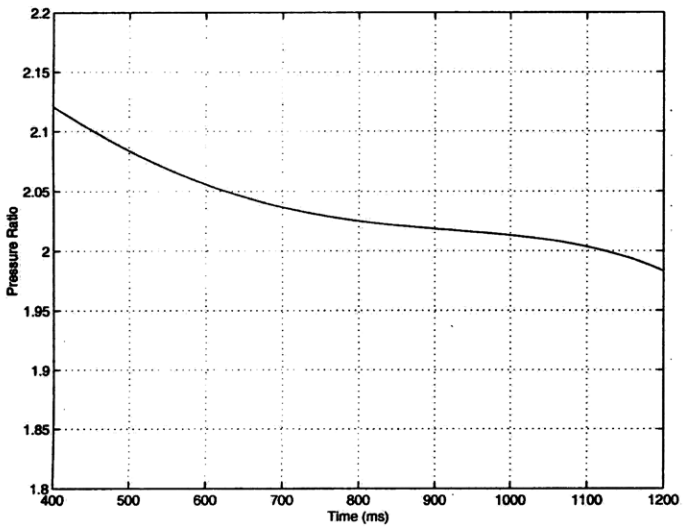

(a) Pressure ratio

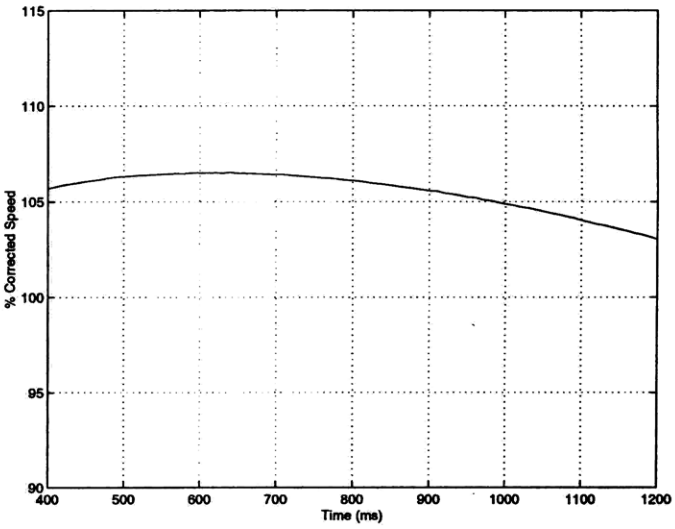

(b) Corrected speed

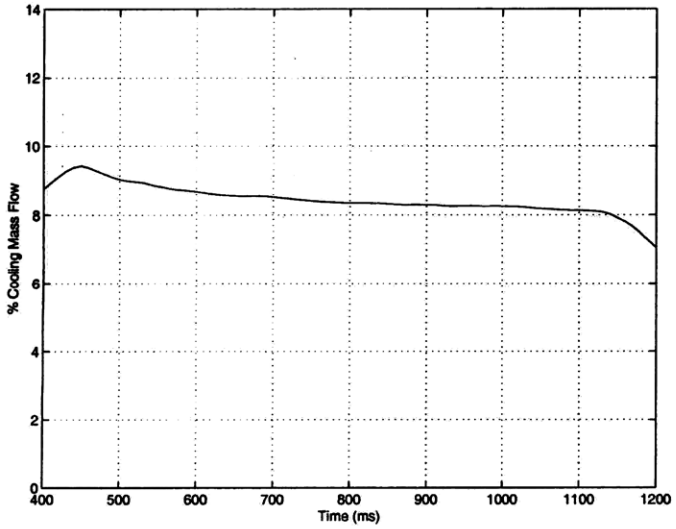

(c) Coolant mass flow

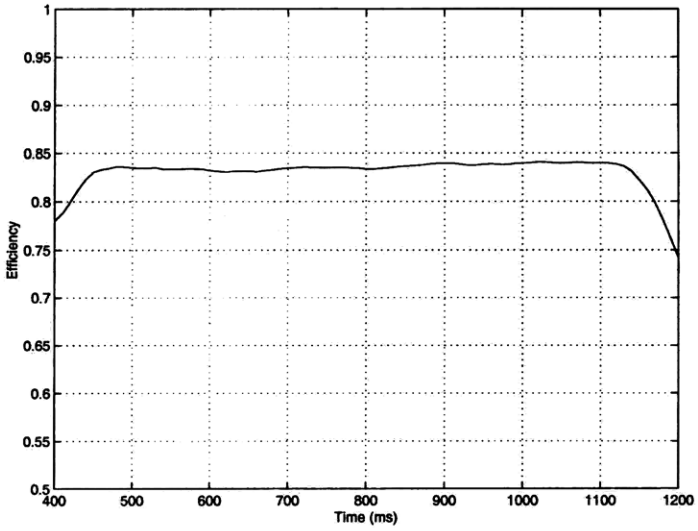

(d) Efficiency

Figure C-2: Film-cooled turbine test #002.

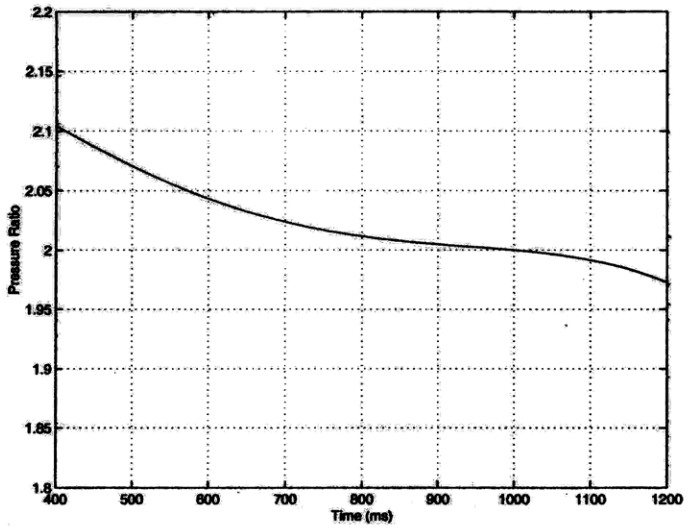

(a) Pressure ratio

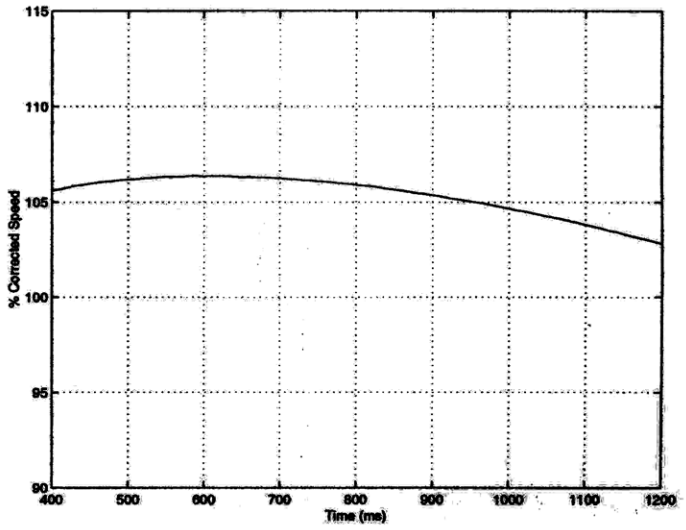

(b) Corrected speed

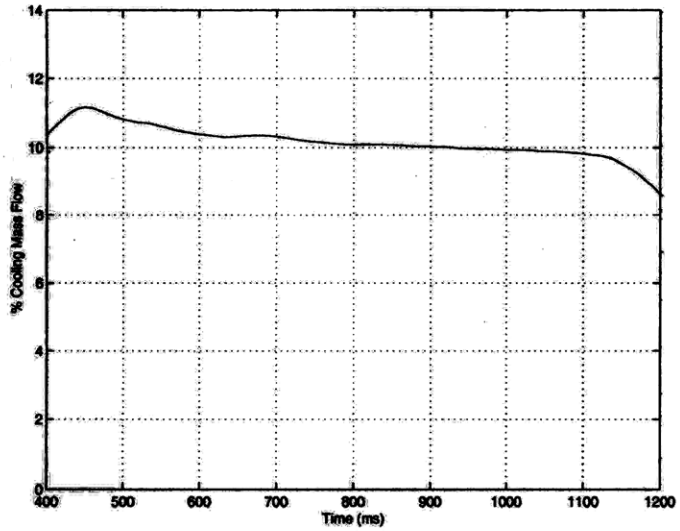

(c) Coolant mass flow

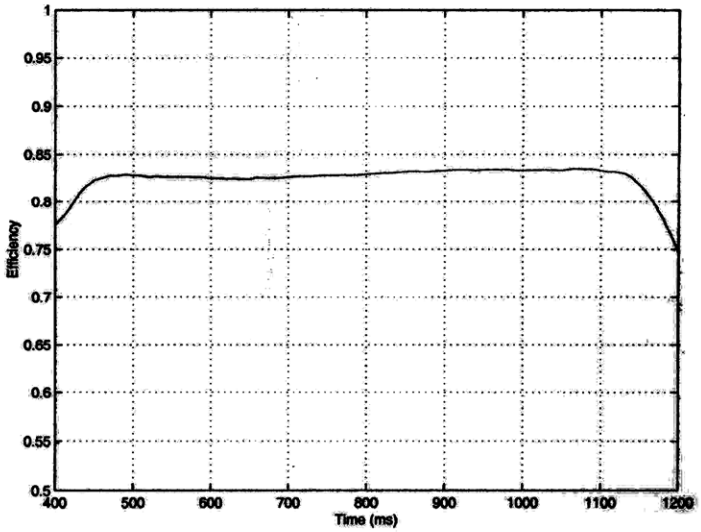

(d) Efficiency

Figure C-3: Film-cooled turbine test #003.

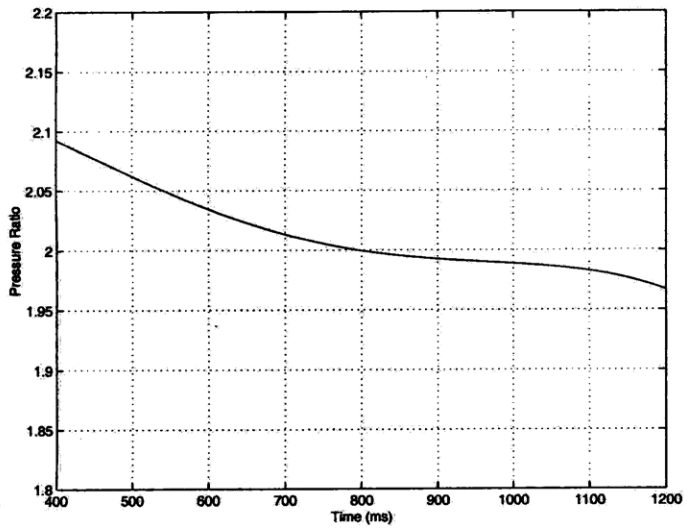

(a) Pressure ratio

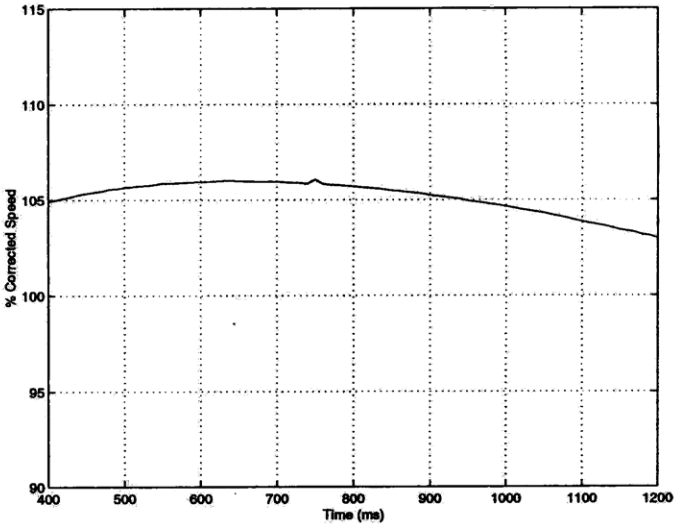

(b) Corrected speed

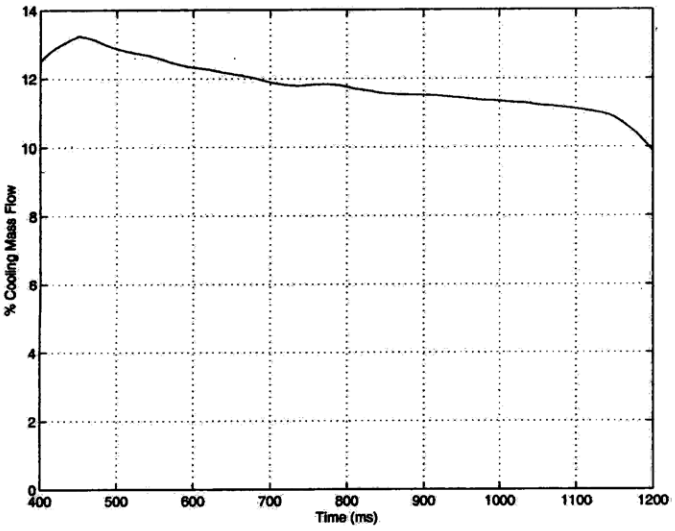

(c) Coolant mass flow

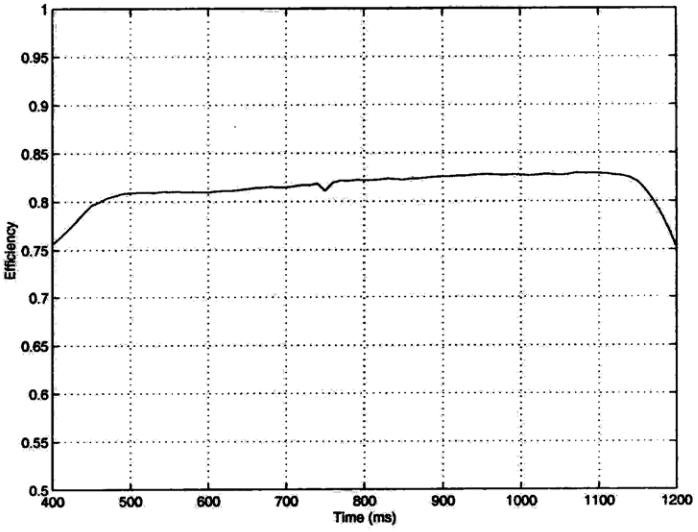

(d) Efficiency

Figure C-4: Film-cooled turbine test #004.

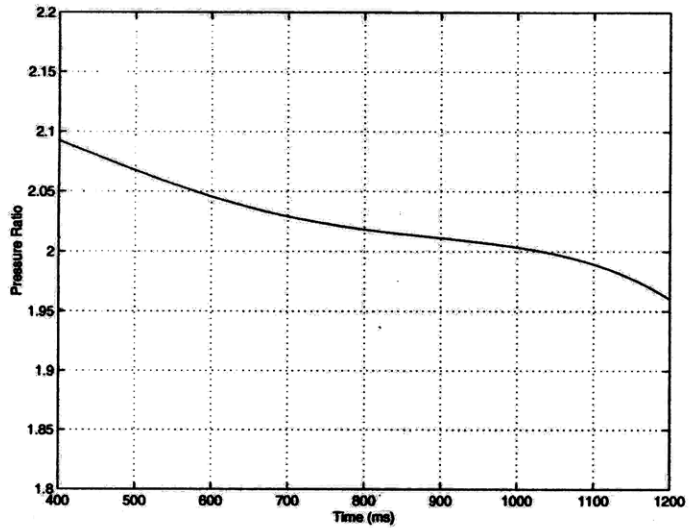

(a) Pressure ratio

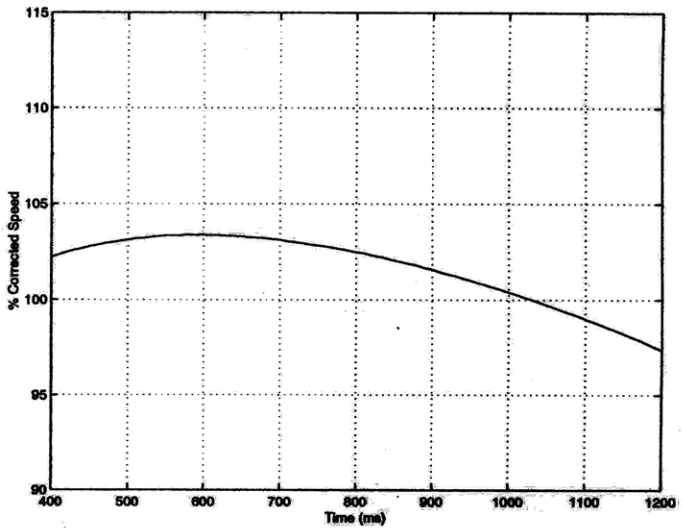

(b) Corrected speed

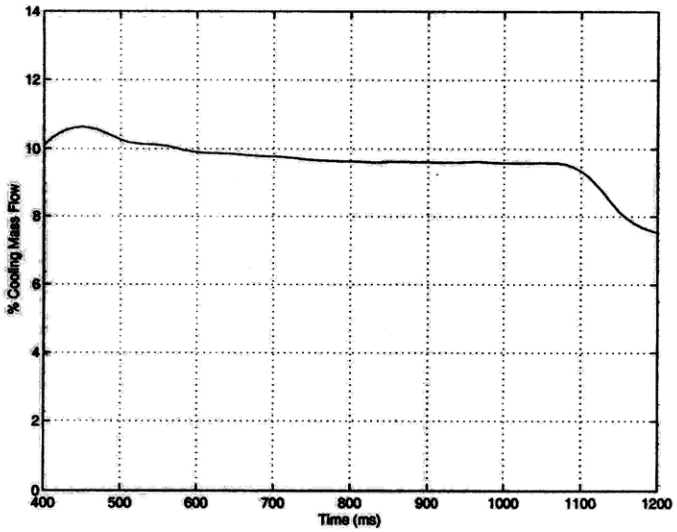

(c) Coolant mass flow

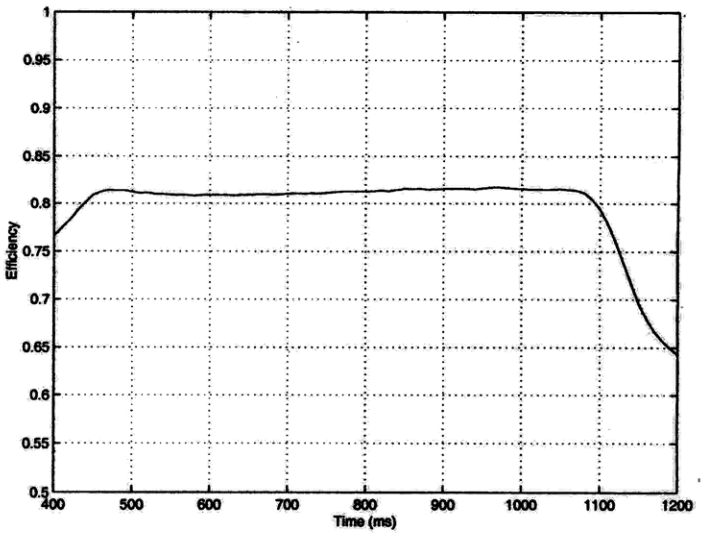

(d) Efficiency

Figure C-5: Film-cooled turbine test #005.

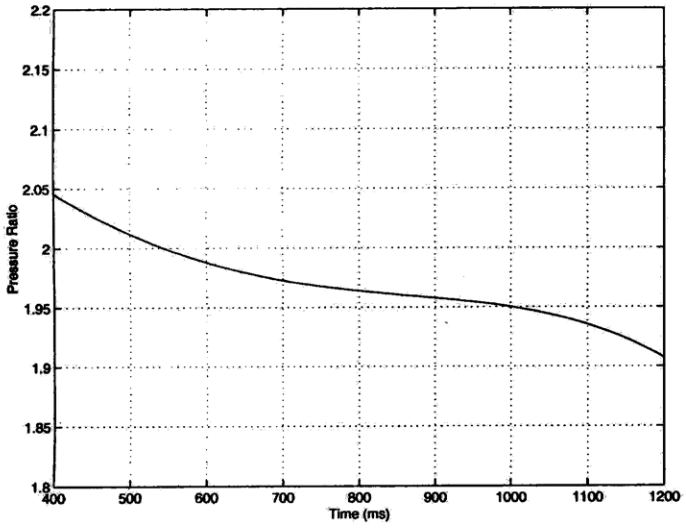

(a) Pressure ratio

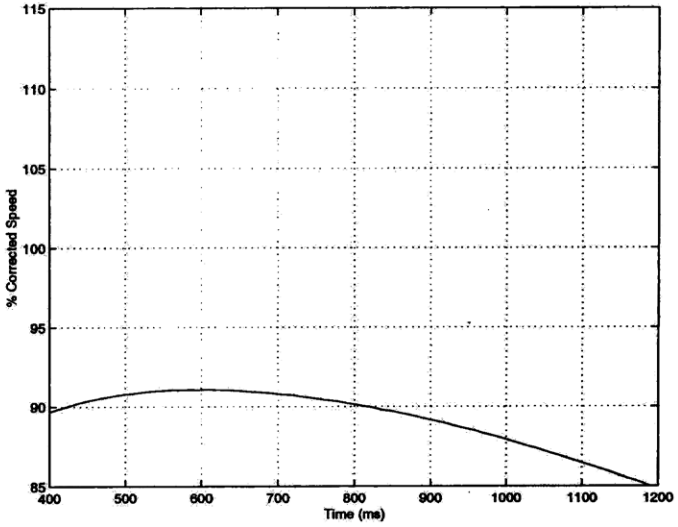

(b) Corrected speed

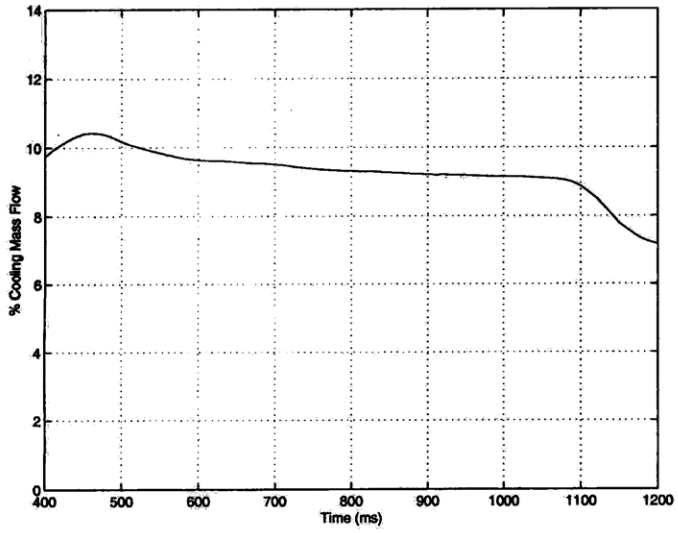

(c) Coolant mass flow

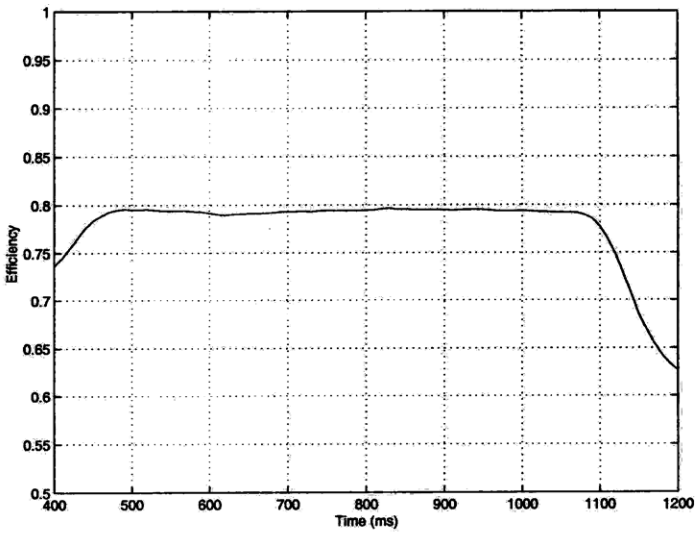

(d) Efficiency

Figure C-6: Film-cooled turbine test #006.

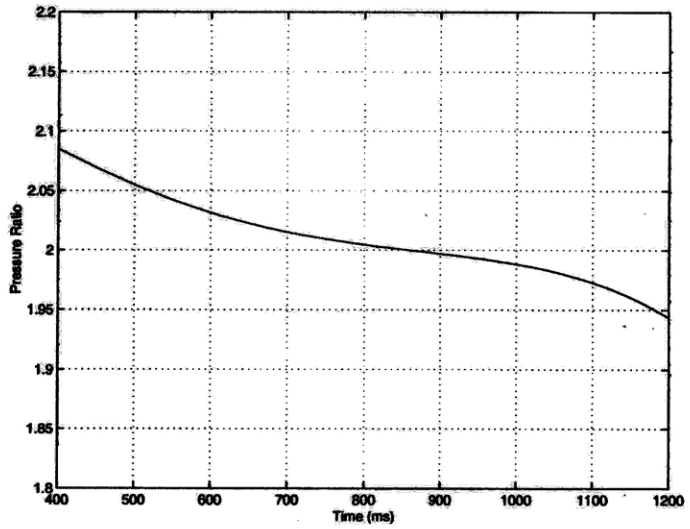

(a) Pressure ratio

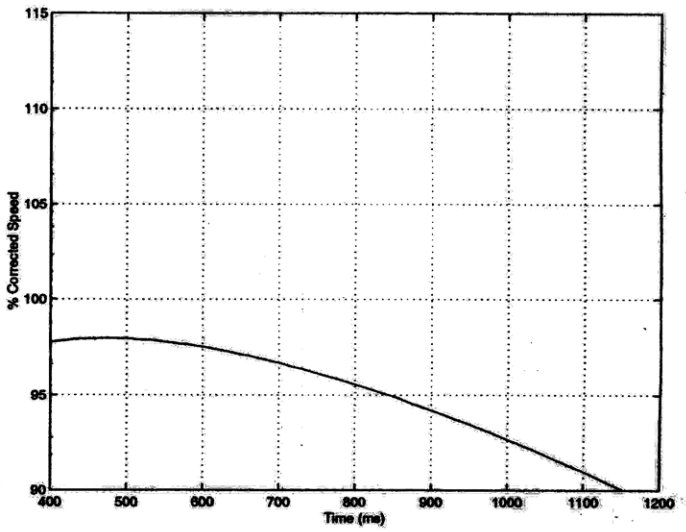

(b) Corrected speed

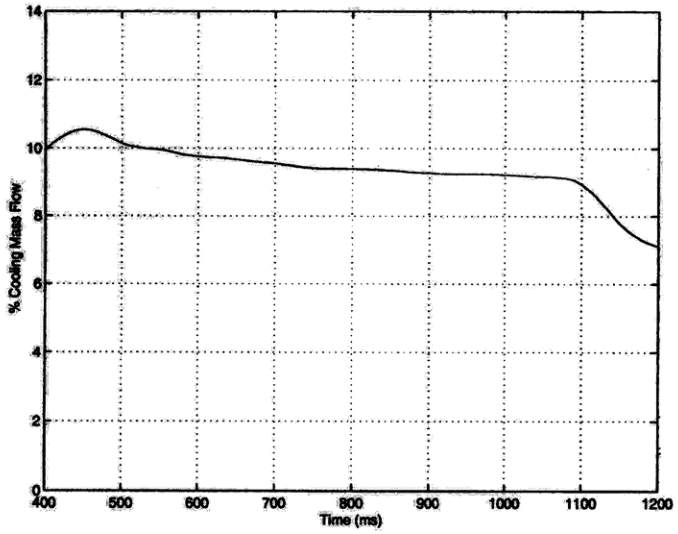

(c) Coolant mass flow

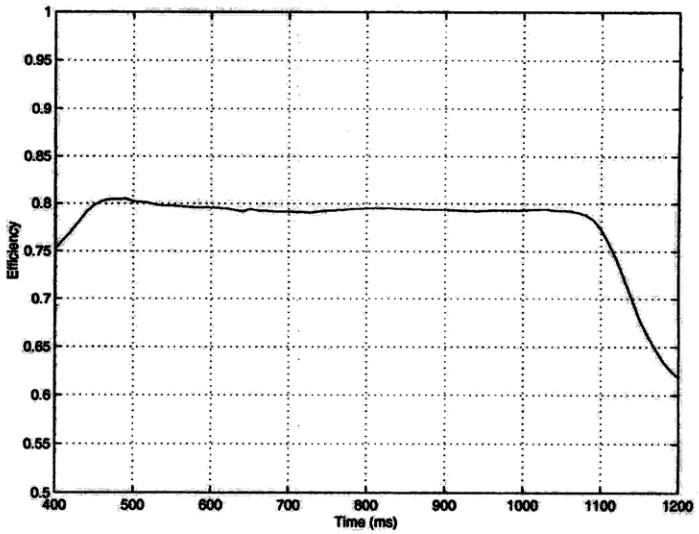

(d) Efficiency

Figure C-7: Film-cooled turbine test #007.

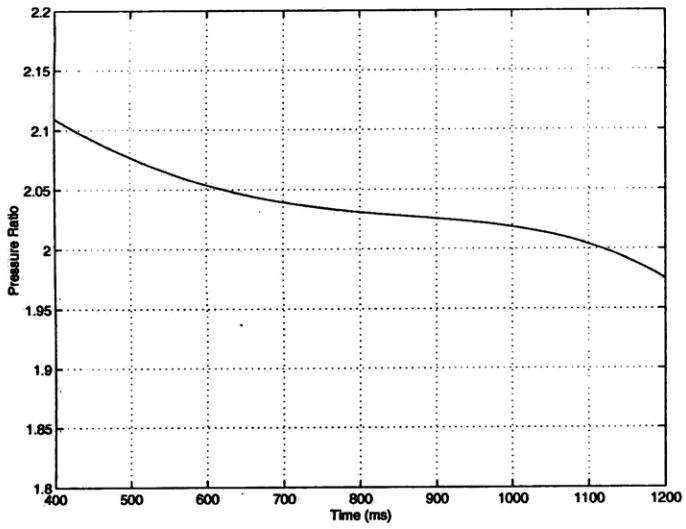

(a) Pressure ratio

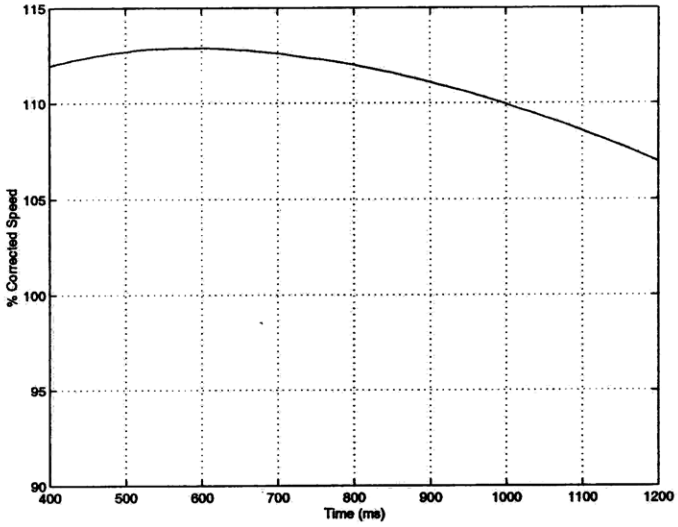

(b) Corrected speed

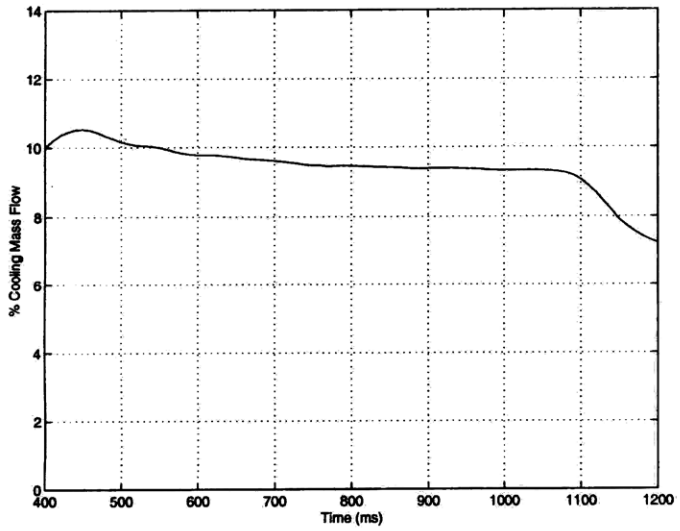

(c) Coolant mass flow

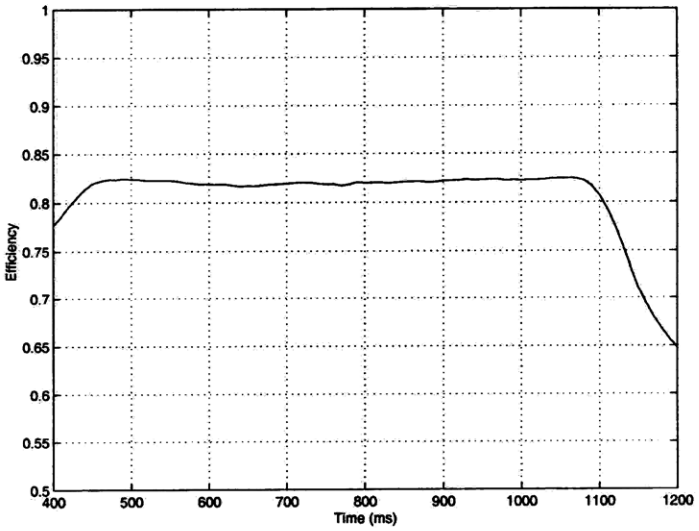

(d) Efficiency

Figure C-8: Film-cooled turbine test #008.

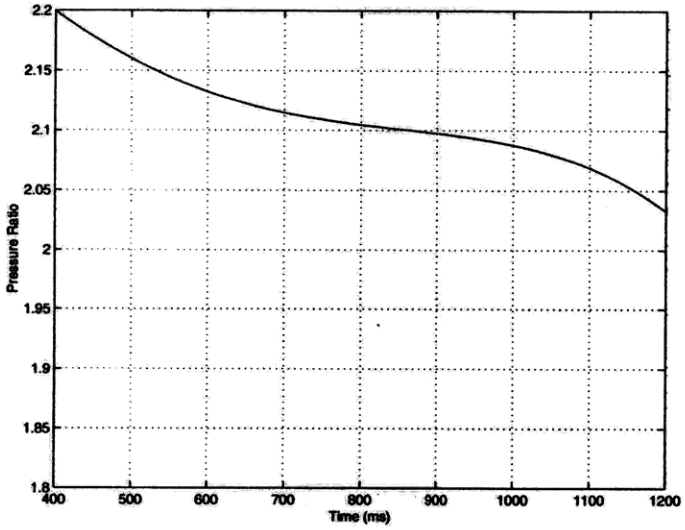

(a) Pressure ratio

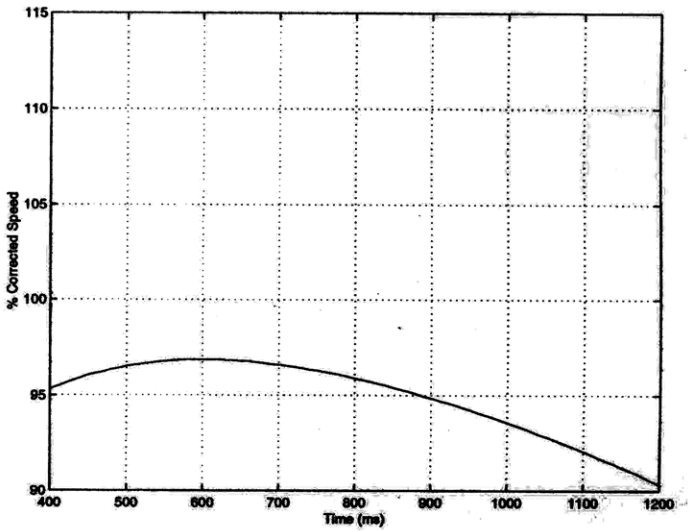

(b) Corrected speed

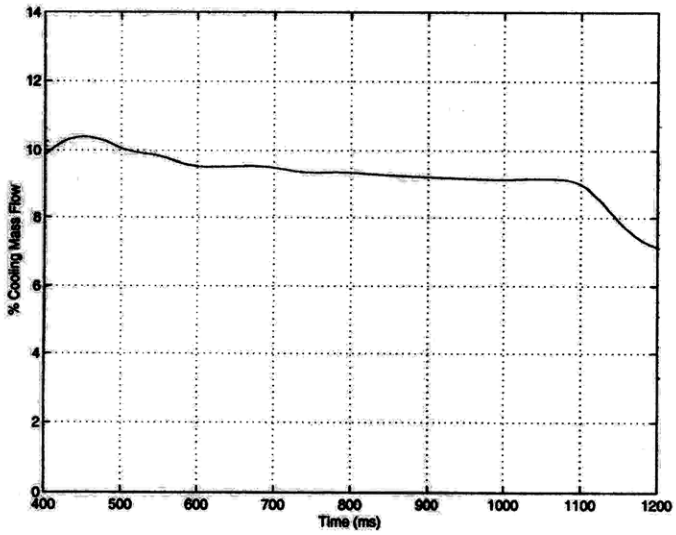

(c) Coolant mass flow

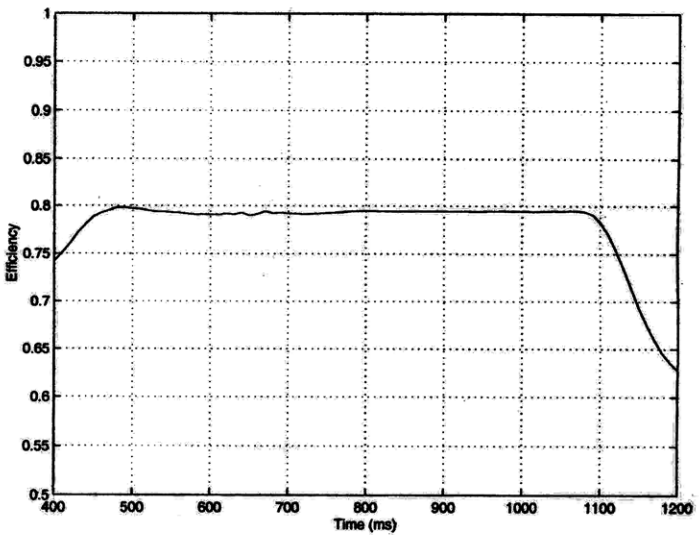

(d) Efficiency

Figure C-9: Film-cooled turbine test #009.

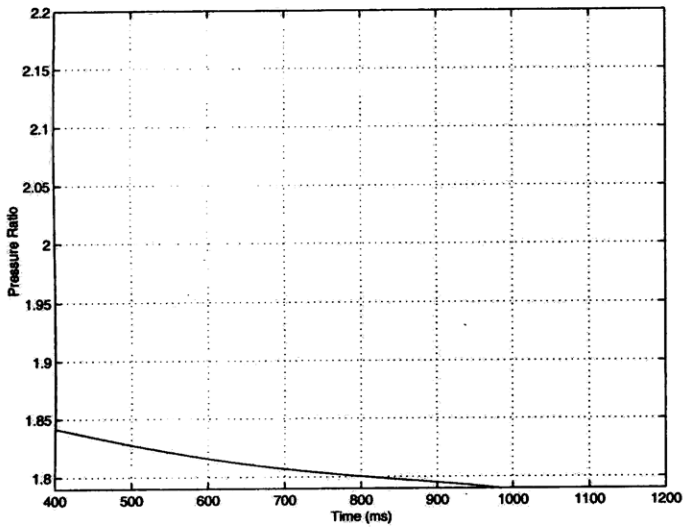

(a) Pressure ratio

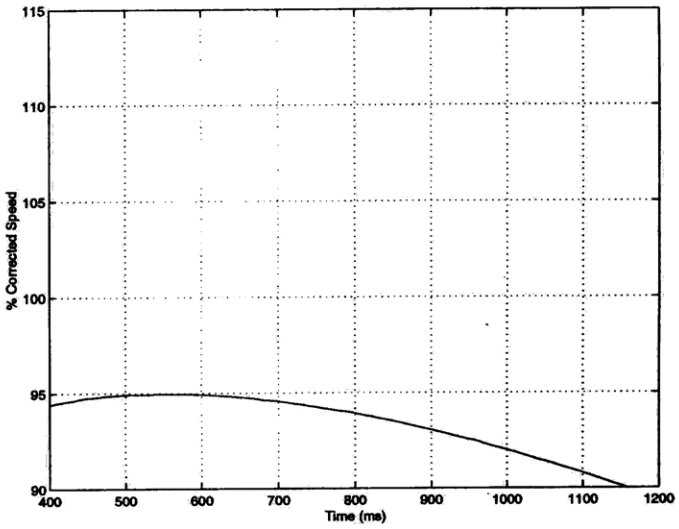

(b) Corrected speed

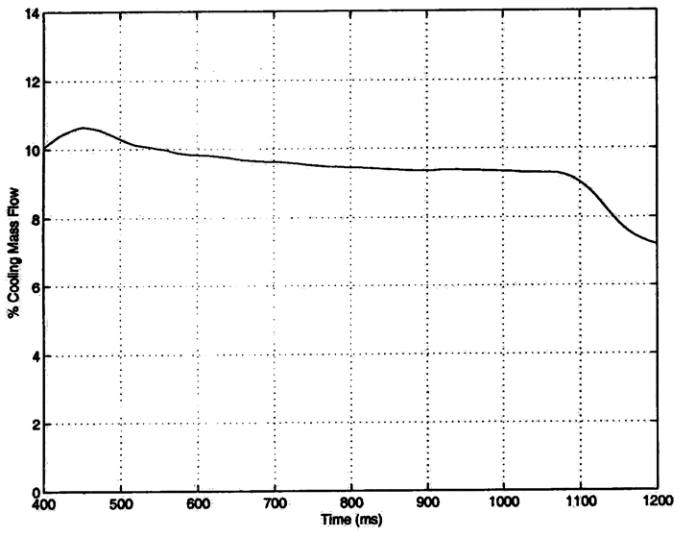

(c) Coolant mass flow

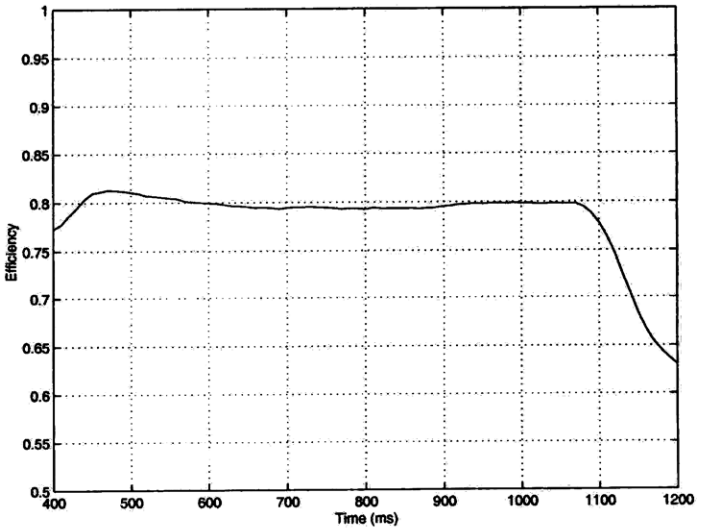

(d) Efficiency

Figure C-10: Film-cooled turbine test #010.

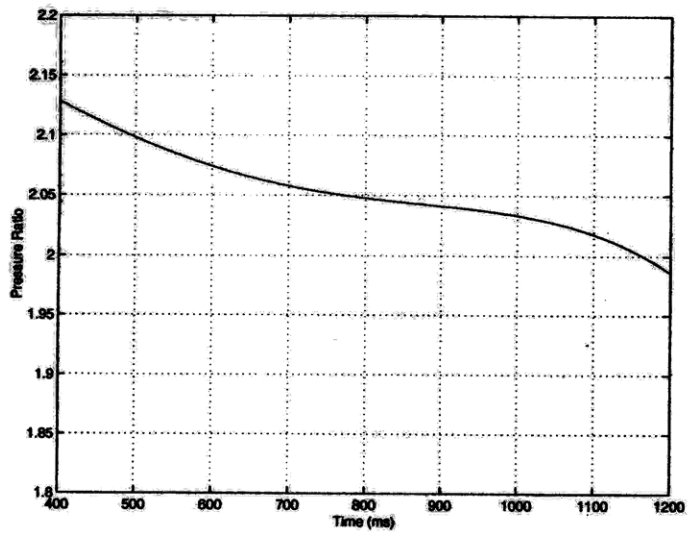

(a) Pressure ratio

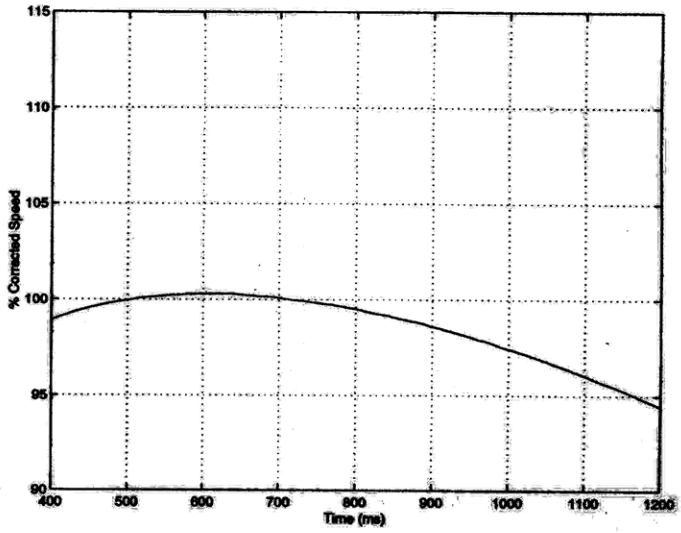

(b) Corrected speed

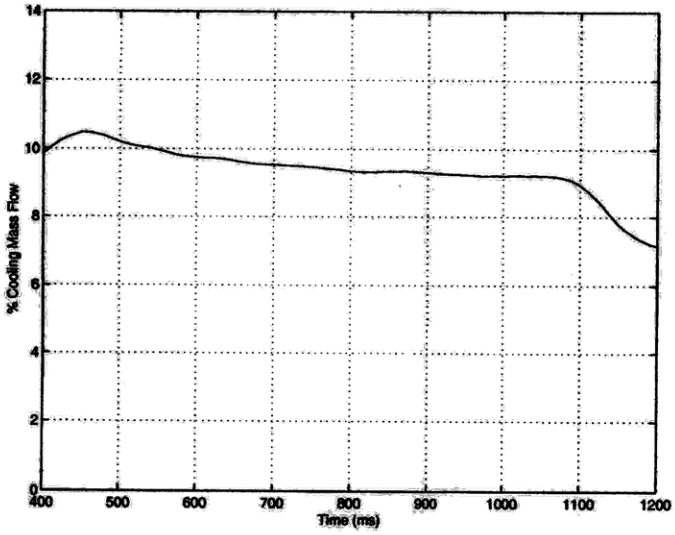

(c) Coolant mass flow

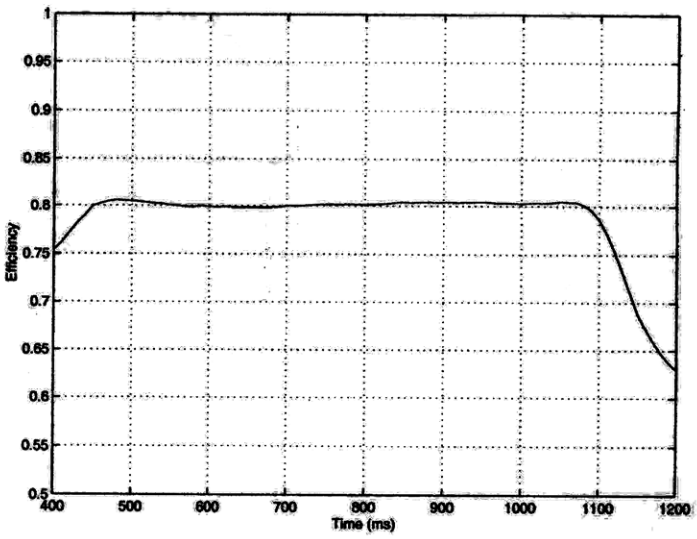

(d) Efficiency

Figure C-11: Film-cooled turbine test #011. This is an additional test which is not included in the test matrix presented in Chapter 7. It is close to the baseline conditions.

BIBLIOGRAPHY

[1] EPSTEIN, A.H., "Short Duration Testing for Turbomachinery Research and Development," Second Int. Symp. on Transport Phenomena, Dynamics, and Rotating Machinery, Honolulu, HI, 1988.

[2] EPSTEIN, A.H., GUENETTE, G.R., AND NORTON, R.J.G., "The MIT Blowdown Turbine Facility," ASME Paper 84-GT-116, 1984.

[3] GUENETTE, G.R., EPSTEIN, A.H., AND ITO, E., "Turbine Aerodynamic Performance Measurements in Short Duration Facilities," AIAA-89-2690, AIAA/ASME/SAE/ASEE Joint Propulsion Conference, Monterey, CA, 1989.

[4] GUENETTE, G.R., "A Fully Scaled Short Duration Turbine Experiment," Sc.D. Thesis, Massachusetts Institute of Technology, August 1985.

[5] ABHARI, R.S., "An Experimental Study of the Unsteady Heat Transfer Process in a Cooled Fully Scaled Transonic Turbine Stage," Ph.D. Thesis, Massachusetts Institute of Technology, January 1991.

[6] SHANG, T., "Influence of Inlet Temperature Distortion on Turbine Heat Transfer," Ph.D. Thesis, Massachusetts Institute of Technology, February 1995.

[7] GRÉPIN, L.M., "Aerodynamic Measurement and Analysis of the Flow in an Uncooled Turbine Stage," Masters Thesis, Massachusetts Institute of Technology, June 1998.

[8] KEOGH, R., "Shaft Efficiency Measurements of a Fully Scaled Turbine in a Short Duration Experiment," Masters Thesis, Massachusetts Institute of Technology, February 1998.

[9] CAI, Y., "Aerodynamic Performance Measurements in a Fully Scaled Turbine," Masters Thesis, Massachusetts Institute of Technology, February 1998.

[10] JACOBS, J.J., "Efficiency Measurements of a Single Stage Turbine in a Short Duration Facility," Masters Thesis, Massachusetts Institute of Technology, June 1998.

[11] HAY, N. AND LAMPARD, D., "Discharge Coefficient of Turbine Cooling Holes: A Review," ASME Paper 96-GT-492, 1984.

[12] ANDREWS, G.E. AND MKPADI, M.C., "Full-Coverage Discrete Hole Wall Cooling: Discharge Coefficients," *Journal of Engineering for Gas Turbines and Power*, Vol. 106, pp. 183-191, January 1984.

[13] OSNAGHI, C., PERDICHIZZI, A., SAVINI, M., HARASGAMA, P., AND LUTUM, E., "The Influence of Film Cooling on the Aerodynamic Performance of a Turbine Nozzle Guide Vane," ASME Paper 97-GT-522, 1997.

[14] WARD-SMITH, A.J., "Critical Flowmetering: The Characteristics of Cylindrical Nozzles with Sharp Upstream Edges," *International Journal of Heat and Fluid Flow*, Vol. 1, No. 3, pp. 123-132, July 1979.

[15] ASME/ANSI MFC-7M-1987 "Measurement of Gas Flow by Means of Critical Flow Venturi Nozzles," *An American National Standard*, The American Society of Mechanical Engineers, 1987.

[16] MILLER, R.W., *Flow Measurement Engineering Handbook*, McGraw-Hill, third edition, 1996.

[17] NIST 14, *NIST Mixture Property Database*, Standard Reference Database 14, Version 9.08, 1992, Fluid Mixtures Data Center, NIST Thermophysics Division 838.02, Boulder, CO.

[18] KERREBROCK, J.L., *Aircraft Engines and Gas Turbines*, The MIT Press, second edition, 1992.